DEVELOPING 1-D HEAT TRANSFER CORRELATIONS FOR SUPERCRITICAL WATER AND CARBON DIOXIDE IN VERTICAL TUBES

by

Sahil Gupta

A Thesis Submitted in Partial Fulfillment
of the Requirements for the Degree of
Master of Applied Science
Nuclear Engineering

The Faculty of Energy Systems and Nuclear Science
University of Ontario Institute of Technology

March, 2014

ABSTRACT

Taking into account the expected increase in global energy demands and increasing climate change issues, there is a pressing need to develop new environmentally sustainable energy systems. Nuclear energy will play a major role in being part of the energy mix since it offers a relatively clean, safe and reliable source of electrical energy. However, opportunities for building new generation nuclear systems will depend on their economic and safety attractiveness as well as their flexibility in design to adapt in different countries and situations. Keeping these objectives in mind, a framework for international cooperation was set forth in a charter of Generation IV International Forum (GIF) (GIF Charter, 2002) and six design concepts were selected for further development.

To achieve high thermal efficiencies of up to 45 – 50%, the use of SuperCritical Fluids (SCFs) as working fluids in heat transfer cycles is proposed Generation IV designs. An important aspect towards development of SCF applications in novel Gen IV Nuclear Power Plant (NPP) designs is to understand the thermodynamic behavior and prediction of Heat Transfer Coefficients (HTCs) at supercritical (SC) conditions. In addition to the nuclear power industry applications; SCFs are also expected to play a vital role in a number of other important technologies such as refrigeration systems, and geothermal systems, to name a few.

Given the potential for vast number of applications of SCFs in industry, the objective of this work was to gain an understanding on the behavior of SCFs and to develop a fundamental knowledge of the heat-transfer processes and correlations for SC Water and SC CO_2 flowing in bare circular tubes.

Experimental datasets for SC Water and SC CO_2 were compiled and used to obtain a basic 1-D empirical correlation that can predict HTC in bare circular tubes during the transient phases. The accuracy of these correlations was also analyzed using statistical techniques. Limitations and applications for 1-D correlations are discussed as well. The new correlations showed promising results for HTC and T_w calculations for the reference dataset with uncertainty of about ±25% for HTC values and about ±10-15% for the calculated wall temperature.

Keywords: Supercritical Water, Supercritical Water-cooled Reactors (SCWR), Heat-Transfer Correlations, Supercritical Fluids.

ACKNOWLEDGEMENTS

Foremost, I would like to acknowledge my supervisor, Dr. Igor Pioro, for his relentless support with this thesis project. The completion of this thesis was not possible without his insightful discussions and valuable direction on the subject.

I thank my parents for their undying support and encouragement through my life. I also thank all my friends, especially, Eugene Saltanov and Sarah Mokry for providing valuable technical consultation and guidance during every phase of the project. Their previous work on this subject laid the foundation of my work.

Financial support received from NSERC/NRCan/AECL Generation IV Energy Technologies Program and NSERC Discovery Grant is greatly acknowledged.

Finally, I would like to thank the University of Ontario Institute of Technology (UOIT) for providing me with a wonderful platform to pursue my research interest.

EXECUTIVE SUMMARY

Chapter 1: Chapter 1 focusses on the present-day status of Nuclear Energy and the need to develop advanced (Generation IV) reactor concepts to meet future energy demands. To compete with the economics of fossil fuel plants, nuclear power plants would have to make use of high temperatures and pressures fluids to reach increased thermal efficiencies (upto 50%). Thus the use of Supercritical Fluids will be vital in next generation Power Applications. It is noted that there are many similarities in the thermo-dynamic cycles of NPP involving SCFs for Generation IV designs. Furthermore, applications of SuperCritical Fluids (SCFs) in Power Engineering and other industrial applications are discussed with the emphasis on the applications for SC water in Rankine cycles and SC CO_2 for Brayton cycle. The objectives and scope of the thesis report have been laid out in this chapter.

Chapter 2: This chapter discusses the background information and the basic thermodynamics involved in SCFs. Various parametric trends in thermodynamic properties involved in transitions to supercritical regions are demonstrated with the use graphs and experiment. It is noted that thermodynamic properties of fluids undergo rapid variations within the pseudocritical regions. Due to these variations, the transition behaviour of the SC fluids is complex and it is difficult to predict the heat transfer characterises of fluid at these conditions. Existing HTC empirical correlations for forced convection are also discussed. The majority of these correlations were proposed in the era of 1960s and 1970s for sub-critical conditions. Their use in superficial fluids data does not achieve the desired level of accuracy and significant deviations of calculated values can be noted especially within the pseudocritical range. A need to develop new correlations that are better aligned with experimental data was identified.

Chapter 3: This chapter the methodology that was adapted to develop 1-D empirical correlations. Time tested approach of using dimensional analysis was employed to formalize a HTC model equation. This model equation can then be coupled with experimental datasets using various curve-fitting techniques to obtain the coefficients of proportionality. Selection of characteristic temperatures and experimental test facilities considerations were also evaluated and discussed.

Chapter 4 and 5: These chapters detail the experimental setups and the reference datasets, using which new 1-D empirical correlations were developed. Experimental dataset for water was obtained from the Institute for Physics and Power Engineering (Obninsk, Russia). CO_2 dataset was obtained from Fuel Channel Thermalhydraulics (FCT) laboratory located at Chalk River (CRL). These datasets were selected as they had well documented/controlled experimental procedures and test uncertainties and hence provides credibility to the data points.

Experimental data in the form of graphs of internal wall and bulk-fluid temperatures and HTC vs. heated length and bulk-fluid enthalpy are presented. Statistical error calculations were performed using analytical and graphical techniques. Preliminary error analysis shows that the new correlations developed as a part of this project show much better agreement with experimental values with lower RMS and mean errors for HTC and T_w. Further analysis is required to confirm these results and test the proposed correlations on datasets from other sources and under different geometrical and flow conditions. Lack of credible datasets that is available in open source is a challenge.

Chapter 6: Chapter 6 focuses on some key applications of the proposed HTC correlations that may be used for (1) preliminary heat-transfer calculations in SCWR fuel channels as a conservative approach; (2) calculations of supercritical-water heat-transfer in heat exchangers in SCWR indirect-cycle concepts; (3) calculations of heat-transfer in heat exchangers for the co-generation of hydrogen at SCW NPPs; (4) future comparisons with other independent datasets and with data for fuel bundles; (5) the verification of computer codes for SCWR core thermalhydraulics; and (6) the verification of scaling parameters between water and modelling fluids (CO2, refrigerants, etc).

It further presents the limitations for the proposed correlations, future work and a summary of key conclusions. It is concluded that the objectives set forth in Chapter 1 were successfully met.

TABLE OF CONTENTS

LIST OF FIGURES

LIST OF TABLES

LIST OF EQUATIONS

NOMENCLATURE

Symbols

C	constant
c_p	specific heat at constant pressure, J/kg·K
$\bar{c}_p$	average specific heat, J/kg·K, $\left(\frac{H_w - H_b}{T_w - T_b}\right)$
D	inside diameter, m
f	function
G	mass flux, kg/m^{2}s
H	enthalpy, J/kg
h	heat transfer coefficient, W/m^{2}K
k	thermal conductivity, W/m·K
L	length, m
P	pressure, Pa
q	heat flux, W/m^2
R_a	surface roughness, μm
T	temperature, ºC
V	velocity, m/s
x	axial location, m

Greek Letters

μ	dynamic viscosity, Pa·s
ρ	density, kg/m^3
δ	thickness, mm

Dimensionless numbers

Nu	Nusselt number $\left(\frac{h \cdot D}{k}\right)$
Pr	Prandtl number $\left(\frac{\mu \cdot c_p}{k}\right)$
$\overline{\mathbf{Pr}}$	average cross-sectional Prandtl number $\left(\frac{\mu \cdot \bar{c}_p}{k}\right)$
Re	Reynolds number $\left(\frac{G \cdot D}{\mu}\right)$

Subscripts

ave	average
b	bulk
calc	calculated
cr	critical
dht	deteriorated heat-transfer
exp	experimental
h	heated
in	inlet
out	outlet
pc	pseudocritical
w	wall

Abbreviations:

AECL	Atomic Energy Canada Limited
AGRs	Advanced Gas cooled Reactors
Ave.	Average (error)
BOP	Balance of Plant
CANDU	CANada Deuterium Uranium (reactor)
CFD	Computational Fluid Dynamics
CRL	Chalk River Laboratories
DAS	Data Acquisition System
DHT	Deteriorated Heat-Transfer
EGS	Enhanced Geothermal Systems
ELSY	European Lead-cooled System
EU-JRC	European Joint Research Center
Gen IV	Generation IV
GFR	Gas-cooled Fast Reactor
GIF	Generation IV International Forum
GWP	Global (or Greenhouse) Warming Potential
HPLWR	High Performance Light Water Reactor
HT	Heat Transfer
HTC	Heat Transfer Coefficient
HTR	High Temperature Reactor
HWRs	Heavy Water Reactors
IAEA	International Atomic Energy Agency
ID	Inside Diameter
IHT	Improved Heat-Transfer
INEEL	Idaho National Engineering and Environmental Laboratory
IPPE	Institute of Physics and Power Engineering
JAEA	Japan Atomic Energy Agency
JSCWR	Japan Super Critical Water Reactor
KAERI	Korea Atomic Energy Research Institue
LFR	Lead Fast Reactor
LWRs	Light Water Reactors
MSR	Molten Salt Reactor
NHT	Normal Heat Transfer
NIST	National Institute of Standards and Technology
NPP	Nuclear Power Plant
NU	Natural Uranium
ODP	Ozone Depleting Potential
PFBR	Prototype Fast Breeder Reactor
PT	Pressure Tube (reactor)
PV	Pressure Vessel (reactor)
RMS	Root-Mean-Square (error)
SC	Super Critical
SCFs	SuperCritical Fluids
SCW	SuperCritical Water
SCWO	SuperCritical Water Oxidation
SCWR	SuperCritical Water Reactor
SFL	Supercritical Fluids Leaching
SFR	Sodium-cooled Fast Reactor
SJTU	Shanghai Jiao Tong University
SSTSR	Small Secure Transportable Autonomous Reactor
USC	Ultra-Super-Critical
VHTR	Very High Temperature Reactor
VVER-SCP	Water –Cooled, water moderated power reactor at SuperCritical Pressure (in Russian abbreviations)

CHAPTER 1 INTRODUCTION

1.1 Current Status of Electricity Generation

Availability of cheap and clean electricity is a key ingredient for our civilizations advancement. The amount of electricity consumed by a country can be directly correlated to its prosperity and standard of living. In general the electricity demand is expected to increase proportionally with the rise in population and our continuous pursuit of industrialization. Currently, electricity can be generated by: 1) non-renewable-energy sources such as coal, natural gas, oil, and nuclear[1]; and 2) renewable-energy sources such as hydro, wind, solar, biomass, geothermal and marine. Oil, natural gas, and coal, the traditional fossil fuels that have powered modern societies since the Industrial Revolution, remain the dominant world energy sources today (see Figure 1-1).

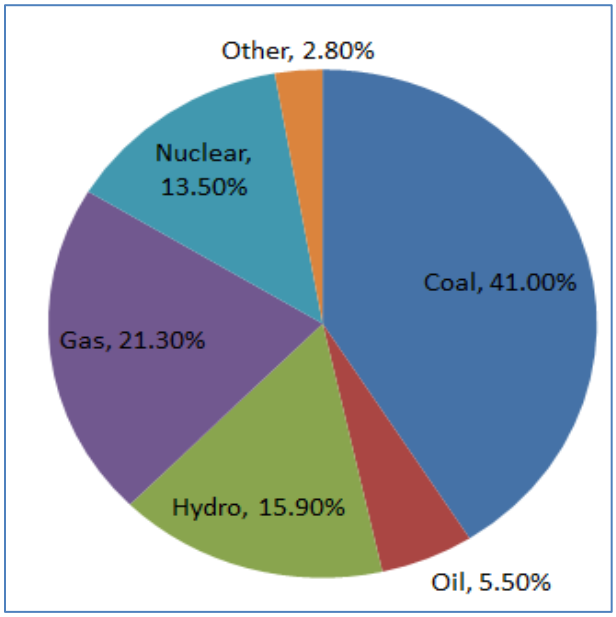

Figure 1-1: World Energy Distribution by Source, in total 20,183 TWh (Pioro and Kirillov, 2013).

While the renewable-energy sources such as wind, solar show good potential; their application towards baseload power generation remains questionable due to low availability factors[2]. Considering the availability and capacity factors (see Table 1-1), the main sources for base-load

[1] Note that Nuclear can be considered as a renewable source if fast spectrum breeder fuel cycles involving U238 or Thorium Th232 are utilized.

[2] The availability factor of a power plant is the amount of time that it is able to produce electricity over a certain period, divided by the amount of the time in the period.

electrical-energy generation are: 1) thermal - coal and natural gas; 2) hydro and 3) nuclear. A mix of these three power sources in the right proportion[3] is perhaps the most feasible option for baseload generation on an electrical grid.

Table 1-1: Average (typical) capacity factors of various power sources (Pioro and Kirillov, 2013)

No.	Power Plant type	Location	Year	Capacity factor[4], %
1	Nuclear	USA	2010	91
		UK	2011	66
2	Combined-cycle	UK	2011 2007-2011	48 62
3	Coal-fired	UK	2011	42
4	Hydroelectric[5]	UK	2011	39
		World (average)	-	44
		World (range)	-	10-99
5	Wind	UK	2011	30
		World	2008	20-40
6	Wave	Portugal	-	20
7	Concentrated-solar thermal	USA California	-	21
8	Photovoltaic solar	USA Arizona	2008	19
		USA Massachusetts	-	12-15
		UK	2011 2007-2011	5.5 8.3
9	Concentrated-solar photovoltaic	Spain	-	12

[3] The right proportion depends on a number of variables such as countries natural resources, economics, energy policies etc.

[4] Capacity factor is the ratio of the actual output of a power plant in a given year and its potential output if it had operated at full nameplate capacity the entire time. Capacity factors vary significantly depending on the type of a plant.

[5] Capacity factors for hydroelectric plans depend significantly on a design, size and location (water availability). Small plants built on large rivers will always have enough water to operate at a full capacity.

1.2 Move towards Higher Thermal Cycle Efficiencies

To increase economic appeal, scientists around the world continuously push the envelope of gaining higher efficiencies in electricity generation. In the last 50 years, thermal-power industry has made significant improvements in thermal efficiencies of power plants. Today, one can see efficiencies of 50 – 53% for coal-fired plants and 55 – 60% for combined gas-fired plants (see Table 1-2 for more details). A significant reason for higher efficiencies at coal-fired power plants is due to the transition from subcritical water/steam with pressure up to 16 MPa to supercritical water/steam with pressures ranging from 23.5 MPa to 38 MPa. However, nuclear-power industry is still facing lower-range thermal efficiencies of about 30 – 35% in the case of water cooled nuclear reactors (Gupta et al., 2010). Advanced Generation IV (see Section 1.3) designs of Nuclear Power Plants (NPPs) are being considered for development throughout the world. An important goal towards development of the next generation NPPs is to increase the thermal efficiency to the level of 45 – 50%.

Table 1-2: Typical ranges of thermal efficiencies of modern power plants (Pioro, 2013).

No.	Power Plant	Cycle Efficiency %
1	Combined-cycle power plant (combination of Brayton gas-turbine cycle (fuel - natural or Liquefied Natural Gas (LNG); combustion-products parameters at the gas-turbine inlet: $T_{in} \approx 1650$°C) and Rankine steam-turbine cycle (steam parameters at the turbine inlet: $T_{in} \approx 620$°C ($T_{cr} = 374$°C)).	Up to 62
2	Supercritical-pressure coal-fired thermal power plant (new plants) (Rankine-cycle steam inlet turbine parameters: $P_{in} \approx 25 – 38$ MPa ($P_{cr} = 22.064$ MPa), $T_{in} \approx 540$ - 625°C ($T_{cr} = 374$°C) and $T_{reheat} \approx 540$ - 625°C).	Up to 55
3	Internal-combustion-engine generators (Diesel cycle and Otto cycle with natural gas as a fuel).	Up to 50
4	Subcritical-pressure coal-fired thermal power plant (older plants) (Rankine-cycle steam: $P_{in} \approx 17$ MPa, $T_{in} \approx 540$°C ($T_{cr} = 374$°C) and $T_{reheat} \approx 540$°C).	Up to 40
5	Concentrated-solar thermal power plants with heliostats, solar receiver (heat exchanger) on a tower and molten-salt heat-storage system: Molten salt maximum temperature is about 565°C, Rankine steam-turbine power cycle used.	Up to 20

1.3 Generation-IV Reactor Concepts

The current fleet of NPPs is classified as Generation II and III[6] and have relatively low operating temperatures (below 350 °C), significantly limiting their thermal cycle efficiencies to around 30%. The latest designs of NPPs that are commercially available are Generation III+ that are enhanced Gen III designs and they incorporate over 50 years of operating experience. However, considering the expected increase in global energy demands and increasing climate change concerns there is a pressing need to develop new environmentally sustainable energy systems. As discussed in earlier sections, nuclear energy is expected to play a major role in the energy mix since it offers a relatively clean, safe and reliable source of energy. For the longer term, more innovative nuclear energy technologies and fuel cycles, known collectively as Generation IV systems, are being developed through international co-operation. Figure 1-2 shows the successive generations of NPPs along with their deployment timeline (Nuclear Energy Today, 2012).

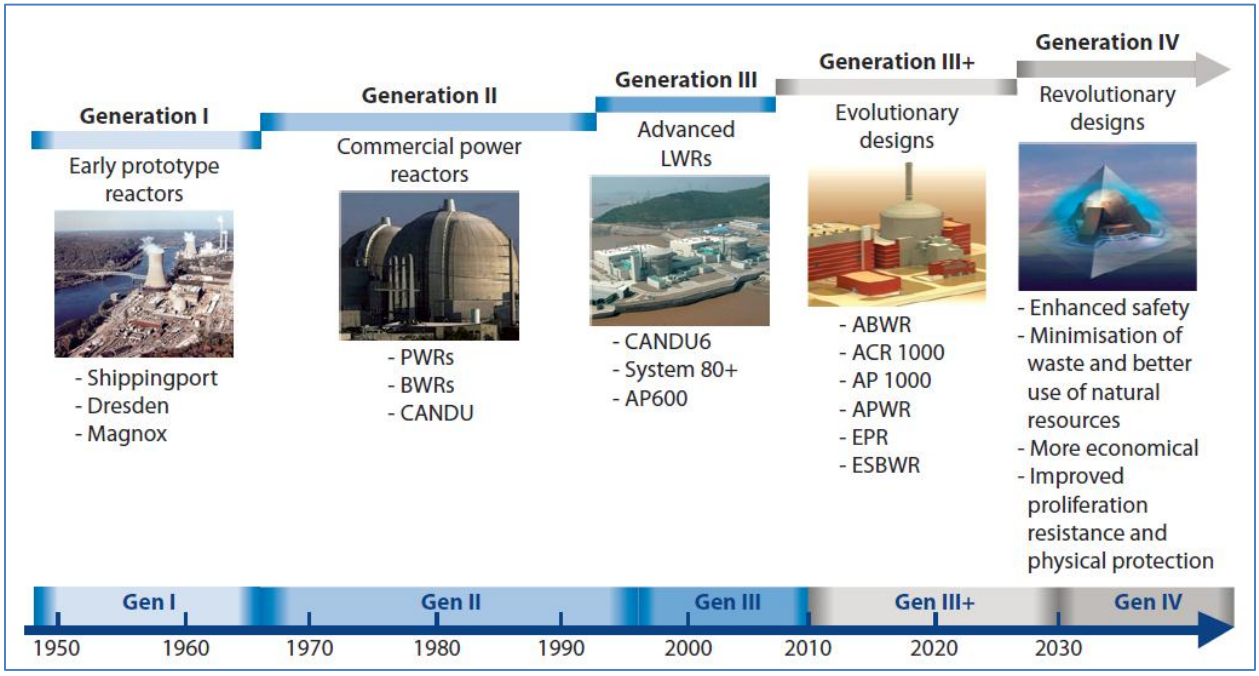

Figure 1-2: Nuclear Reactors Evolution (Nuclear Energy Today, 2012)

[6] A limited number of Generation III+ reactors (mainly, Advanced Boiling Water Reactors -ABWRs) operate in some countries.

1.4 Generation IV-International Forum

Opportunities for building new generation IV nuclear systems will depend on their economic and safety attractiveness as well as flexibility in design to adapt in different countries and situations. Keeping these objectives in mind, a framework for international cooperation was set forth in a charter of Generation IV International Forum (GIF)[7] (GIF Charter, 2002). The main design goals for the Generation IV nuclear system concept were to improve economic gains, enhance safety, extend sustainability, and strengthen proliferation resistance by building upon the platform set by the current fleet of reactors recognizing the shortcomings, positive design features and operating experience. Since its conception, the Gen-IV program has narrowed its goals to the 3 major objectives:

1. **Electricity Generation:** innovative improvements in economics and to be cost competitive in a number of market environments, while seeking further advances in safety, proliferation resistance and physical protection, and sustainability.

2. **Hydrogen Production, Cogeneration, and other Uses:** Designed to utilize waste/process heat for various purposes such as supporting steam-reforming, steam electrolysis, or thermochemical production of hydrogen, as well as other chemical production processes. Application to desalination for potable water production may be an important use for the rejected heat.

3. **Actinide Management:** Designed to minimize nuclear waste and long-term assurance of fuel availability.

The Generation IV International Forum (GIF) Program has narrowed design options of nuclear reactors to six concepts. These concepts are: 1) Gas-cooled Fast Reactor (GFR) or High Temperature Reactor (HTR), 2) Very High Temperature Reactor (VHTR), 3) Sodium-cooled Fast Reactor (SFR), 4) Lead-cooled Fast Reactor (LFR), 5) Molten Salt Reactor (MSR), and 6) SuperCritical Water-cooled Reactor (SCWR).

These nuclear-reactor concepts differ from each other in terms of their design, neutron spectrum, coolant, moderator, operating temperatures and pressures. Some of these reactor designs could

[7] Canada, EU, Japan, Russia and USA are among the major participants of Gen-IV forum.

be demonstrated within the next decade, with commercial deployment beginning in the 2030s. Today, China has begun construction of a prototype High Temperature Reactor, a first step towards the development of the VHTR, and both France and Russia are developing advanced sodium-fast reactor designs for near-term demonstration. A prototype lead fast reactor is also expected to be built in Russia in the 2020 time frame. Table 1-3 provides an overview of the Generation IV systems and a brief description of each concept has been provided in subsequent sections (Gen IV, 2009).

Table 1-3: Overview of six Generation IV Systems

System	Neutron spectrum	Coolant	Temp. Range °C	Operating Pressure MPa	Power Cycles[8]		Thermal Efficiency %
					Primary	Alternative	
VHTR	Thermal	Helium	640 – 1000	7 – 9	Direct Brayton helium gas-turbine	Indirect gas mixture Brayton Cycle or Rankine Steam cycle	> 50
SFR	Fast	Sodium	500 – 550	~ 0.1	Indirect Steam Rankine[9]	Indirect SC CO_2 Brayton	40 – 42
SCWR	Thermal/fast	Water	510 – 625	25	Direct Steam Rankine	Indirect SC Steam Rankine Cycle	
GFR or HTR	Fast	Helium	490 – 850	9	Direct Brayton helium gas-turbine	Indirect Steam Rankine cycle/indirect SC CO_2 Brayton	~ 48
LFR	Fast	Lead	480 – 570	~ 0.1	Indirect SC CO_2 Brayton (in USA)	Indirect Steam Rankine (in Russia)	~ 43
MSR	Thermal/fast	Fluoride salts	700 – 800	~ 0.1	Indirect Steam Rankine	Indirect SC CO_2 Brayton cycle	45 – 50

1.4.1 Gas-cooled Fast Reactor (GFR) or High Temperature Reactor (HTR)

Gas-cooled Fast Reactor (GFR) or High Temperature Reactor (HTR) is fast-neutron-spectrum reactor with a closed fuel cycle, which can also be for co-generation of hydrogen through thermochemical cycles or high-temperature electrolysis. The coolant is helium with inlet and

[8] Most of the Gen – IV reactor concepts are looking to utilize direct thermal cycles to avoid the need for Heat Exchangers (HX). However, due to design and operational concerns limitations, indirect cycles utilizing HX are also being looked as a backup plan.

[9] Utilizing Steam cycle in Sodium SFR is potentially unsafe option since piping leaks can lead to mixing of the water and sodium together which results in a violent chemical reaction. An indirect SC CO_2 Brayton cycle is must safer option.

outlet temperatures of 490 and 850°C, respectively with direct Brayton helium-gas-turbine cycle. Indirect Rankine steam cycle or even indirect supercritical carbon-dioxide Brayton gas-turbine cycle are also considered. It combines the advantages of fast-spectrum systems[10] with those of high-temperature systems[11].

1.4.2 Very High Temperature Reactor (VHTR)

Very High Temperature Reactor (VHTR) is a thermal-neutron-spectrum reactor and is primarily dedicated to the co-generation of hydrogen through high-temperature electrolysis and process heat. In a VHTR, graphite and helium have been chosen as the moderator and the coolant, respectively. The inlet and outlet temperatures of the coolant are 640 and 1000°C, respectively, at a pressure of 7 – 9 MPa (US DOE, 2002). Due to such high outlet temperatures, the thermal efficiency of VHTR is projected to be above 50% and it also becomes extremely attractive for chemical, oil and iron industries. The electric power conversion may employ either a direct (helium gas turbine) or indirect (gas mixture turbine) Brayton cycle.

1.4.3 Sodium-cooled Fast Reactor (SFR)

Similar to GFR, SFR is a fast-neutron-spectrum reactor that uses liquid sodium as the reactor coolant, allowing high power density with low coolant volume fraction. SFR closed fuel cycle enables breeding of fissile fuel and facilitates the management of high-level radioactive wastes. The primary choices of fuel for SFR are oxide and metallic fuels with supercritical CO_2 as a working fluid for power conversion thermo system.

Currently, SFR is the only one Generation IV power reactor implemented in the power industry. Russia and Japan are leaders within this area. India also has a Prototype Fast Breeder Reactor (PFBR) which is 500MWe pool type, sodium cooled nuclear reactor currently under advanced stage of construction. Much of the basic technology for the SFR has been established in former fast reactor programs and is being confirmed by Phenix end-of-life tests in France, the lifetime extension of BN-600, the restart of Monju in Japan, startup of BN-800/BN-1200 in Russia, and the startup of the China Experimental Fast Reactor (Gen IV, 2009).

[10] Fast spectrum affords a more sustainable use of uranium resources and waste minimization through fuel recycling and burning of long-lived actinides.

[11] High temperature affords increased thermal-cycle efficiency and industrial use of the generated heat that can be used for various applications such as hydrogen co-production.

1.4.4 Lead-cooled Fast Reactor (LFR)

LFR is a fast-neutron-spectrum reactor with a closed fuel cycle, which uses lead or lead-bismuth as the reactor coolant. The outlet temperature of the coolant is about 550°C (but can be as high as 800°C) at atmospheric pressure. The primary choice of fuel is a nitride fuel. The supercritical carbon-dioxide Brayton gas-turbine cycle has been chosen as a primary choice for the power cycle in US and some other countries, while the supercritical-steam Rankine cycle is considered as the primary choice in Russia.

The designs that are currently proposed as options are two pool-type reactors (Gen IV, 2009) - the small secure transportable autonomous reactor (SSTAR) and the European lead-cooled system (ELSY).

1.4.5 Molten Salt Reactor (MSR)

MSR is a thermal-neutron-spectrum reactor, which uses a molten fluoride salt with dissolved uranium while the moderator is made of graphite. The inlet temperature of the coolant (e.g., fuel-salt mixture) is 565°C while the outlet temperature reaches 700°C. However, the outlet temperature of the fuel-salt mixture can even increase to 850°C when co-generation of hydrogen is considered as an option. Compared with solid-fueled fast reactors, thermal-spectrum MSRs have lower fissile inventories, no radiation damage constraint on fuel burnup, no fabrication of fuel forms, no spent nuclear fuel assemblies, and a homogeneous isotopic composition of fuel in the reactor (Gen IV, 2009). These unique design features of MSRs, high thermal efficiencies (between 45 and 50%) and inherent safety features make MSRs extremely attractive option for future reactors.

1.4.6 SuperCritical Water-cooled Reactor (SCWR).

SuperCritical Water-cooled Reactor (SCWRs) is a Generation IV concept that is being designed to operate at high temperatures and supercritical pressures similar to that of modern coal-fired power plants. While the reactor size, design and operating conditions differ for each concept, they are all designed for operating pressures around 25 MPa and use SC water for heat transfer. The design of SCW nuclear reactors can be seen as the natural and ultimate evolution of today's conventional modern light water reactors (LWRs) and heavy water reactors (HWRs). While the

design can be 1) Pressurized-Vessel (PV) type, 2) Pressurized-Tube (PT)/Pressure-Vessel (PV) type, or a hybrid design, the overall design approach is to match the reactor core operating conditions to those of existing supercritical turbines, avoiding the need for a new turbine development effort. Majority of the SCWR concepts are focussed on the Pressure Vessel type, however Canada (AECL) has focussed its research on Pressure-Tube type (see Figure 1-3 and Figure 1-4). Both thermal and fast spectrums have been proposed as a potential option (Oka, 2010). Therefore, the typical outlet temperatures of the SCWR designs vary from 550°C to 625°C.

1.4.6.1 Pressure Vessel Type (PV)

Pressure Vessel type designs are evolutionary designs adapted from PWRs and BWR designs. Since supercritical water is a single-phase fluid, the reactor pressure vessel (PV) is simpler than in a BWR without the need for steam-water separators above the core and the possibility for the control rods to be inserted through the top of the vessel, as in a PWR (US DOE, 2002). But like a BWR (and in a supercritical fossil fired power plant), a direct cycle is possible with steam exiting the core at 500°C being fed directly to the high pressure steam turbine. The simplicity in design offers huge cost savings since it eliminates the need for a separated primary and secondary loop and the use of steam generators.

1.4.6.2 Pressure-Tube Type (PT)

A core of a PT SCWR consists of distributed pressure channels analogous to CANDU and RBMK reactors, respectively (see Figure 1-3 and Figure 1-4). Direct cycle is proposed and the high-pressure SCW from the core will be directly fed into the SCW turbines with operational pressure of 25 MPa and temperate of 625°C (Pioro et al., 2008). This design builds on the current advanced high pressure turbine configurations of SCW fossil power plants. The design offers increased thermal efficiency and also simplifies the system by eliminating the need to transfer energy to a secondary cycle via a steam generator and its associated components (Duffey et al., 2008). Some variants, such as options for reheat channels and dual cycles are also being considered.

Proposed operating conditions of the SCWR are shown in Table 1-4 CO_2 equivalent (scaled down) conditions are also shown.

Table 1-4: Critical and nominal operating parameters (NIST, 2007)

Parameter	Unit	Water	CO_2
Critical parameters			
Critical pressure	MPa	22.1	7.38
Critical temperature	ºC	374.1	31.0
Critical density	kg/m^3	315	468
Operating parameters			
Operating pressure	MPa	25	8.34
Inlet temperature	ºC	350	20
Outlet temperature	ºC	625	150

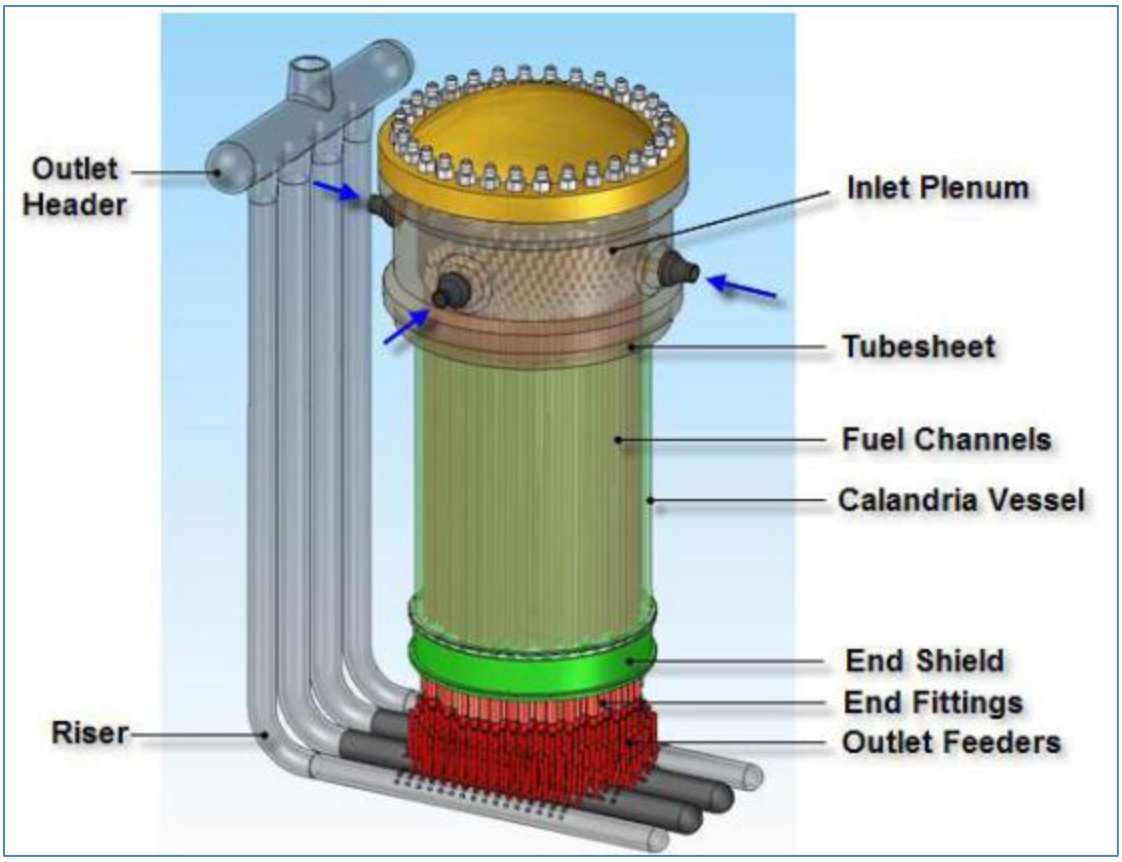

Figure 1-3: Schematic Diagram of the Pre-Conceptual Canadian SCWR Design

(Courtesy of AECL, CANADA)

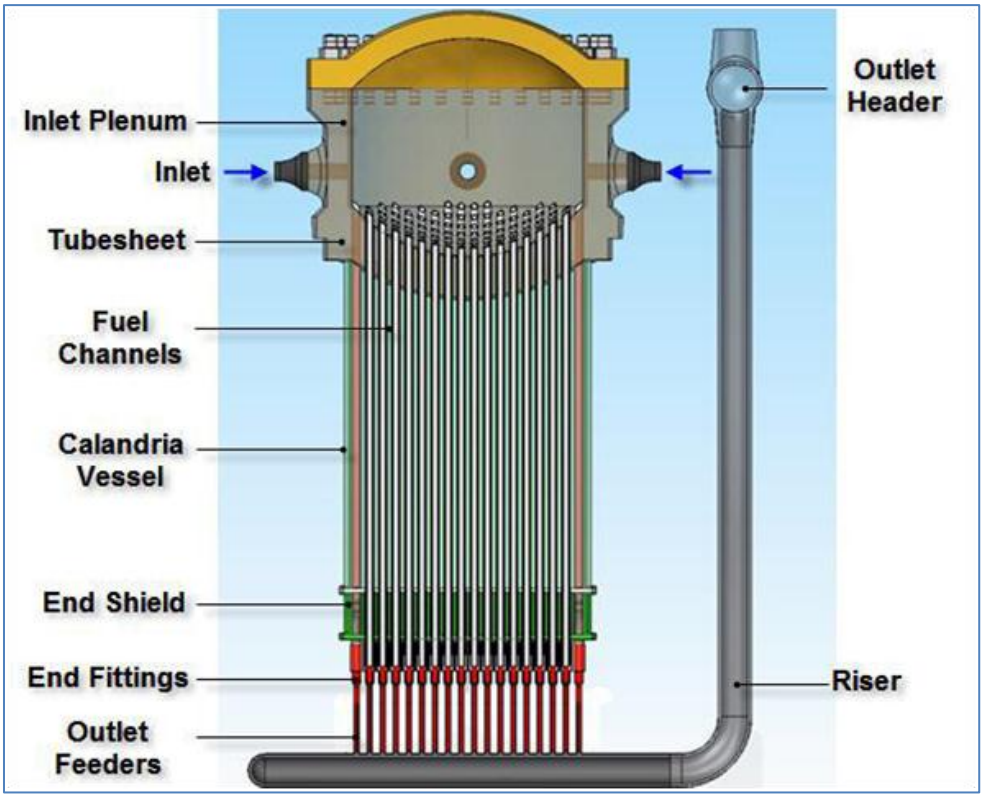

Figure 1-4: Cross Sectional View of the Pre-Conceptual Canadian SCWR Design
(Courtesy of AECL, CANADA)

1.5 SCWR Concepts around the world

Through the GEN-IV forum, a number of countries are leading a coordinated research effort toward developing the SCWR technology. Table 1-5 summarizes the various conceptual design parameters.

Note that a number of these reactor concepts are still in their infancy stages and design parameters are evolving. While the reactor core and fuel designs differ significantly, there are many similarities between the secondary side cycles and safety features. Most design concepts are still facing challenges, particularly cladding material selection to withstand high temperatures during normal operations and postulated accident scenarios. Improvement in heat-transfer prediction accuracy would provide a realistic estimation of cladding temperature, which may ease the cladding material requirement.

Furthermore, all SCWR concepts may utilize Heat Exchangers (HX) and heat transfer correlations would be required for calculations involving flow temperatures and HX designs.

Table 1-5: Proposed Design Parameters for SCWR Concepts around the world[12]

Parameters	**Units**	**Canada**	**China**	**Europe**	**Japan**		**Korea**	**Russia**	**USA**
Organization	-	AECL	SJTU	EU-JRC	Various		KAERI	OKB IPPE	INEEL
Reactor Type	-	PT	PV	PV	PV	PV	PV	PV	PV
Power (Thermal)	MW_{th}	2540	3800	2300	4039	1602	3182	3830	3575
Spectrum		Thermal	Mixed	Thermal	Thermal	Fast	Thermal	Fast-resonance	Thermal
Thermal efficiency	**%**	48	~44	43.5	42.7	~44		43-45	45
Operation Pressure	MPa	25	25	25	25	25	25	24.5	25
T_{in} coolant	ºC	350	280	280	290	280	280	290	280
T_{out} coolant	ºC	625	510	500	510	508	510	540	500
Flow rate	kg/s	1512	1927	1179	2105	820		1890	1843
Fuel	–	Pu-Th	UO_2/MOX	UO_2	UO_2	MOX	UO_2	MOX	UO_2

[12] Data compiled from various sources and published papers

1.6 Use of Supercritical Fluids in Power Applications

Use of supercritical water in power-plant "steam" generators is the largest application of a fluid at supercritical pressures in the industry (Pioro, 2011). Use of supercritical pressures in power generation is very attractive since it can lead to significant increase in efficiency and there is no liquid-vapor phase transition; therefore, there is no such phenomenon as critical heat flux or dryout[13]. Temperatures at the boiler exit were initially around 550°C, but recent advances in materials and turbine technology have led to using 625°C at 25 MPa. Further research is proceeding towards adopting outlet temperatures of over 750°C at the pressure of 35 MPa (DOE, 2009). The Ultra-Super-Critical (USC) turbine manufacturers now claim that developments in thermal (coal-fired) power plants will lead to thermal cycle efficiencies of greater than 50% (World Coal Institute, 2010).

In general, the development of SCFs in power applications focuses on:

- Increasing the efficiency of the existing ultra-supercritical and supercritical "steam" generators (Smith 1999);
- Developing supercritical water-cooled nuclear reactors (Kirillov 2001a,b; Oka 2003);
- Using supercritical water in the Rankine cycle for lead-cooled nuclear reactors (Boehm et al. 2005) and in the Brayton cycle (Sohn et al. 2005) including the Brayton cycle for future Sodium Fast Reactors (SFRs);
- Using supercritical carbon dioxide in an indirect cycle of the gas cooled fast reactors (Hejzlar et al. 2005; Kato et al. 2005);

1.6.1 Advantages of using Supercritical Fluids in Nuclear Reactors

In the 1950s, the idea of using supercritical water appeared to be rather attractive for the thermal-power industry (Pioro and Duffey, 2007). The objective was increasing the total thermal efficiency of coal-fired power plants. Between late 1950s and early 1960s, studies were conducted to investigate the possibility of using supercritical water in nuclear reactors (Pioro and Duffey, 2007). Several designs of nuclear reactors using supercritical water were proposed in Great Britain, France, the USA, and the former USSR. However, the idea was abandoned for

[13] Note however that within certain range of parameters, deterioration of heat transfer (DHT phenomenon) may occur. Refer to Section 2.3 for more details.

almost 30 years with the emergence and great success of Light Water Reactors (LWRs). SCW technology regained interest in the 1990s following LWRs maturation.

The current fleet of nuclear reactors are significantly lagging behind in terms of thermodynamic efficiencies. With the exception of Advanced Gas cooled Reactors (AGRs), the efficiencies are limited in ranges of 30 – 38%. In order to create a significant step change in cycle efficiencies, nuclear industry has to move towards using coolants at supercritical conditions. Fluids at supercritical pressures are considered to be very promising as coolants for the next fleet of reactors as they also simplify the overall design of the nuclear plants (Gallaway, 2009) while increasing the efficiencies to the range of 50 – 55%. Higher temperatures also allow opportunities for hydrogen co-generation, increase in the specific fuel utilization and reduction in the waste heat rejection.

In addition to SC water, SC CO_2 also offers widespread applications in power industry. SC CO_2 is proposed to be the working fluid in Brayton-cycle power plant applications due to its attractive thermophysical properties, low operational and capital costs, and minimal safety concerns as well as particularly small dimensions of turbomachinery. Use of SC CO_2 in combined cycles offer significant advantages such as high thermal efficiencies, optimal thermal input for CO_2 and fewer problems with erosion and corrosion of materials (Hajek, 2009). Supercritical CO_2 cycles can also be optimally used in combined cycles with water or Sodium.

Thus, a basic understanding of the thermodynamic behaviour of SCFs is very critical to assist in developments of the above mentioned power applications. Keeping this objective in mind, this thesis report focuses on analyzing SC Water and CO_2 flow in bare tubes.

It must be pointed out here that while the use of high temperature and pressure fluid offers significant advantages in terms of net increase to the thermal efficiencies, it does tend to add operational and maintenance complexities. Special metallurgical considerations would also have to be made to find materials that can withstand the higher temperatures and have with minimal neutron absorption cross section area. Furthermore, high temperatures also increase the corrosion rates and may lead to an overall decrease in the operational life of the plant systems. Thus, there is a fine balance that needs to be realized in any system design involving SCFs to balance the economic gains of higher efficiencies vs. the associated costs of enhanced material, operational and maintenance constraints.

1.7 Other Uses of Supercritical Fluids

Applications for Supercritical Fluids (SCFs) are not limited to the power industry. Recent advancements in this area have proposed use of SCFs in much wider applications such as (Pioro and Duffey, 2007)[14]:

- Using supercritical carbon dioxide for cooling of a printed circuit
- Use of near-critical helium to cool the coils of superconducting electromagnets, superconducting electronics and power-transmission equipment
- Use of supercritical hydrogen as a fuel for chemical and nuclear rockets
- Use of liquid hydrocarbon coolants and fuels at supercritical pressures in the cooling jackets of liquid rocket engines and in fuel channels of air-breathing engines
- Use of supercritical carbon dioxide as a refrigerant in air-conditioning and refrigerating systems
- Use of a supercritical cycle in the secondary loop for transformation of geothermal energy into electricity
- Use of supercritical water oxidation technology (SCWO) for treatment of industrial and military wastes
- Use of carbon dioxide in the supercritical fluid leaching (SFL) method for removal of uranium from radioactive solid wastes and in decontamination of surfaces
- Use of supercritical fluids in chemical and pharmaceutical industries in such processes as supercritical fluid extraction, supercritical fluid chromatography, polymer processing and others

Some of the applications for SC CO_2 are discussed in further details in subsequent sections.

[14] For detailed references refer to Chapter 1 of Pioro and Duffy, 2007

1.7.1 Air Conditioning Systems (Refrigeration Cycles)

Refrigerant 134a has long been used in air conditioning (A/C) systems for automotive and commercial purposes. However R-134a's Global (or Greenhouse) Warming Potential (GWP) is quite large and also breaks down the ozone layer as it leaks into the atmosphere from the A/C systems (Mathur, 2000). As a result, Carbon Dioxide (CO_2) has been widely investigated for use as a working fluid in refrigeration cycles, because it has no ozone depleting potential (ODP) and low Global Warming Potential (GWP). It is also inexpensive, non-explosive, non-flammable and abundant in nature.

1.7.2 Enhanced Geothermal Systems (EGS)

Supercritical CO_2 is being proposed to be used as a working fluid in Enhanced Geothermal Systems (EGS) as it may hold some advantages over water. An EGS uses dry impermeable rock as a source of energy as opposed to traditional wet permeable rock (Wan, 2011). The idea of using EGS with SC CO_2 was initially proposed by Donald W. Brown (Brown, 2000) with increasing concerns of releasing carbon dioxide into the atmosphere. The use of carbon dioxide as the heat transmission fluid in an EGS would combine recovery of geothermal energy and geological storage of carbon dioxide.

The advantages of using carbon dioxide in an EGS also extend to its properties, including larger expansivity and lower viscosity, and it being a poor solvent for rock minerals. The larger expansivity compared to water is especially attractive because it would increase buoyancy forces and reduce the parasitic power consumption of the fluid circulation system (Wan, 2011).

1.7.3 Solar trough Power Plants

There is a continuous effort to optimize the efficiency of concentrating solar trough power plants. Traditionally, these large parabolic concentrating solar power plants have relied on steam Rankine cycle (steam or oil) since their output temperatures are not hot enough for gas Brayton Cycle (generally <400 ^{o}C). However, considering the recent material improvements in low-emissivity receiver coating and advancements in heat transfer fluid thermal limits; use of SC CO_2 Brayton cycle or a combined Rankine cycle is a real possibility (Chapman and Arias, 2009).

1.8 Use of Carbon Dioxide as a Modelling Fluid

Performing experiments in SC water can be extremely expensive due to the high temperature and pressures involved. On the other hand, CO_2 reaches its supercritical temperatures at much lower conditions (see Table 1-4). Thus fluid such as CO_2 is proposed as a modelling fluid to investigate the properties of SC Water and other fluids due to relative safety and lower financial costs. Non-dimensional parameters applied in correlating data are generally applicable to various fluid types.

Furthermore, SC Fluids exhibit very similar thermo-physical properties trends within similar operational transients (refer to Section 2.7 for further discussions).

1.9 Objectives of Thesis

From the discussions in the sections above, it is clear that there is a need to develop advanced reactor concepts that will make use of supercritical fluids in order to achieve high thermal cycle efficiencies. SC Water and SC CO_2 are expected to play a pivotal role in next generation power generation systems due to their attractive thermophysical properties as heat transfer coolants. It should be noted that all Generation- IV NPP can be connected to SC "Steam" Rankin cycle. There are other applications of SC Pressure technology in Gen-IV such as 1) SC Pressure HXs for indirect cycles; 2) SCW heaters; 3) SCW – Superheated steam HX for hydrogen co-generation; 4) SCW fuel channels in SCWRs and 5) SC CO_2 Brayton cycle for SFRs and MSRs.

In order to develop the above mentioned applications, it is very important to understand the thermodynamic behaviour of the fluids and to accurately predict the heat transfer coefficients for the given flow conditions.

The primary objective of the thesis is to study and develop empirical 1-D heat transfer correlations for SC Water and SC CO_2 flowing in bare tubes that can be used in basic heat transfer calculations. The scope of the thesis is limited to the following activities:

- Study Thermodynamic behaviour and properties of SCFs and investigate its use in future technological applications.
- Investigate the phenomenon of Deteriorated Heat Transfer (DHT) and develop prediction models for the onset of deterioration.

- Investigate the use of Carbon Dioxide as a Modelling fluid to study the behaviour of Supercritical Water and compare the two.
- Analyse Existing Heat Transfer Correlations and check their applicability on Supercritical data.
- Consolidate Test Data from SC Experimental Facilities and develop New 1-D empirical HTC correlations for SC Water and SC CO_2 using the compiled Datasets.
- Perform Error Analysis on the proposed HTC correlations and compare them with independent datasets.
- Analyze the applications and limitations of the 1-D HTC Correlations as it applies towards the advancement of SCWR concepts.

CHAPTER 2 BACKGROUND AND LITERATURE REVIEW

2.1 General Definitions Related to Fluids at Critical and Supercritical Pressures

Prior to discussing heat-transfer calculations, it is necessary to define special terms and expressions, which are listed below (Pioro and Duffey, 2007).

Compressed fluid is a fluid at a pressure above the critical pressure, but at a temperature below the critical temperature.

Critical point (also called a *critical state*) is a point in which the distinction between the liquid and gas (or vapour) phases disappears, i.e., both phases have the same temperature, pressure and volume or density. The *critical point* is characterized by the phase-state parameters T_{cr}, P_{cr} and V_{cr} (or ρ_{cr}), which have unique values for each pure substance.

Deteriorated Heat Transfer (DHT) is characterized by lower values of the wall heat transfer coefficient compared to those at the normal heat transfer; and hence has higher values of wall temperature within some part of a test section or within the entire test section.

Improved Heat Transfer (IHT) is characterized by higher values of the wall heat transfer coefficient compared to those at the normal heat transfer; and hence lower values of wall temperature within some part of a test section or within the entire test section. In our opinion, the improved heat-transfer regime or mode includes peaks or "humps" in the heat transfer coefficient near the critical or pseudocritical points.

Near-critical point is actually a narrow region around the critical point, where all the thermophysical properties of a pure fluid exhibit rapid variations.

Normal Heat Transfer (NHT) can be characterized in general with wall heat transfer coefficients similar to those of subcritical convective heat transfer far from the critical or pseudocritical regions, when are calculated according to the conventional single-phase Dittus-Boelter-type correlations: $\mathbf{Nu} = 0.0243\ \mathbf{Re}^{0.8}\ \mathbf{Pr}^{0.4}$

Pseudo-boiling is a physical phenomenon similar to subcritical pressure nucleate boiling, which may appear at supercritical pressures. Due to heating of supercritical fluid with a bulk-fluid temperature below the pseudocritical temperature (high-density fluid, i.e., "liquid"), some layers

near a heating surface may attain temperatures above the pseudocritical temperature (low-density fluid, i.e., "gas"). This low-density "gas" leaves the heating surface in the form of variable density (bubble) volumes. During the pseudo-boiling, the wall heat transfer coefficient usually increases (improved heat-transfer regime).

Pseudocritical line is a line, which consists of pseudocritical points (see Figure 2-1).

Pseudocritical point (characterized with P_{pc} and T_{pc}) is a point at a pressure above the critical pressure and at a temperature ($T_{pc}>T_{cr}$) corresponding to the maximum value of the specific heat at this particular pressure.

Pseudo-film boiling is a physical phenomenon similar to subcritical-pressure film boiling, which may appear at supercritical pressures. At pseudo-film boiling, a low-density fluid (a fluid at temperatures above the pseudocritical temperature, i.e., "gas") prevents a high-density fluid (a fluid at temperatures below the pseudocritical temperature, i.e., "liquid") from contacting ("rewetting") a heated surface. Pseudo-film boiling leads to the deteriorated heat-transfer regime.

Supercritical fluid is a fluid at pressures and temperatures that are higher than the critical pressure and critical temperature.

Supercritical "steam" is actually supercritical water, because at supercritical pressures fluid is considered as a single-phase substance. However, this term is widely (and incorrectly) used in the literature in relation to supercritical "steam" generators and turbines.

Superheated steam is a steam at pressures below the critical pressure, but at temperatures above the critical temperature.

In order to illustrate these terms and expressions a thermodynamic diagram for water (P_{cr} = 22.064 MPa and T_{cr} = 373.95°C) and thermodynamic diagram for Carbon-dioxide (P_{cr} = 7.38 MPa and T_{cr} = 31.0°C) is shown in Figure 2-1

NHT, DHT, and IHT regimes are also shown in Figure 2-2. Data in Figure 2-2 is obtained from Kirillov et al. for water (inside diameter 10 mm and heated length 4 m).

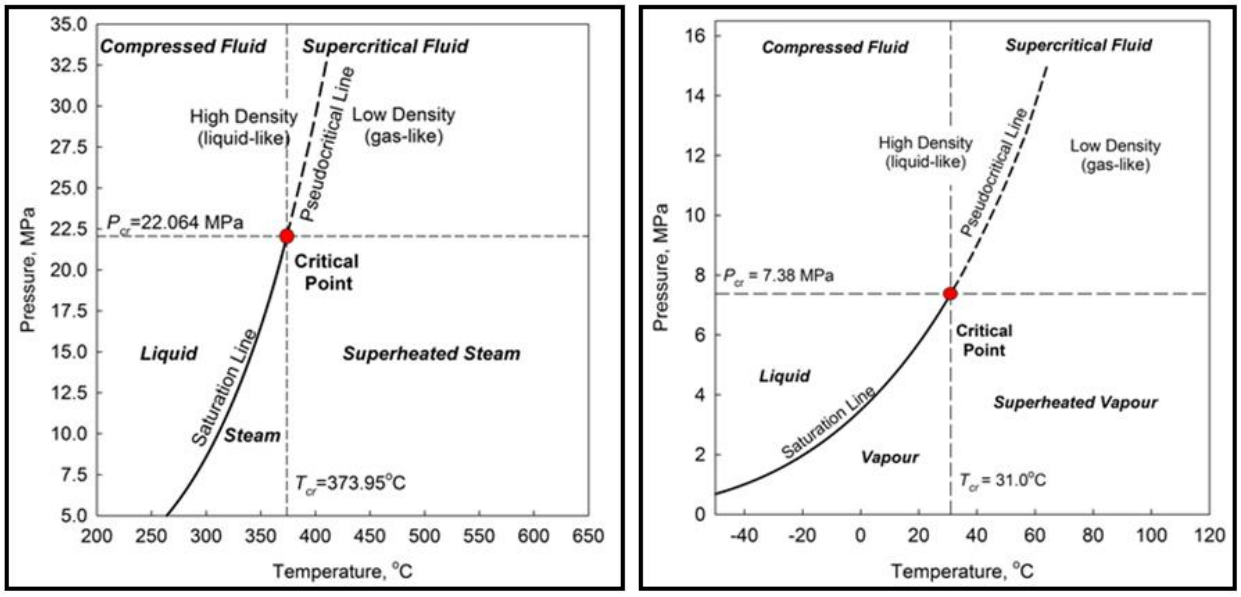

(a) (b)

Figure 2-1: Pressure-Temperature diagram for (a) Water and (b) Carbon Dioxide (NIST, 2007)

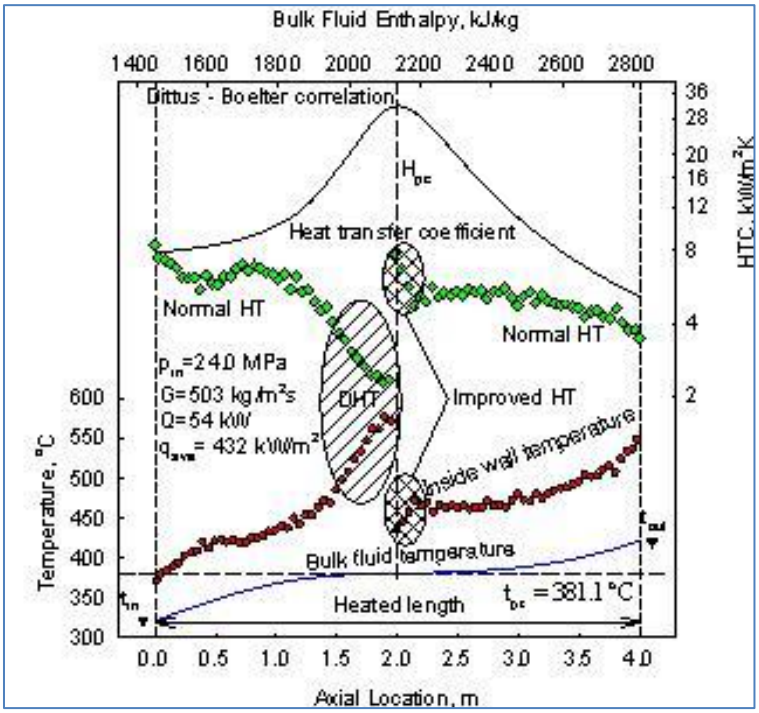

Figure 2-2: Temperature and heat transfer coefficient profiles along heated length of vertical circular tube (Gupta et al., 2011)

2.2 Basics Considerations in Supercritical Heat Transfer

An important aspect in the PT-SCWR reactor concept is calculations of the HTC in fuel bundles and heat exchangers in case of the indirect cycle and for the co-generation of hydrogen. Calculation of HTC is also a critical step in any calculation involving heat transfer analysis of a system. However, the task of calculating HTC at supercritical conditions can get very complicated, because heat transfer at those conditions is influenced by significant changes in thermophysical properties of fluid. It is also highly dependent on the flow geometry and operating parameters such as heat flux, mass flux, Pressure, inlet enthalpy etc.

Supercritical fluids have unique properties. Beyond the critical point (22.1 MPa and 374.1°C for water and 7.38 MPa and 31.0°C for carbon dioxide), the fluid resembles a dense gas. The transition from single-phase liquid to single-phase gas does not involve a distinct phase change under these conditions. Phenomena such as dryout (or critical heat flux) are therefore not relevant (Pioro and Duffey, 2003). The most significant properties variations occur within critical and pseudocritical ranges as shown in Figure 2-9 for H_2O and Figure 2-14 for CO_2.

In addition to the rapid variation of properties in pseudocritical ranges, three major heat-transfer regimes can be noticed at critical and supercritical operating parameters (also see Section 2.3 for more explanation on Deteriorated Heat Transfer regime).

1) Normal Heat Transfer Regime (NHT)

2) Improved Heat Transfer Regime (IHT)

3) Deteriorated Heat Transfer Regime (DHT)

It is important to consider the effects of these distinct regimes in SC heat transfer applications. Also, two special phenomena may appear along the heated surface: 1) pseudo-boiling; and 2) pseudo-film boiling.

These heat-transfer regimes and special phenomena appear to be due to the significant variations of thermophysical properties near the critical and pseudocritical points as previously discussed. The following factors have a considerable impact on heat transfer behaviours at critical and supercritical pressures:

a) Wall and bulk-fluid temperatures are below pseudocritical temperature within a part of or for the entire heated channel

b) Wall temperature is above and bulk-fluid temperature is below pseudocritical temperature within a part of or for the entire heated channel (which may lead to DHT regimes)

c) Wall temperature and bulk-fluid temperature are above pseudocritical temperature within a part of or for the entire heated channel

d) High heat fluxes in comparison to the mass flux (ratio of the two is a critical factor for developing DHT regimes)

e) Presence of entrance region and inlet enthalpy's of the fluids

f) Upward, downward and horizontal flows (orientation of flow)

g) Effect of gravitational forces at lower mass fluxes; etc.

All these above mentioned conditions can affect supercritical heat transfer and further complicate the HT analysis at those conditions.

2.3 Deteriorated Heat Transfer

The phenomenon of DHT at high heat fluxes when transferring heat to a fluid at supercritical pressure has been observed with several fluids by various investigators and the most detailed work on water was reported by Shitman (1963). DHT is the phenomenon resulting in a sudden reduction of the heat transfer coefficient, which consequently results in locally higher values of wall temperatures (see Figure 2-3).

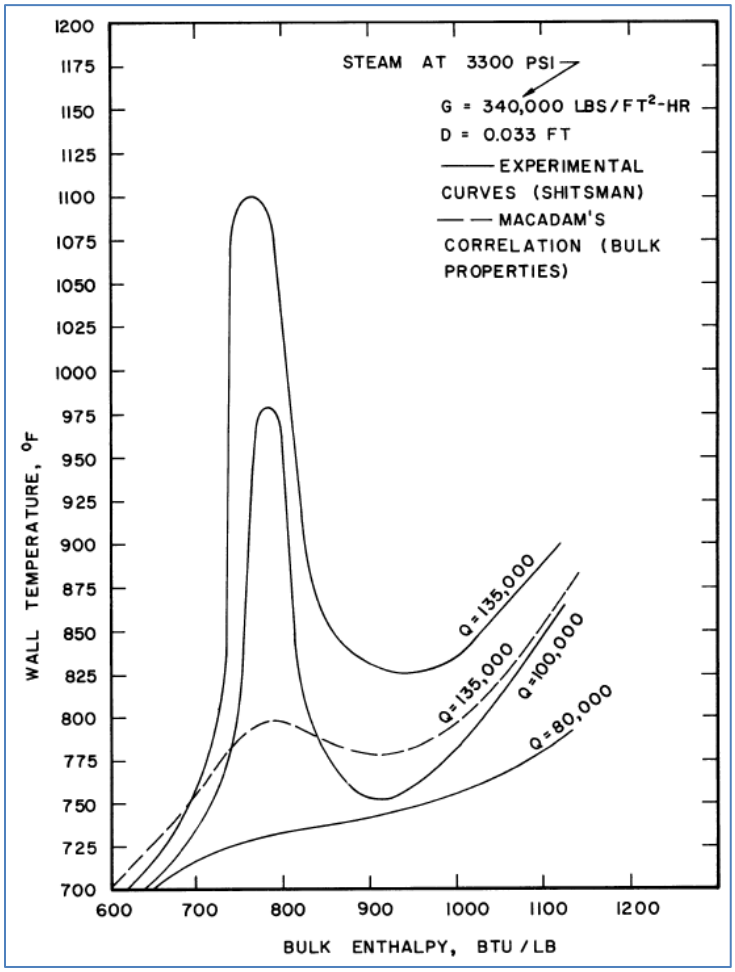

Figure 2-3: DHT Region at High Heat Fluxes (Shitman, 1963)

Figure 2-3 shows a DHT region in water based on the data from Shitman (1963). The dotted line in Figure 2-3 is calculated using Dittus-Boelter type correlation: $\mathbf{Nu} = 0.0243\ \mathbf{Re}^{0.8}\ \mathbf{Pr}^{0.4}$ (McAdams, 1942). Huge peaks in the wall temperature can be noted at high heat fluxes (Q) and the peak heights are proportional to the heat flux (Q). The reason for the nonlinear behavior of the heat-transfer coefficients with the heat flux is the strong variation of the properties of the fluid on the temperature in the vicinity of the critical temperature (see Figure 2-9 and Figure 2-14)

Based on various experimental studies, it is determined that heat flux, mass flux, and the flow geometry are the main parameters that play a major factor in forming the DHT regions.

Typically DHT regimes are developed in conditions of high heat fluxes and low mass fluxes[15] and it is believed to be caused by the local changes of the physical properties of water near the heated wall (Cheng et al., 2002). The conditions under which the deterioration was observed to occur were (Shiralkar and Griffith, 1968):

1. The wall temperature must be above psudocritical temperature and the bulk temperature must be below the psuedocritical temperature (i.e. $T_b < T_{pc} < T_w$).

2. The heat flux must be above a certain value, dependent on the flow rate and pressure.

Shiralkar and Griffith (1968) postulated a simple physical model to explain the deterioration phenomenon, based on the evidence of the computed and experimental results. They established that when $T_b < T_{pc}$ and $T_w > T_{pc}$, the bulk velocity is essentially that of a high density fluid whereas the fluid near the wall is of low density. This condition combined with high heat flux leads to a large temperature difference between T_b and T_w and also causing the shear stress to drop by a substantial amount. The drop in shear stress is largely due to the drop in density and viscosity near the wall without an appreciable increase in the core velocity. The deterioration in heat transfer corresponds to this drop in shear stress. At low heat fluxes, the deterioration is less profound or unable to develop due to the nearness of the T_b and T_w values.

The nature and amount of DHT formation is dependent on a number of flow factors such as:

1. Ratio of Heat Flux and Mass Flux: Typically the higher the ratio of heat flux to the mass flux, the worse is the deterioration and the earlier it occurs.

2. Inlet Enthalpy: The amount of deterioration is strongly influenced by the inlet enthalpy and its worse when the inlet enthalpy is low.

3. Entrance Regions: It has been observed that deterioration is substantially reduced with well mixed fluids

4. Flow Geometry: A tube or channel with turbulence enhancing designs will reduce the amount of deterioration. Swirls, vibrations or flow instabilities tend to disrupt the low

[15] Many authors attribute the ratio of heat to mass fluxes to be major factor for the creation of DHT.

density boundary layer near the wall and, consequently, prevent the formation of DHT regime.

5. Pressure: The deterioration is the worst when the system pressure is close to the critical pressure, where the changes in properties are the most rapid.

6. Orientation of Flow: The DHT regimes are observed in both upwards and downwards flows, however the mechanism associated with each flow type varies. Generally, deterioration has been found to be more profound in upward flows. Further investigation is required to study the impact of flow orientation on DHT regime.

2.3.1 Onset of Deteriorated Heat Transfer

As discussed earlier, DHT regimes are typically developed at high heat flux values and when the condition $T_b < T_{pc} < T_w$ is met. Onset of HT deterioration depends on pressure, mass flux, tube diameter and orientation of the flow channel (Cheng and Schulenberg, 2001). Note that occurrence of DHT regions are much less drastic than onset of DNB (departure from nuclear boiling) and often show slow and smooth behaviors. Therefore, it is very difficult to define a sharp onset point where the heat transfer deterioration starts to occur. Nevertheless, extreme caution must be taken while designing systems using SCFs to ensure that flow parameters do not correspond to the conditions suited to the formation of DHT.

In previous studies such as Shiralkar and Griffith (1968), numerical models using simple eddy diffusivity approach have been proposed to explain development of DHT regions. While the numerical results show good agreement for qualitative trends for test data, quantitatively they over-predict the heat transfer deterioration beyond the peak. Dotted lines in Figure 2-4 show the results of numerical computation by Shiralkar and Griffith (1968) on Shitman's (1963) data and qualitatively similar wall temperature profiles are obtained. However, numerical analyses used for DHT predictions generally over predict the test data.

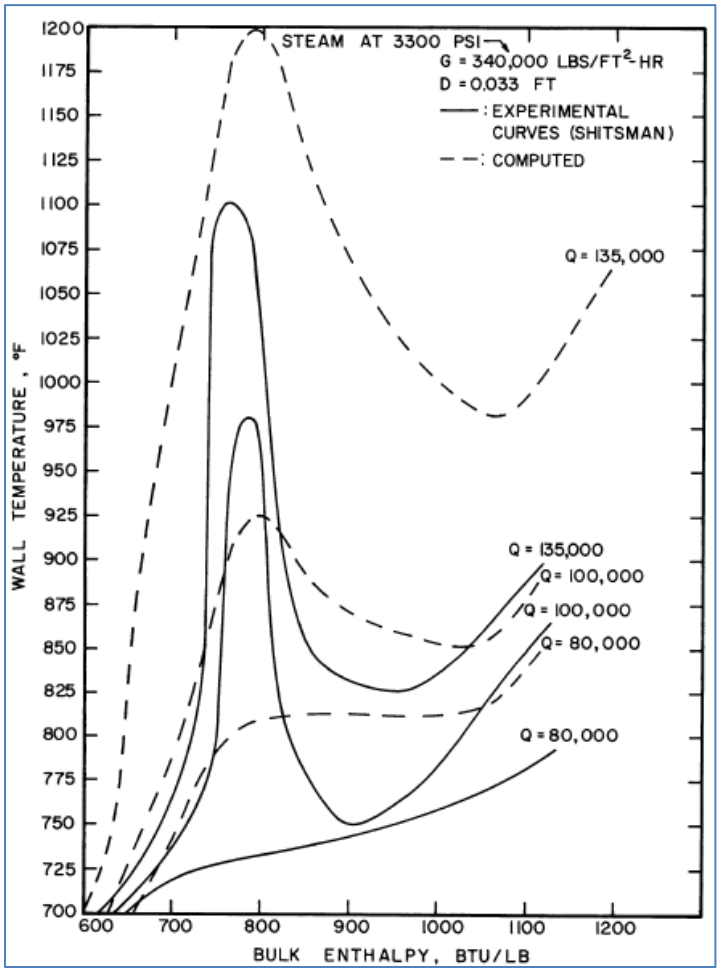

Figure 2-4: Deteriorated Heat Transfer Region and Computed Results using Numerical Analysis (Shiralkar and Griffith, 1968)

Empirical approach is also adapted by various studies and correlations with minimum heat flux (q_{dht}) expressed as a function of mass flux (G) is used for detecting the onset of DHT region. Table 2-1 lists some of the common empirical correlations found in literature.

Table 2-1: Existing correlations for supercritical water.

Correlation	Equation
Yamagata et al. (1972)	$q_{dht}(kW/m^2) = 200\ G^{1.2}$
Styrikovich et al. (1967)	$q_{dht} = 580G$
Pioro et al. (2011)	$q_{dht}(kW/m^2) = -58.97 + 0.745G$

Semi-empirical correlations are also found in literature. Based on analysis of the effect of buoyancy on the shear stress, Jackson et al. (1979) derived the following equation:

Equation 2-1: Jackson et al. (1979) DHT Correlation

$$\frac{q_w}{\rho_B G}\left(\frac{\partial \rho}{\partial h}\right)_{P,b}\left(\frac{\mu_w}{\mu_b}\right)\left(\frac{\rho_w}{\rho_b}\right)^{-0.5}\frac{1}{Re_b^{0.7}} \geq C$$

Where, constant C is determined using test data.

Ogata and Sato (1972), derived the following equation for the onset of DHT in cryogens (He, H_2 and N_2)

Equation 2-2: Ogata and Sato (1972) DHT Correlation in cryogens

$$q_{dht} = 0.034\sqrt{\frac{f}{8}}.\left(\frac{C_P}{\beta}\right)_{pc} G$$

Where, f is the friction factor.

Using similar mechanisms, Petuhkov and Kurganov (1983) derived the following equation:

Equation 2-3: Petuhkov and Kurganov (1983) DHT Correlation in cryogens

$$q \approx 0.187\, f.\left(\frac{C_P}{\beta}\right)_{pc} G$$

An analysis was also conducted based on the general approach presented in Table 2-1 to obtain a new preliminary empirical correlation to predict the onset of DHT region using the AECL SC CO_2 dataset. It must be noted that due to the relatively smooth behaviour of T_w; there is no clear unique definition of the onset of DHT. Thus, the correlation predicting the onset of DHT vary significantly from each study and is subjected to the visual bias[16] of the authors. SC CO_2 data used in this empirical correlation was collected at the MR-1 test facility at Chalk River Lab (CRL), AECL (refer to CHAPTER 5 for details). 41 cases of DHT points were identified from the CRL data (based on visual inspections) and the following correlation is proposed for the minimal heat flux at which deterioration occurs:

[16] The selection of DHT points were done by looking at the trends of plotted data, since there is no well-defined selection criterion and onset of DHT is generally smooth. Thus, there exists a visual bias in identifying DHT points.

Equation 2-4: Proposed q_{dht} correlation in AECL data

$$q_{dht}(kW/m^2) = 66.81 + 0.18G$$

Table 2-2 shows the range of applicability of the new correlation.

Table 2-2: Range of applicability of q_{dht} correlation (Equation 2-4).

***P*, MPa**	***G*, kg/(m^{2}s)**	**q_{dht}, kW/m^2**	**$T_{b,in}$/ $T_{w,in}$,°C**	***D*, mm**
7.57 – 8.85	694 – 2987	180 – 616	22 – 35/ 81 – 159	8.1

Basic empirical and semi-empirical correlations developed to predict the onset of DHT regimes using experimental datasets and curve fitting techniques show good agreement with test data. However, in most cases, ranges of applicability of DHT correlations are not clearly defined. Also, as mentioned; DHT occurs only in the case when condition $T_b < T_{pc} < T_w$ is true. The correlations above do not take this specific limitation into consideration. Furthermore, there is no clear unique definition of the onset of DHT and thus the various correlations found in literature vary quite significantly from each other.

2.4 Thermophysical Properties of Water

The following figures show the variation of important thermophysical properties of water at supercritical operating ranges. Data in these figures were obtained using the NIST REFPROP software (NIST, 2007)

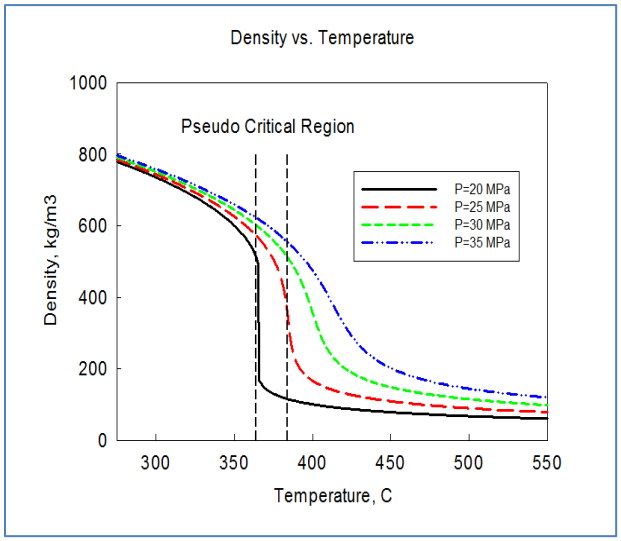

Figure 2-5: Variation of Density vs. Temperature for water

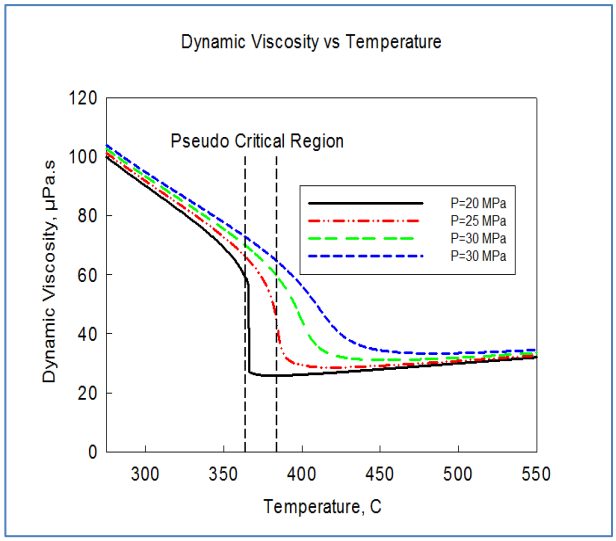

Figure 2-6: Variation of Dynamic Viscosity vs. Temperature for water

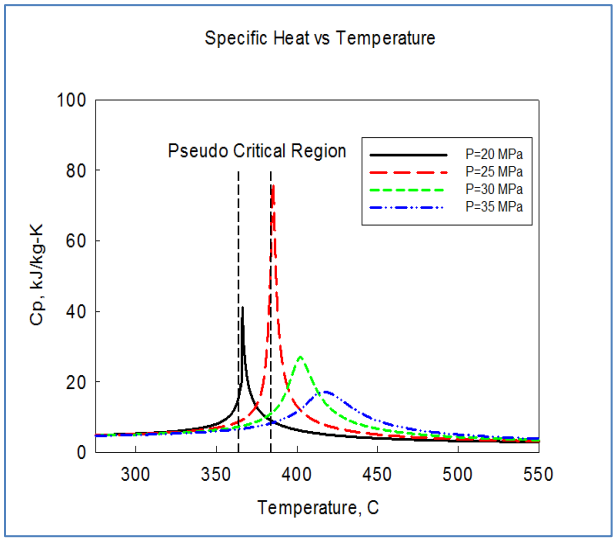

Figure 2-7: Variation of Specific Heat vs. Temperature for water

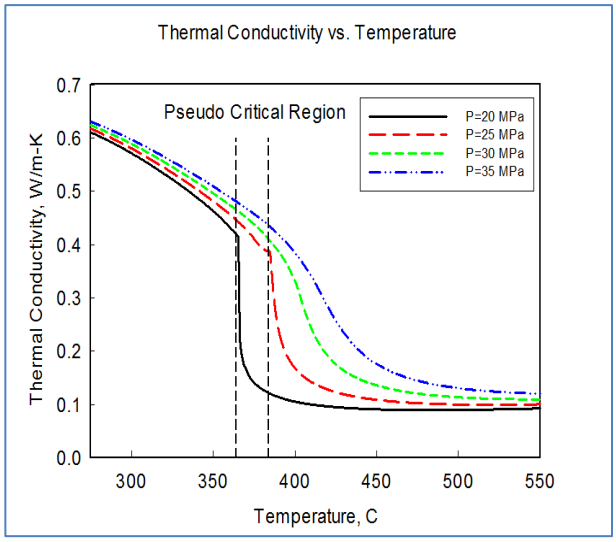

Figure 2-8: Variation of Thermal Conductivity vs. Temperature for water

Figure 2-9 shows the major properties of water at a pressure of 25 MPa within the pseudocritical region. As it can be seen from the graph, density and viscosity sharply drop as they pass through the pseudocritical point. In general, thermal conductivity also experiences a drop. However, it exhibits a small peak at the pseudocritical point, and experiences a less drastic drop. Specific heat has a large peak in the pseudocritical point, but remains fairly constant outside the pseudocritical region.

As discussed earlier, these drastic changes in thermophysical properties further complicate the task of predicting HTC when fluid is transitioning between the pseudocritcal regions.

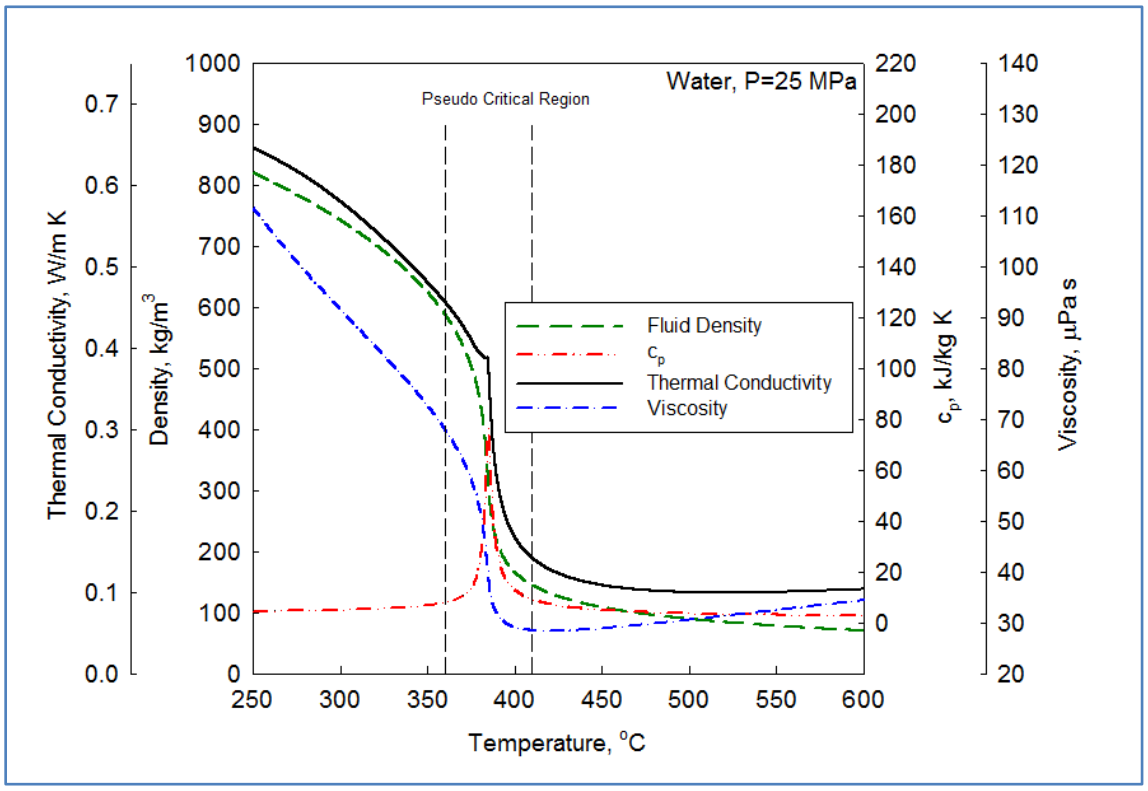

Figure 2-9: Profiles of Density, Thermal Conductivity, Viscosity and specific heat of water with temperature variations at 25 MPa (Gupta et. al, 2012)

2.5 Thermophysical Properties of CO_2

The following figures show the variation of important thermophysical properties of CO_2 at supercritical operating ranges. Data in these figures were obtained using the NIST REFPROP software (NIST, 2007)

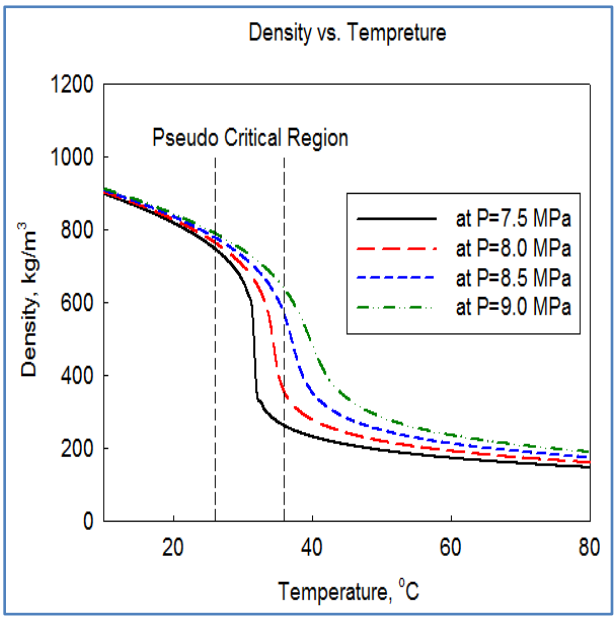

Figure 2-10: Variation of Density vs. Temperature for Carbon Dioxide

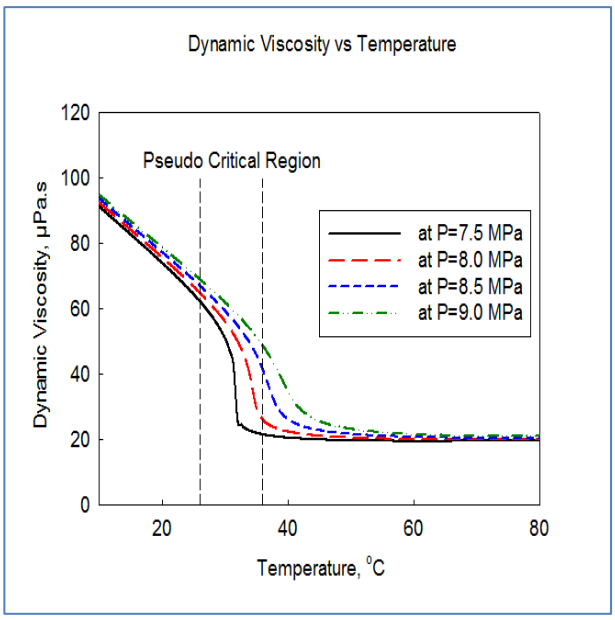

Figure 2-11: Variation of Dynamic Viscosity vs. Temperature for Carbon Dioxide

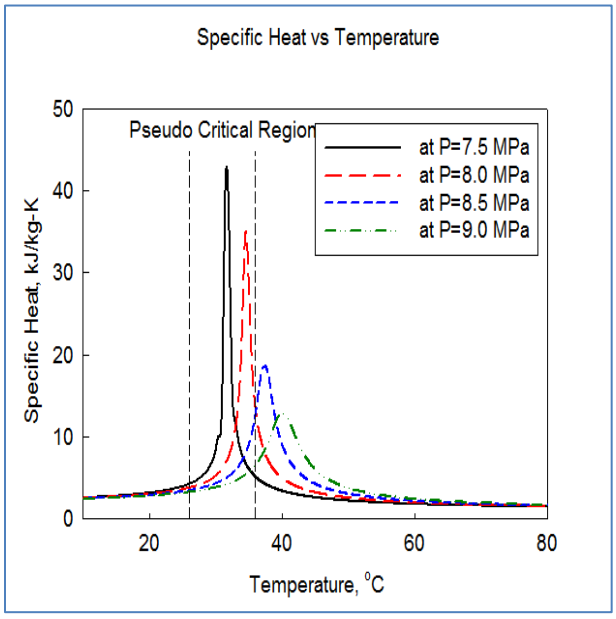

Figure 2-12: Variation of Specific Heat vs. Temperature for Carbon Dioxide

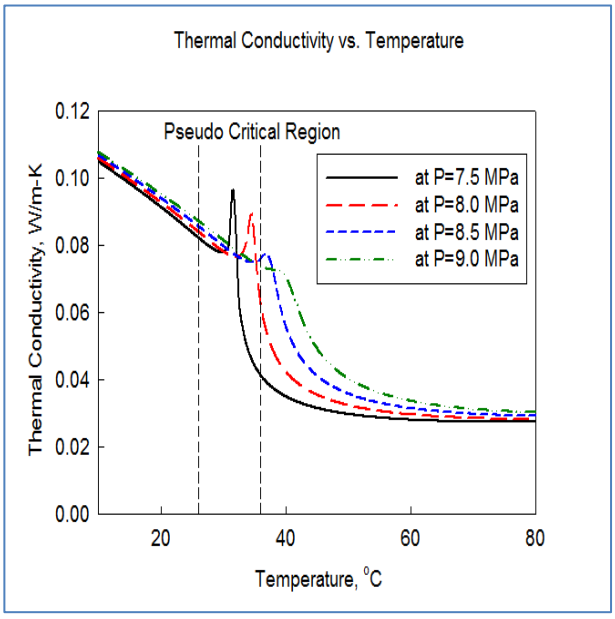

Figure 2-13: Variation of Thermal Conductivity vs. Temperature for Carbon Dioxide

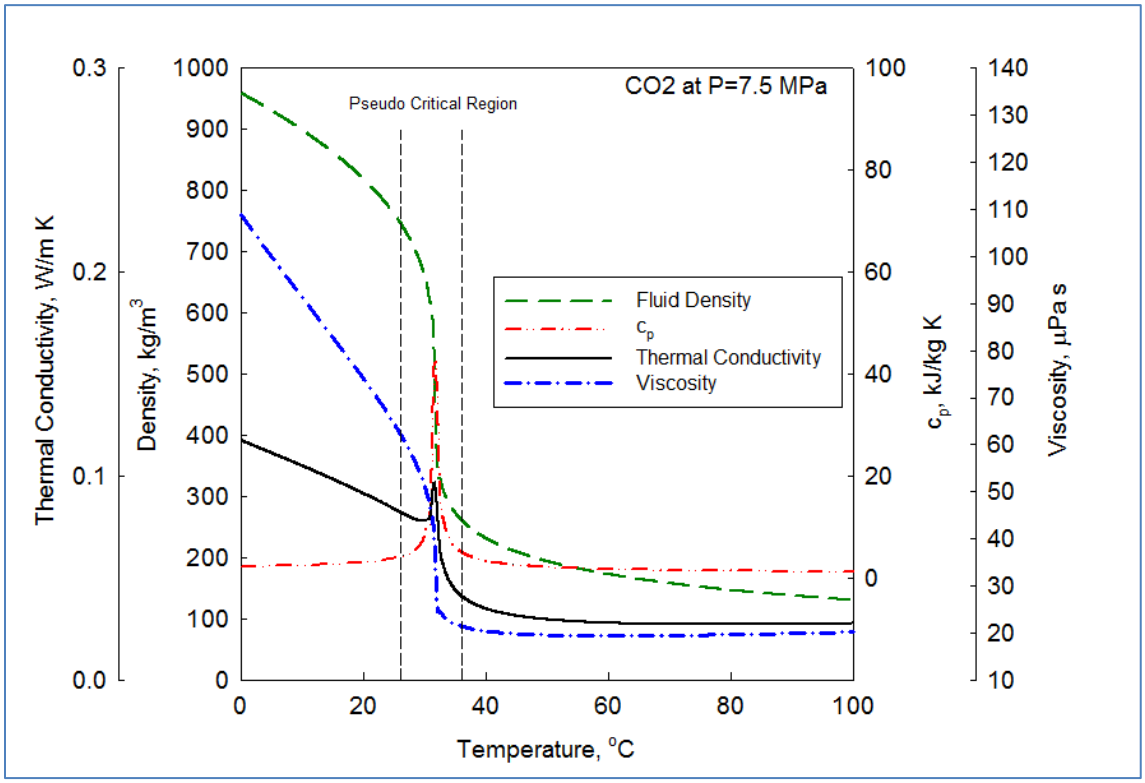

Figure 2-14: Profiles of Density, Thermal Conductivity, Viscosity and specific heat of CO_2 with temperature variations at 7.5 MPa (Gupta et. al, 2013)

2.6 Considerations for Scaling Parameters

As seen in sections 2.4 and 2.5, both SC water and CO_2 demonstrate similar trends in the variation of thermophysical properties during the transition phase. Due to these similarities in the trends, CO_2 is proposed to be used as a modelling fluid to investigate mechanics associated with supercritical water and possibly other fluids as well. Preliminary parameters used for scaling water operating conditions to carbon dioxide-equivalent values are listed in Table 2-3. These scaling parameters were deduced from those proposed by Jackson and Hall in 1979 and Gorban' et al. in 1990. Direct applications of surrogate fluid heat-transfer data in SCWR design and safety analyses require the development of fluid-to-fluid modelling parameters to relate the surrogate-fluid heat-transfer coefficients to water-equivalent values.

Table 2-3: Basic Scaling parameters for CO_2-Water modelling.

Pressure (*P*)	$\left(\frac{P}{P_{cr}}\right)_{CO_2} = \left(\frac{P}{P_{cr}}\right)_{H_2O}$
Bulk fluid temperature *(T)*	$\left(\frac{T_b}{T_{cr}}\right)_{CO_2} = \left(\frac{T_b}{T_{cr}}\right)_{H_2O}$
Mass Flux (*G*)	$\left(\frac{GD}{\mu_b}\right)_{CO_2} = \left(\frac{GD}{\mu_b}\right)_{H_2O}$

2.7 Comparison of Thermophysical Properties of different fluids

Using the scaling parameters mentioned in section 2.6, thermophysical properties of water, carbon dioxide and R134a were also plotted with varying temperature ratios (T/T_{cr}) at the respective pressures (*P*=25 MPa for water, *P*=8.4 for CO_2 and *P*=4.6 MPa for R134a).

The results are shown in Figure 2-15 to Figure 2-21. It can be seen that the three fluids demonstrate similar trend, however there are still significant variations of thermodynamic properties in reference to the absolute values.

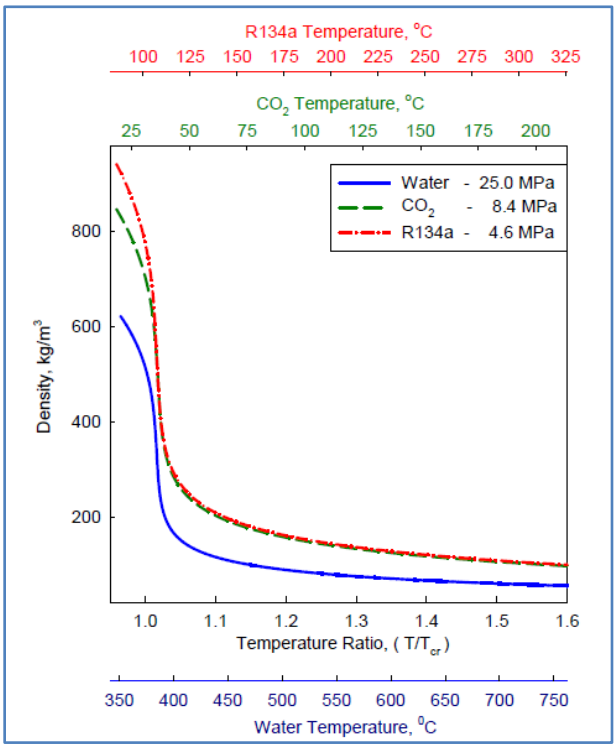

Figure 2-15: Density vs. Temperature Ratio for water, CO_2 and R134a

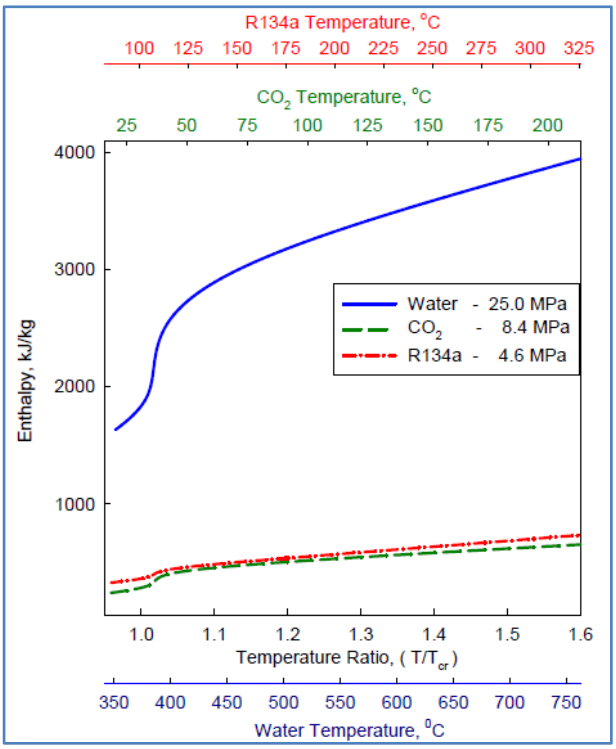

Figure 2-16: Enthalpy vs. Temperature Ratio for water, CO_2 and R134a

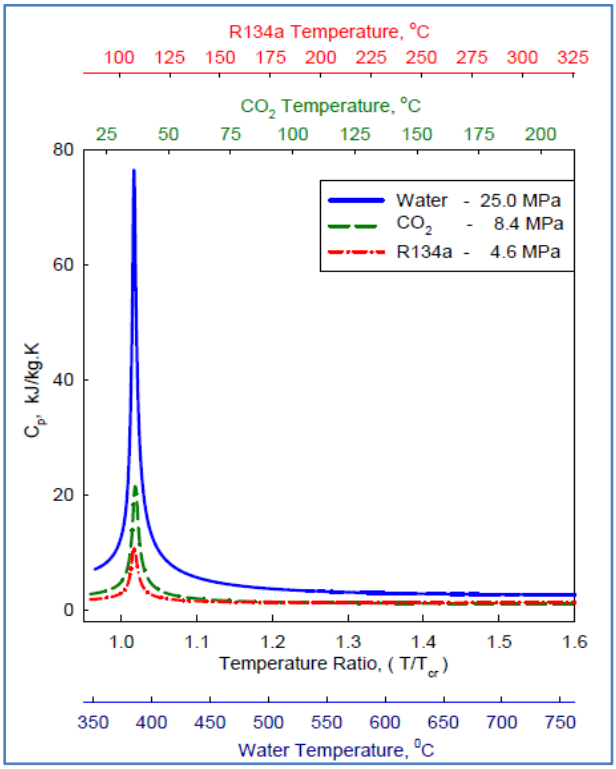

Figure 2-17: Specific Heat vs. Temperature Ratio for water, CO_2 and R134a

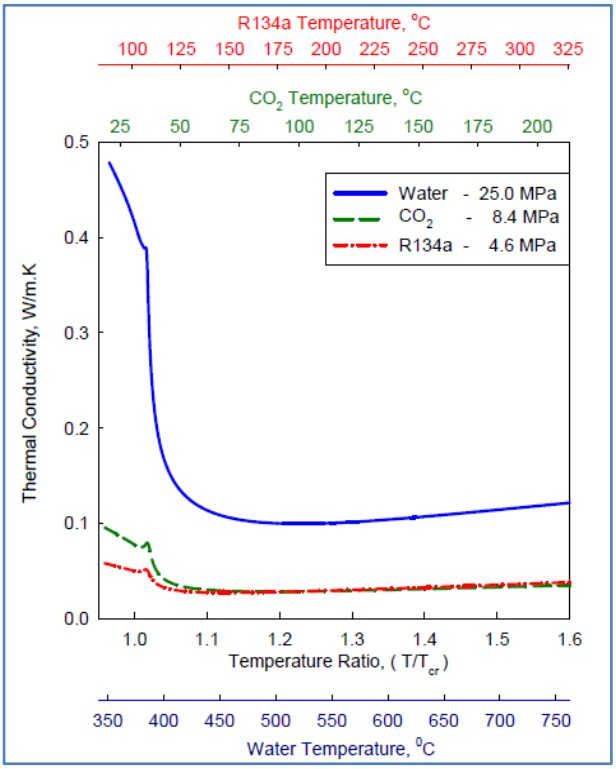

Figure 2-18: Thermal Conductivity vs. Temperature Ratio for water, CO_2 and R134a

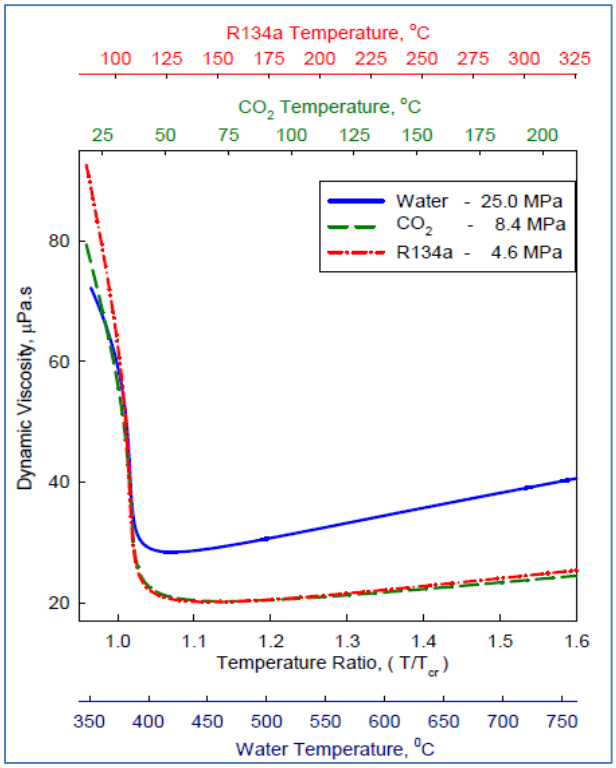

Figure 2-19: Dynamic Viscosity vs. Temperature Ratio for water, CO_2 and R134a

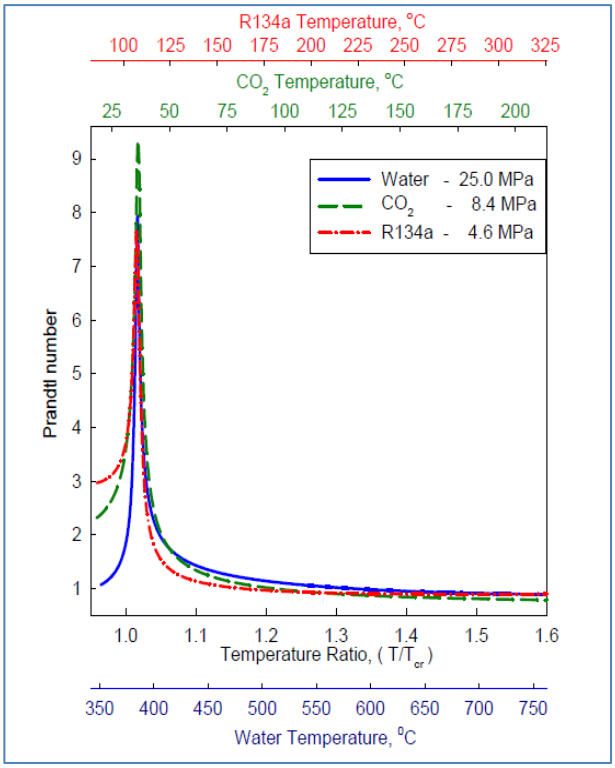

Figure 2-20: Prandtl number vs. Temperature Ratio for water, CO_2 and R134a

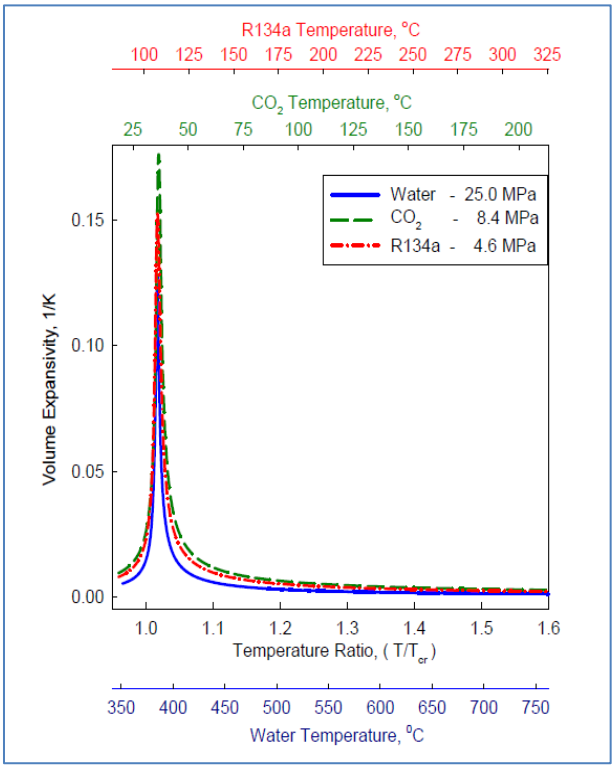

Figure 2-21: Volume Expansivity vs. Temperature Ratio for water, CO_2 and R134a

In an attempt to converge the 3 different fluids properties to a single trend, 2 more approaches were attempted in addition to plotting the absolute values of properties in Figure 2-15-Figure 2-21. The first approach comprised of plotting ratio of property/property$_{critical}$ with varying Temperature Ratios (T/T_{cr}), where property$_{critical}$ is the value at the critical point for the respective fluid (also see Table 2-4). The resulting graphs are shown in Figure 2-22 to Figure 2-28. Note that water has a huge peak in values of specific heat, thermal conductivity, volume expansivity and Prandtl number at the critical point (Table 2-4). Thus, corresponding property/property$_{critical}$ approaches a zero value and the water graph is more a less straight line parallel to the x-axis.

Table 2-4: Values of thermodynamic properties for water, CO_2 and R134a at respective critical points (NIST, 2007).

Fluid	T_{cr} K	P_{cr} MPa	ρ_{cr} kg/m^3	Cp_{cr} KJ/kg-K	H_{cr} KJ/kg	k_{cr} mW/m-K	μ_{cr} µPa-s	Pr_{cr}	β_{cr} 1/K
Water	647.09	22.064	322.10	Sharp Peak*	2084.09	Sharp Peak*	65.21	Sharp Peak*	Sharp Peak*
CO_2	304.1282	7.3768	422.70	952.38	343.70	290.82	29.89	97.88	8.23
R134a	374.21	4.0592	545.63	592.47	385.73	153.22	37.42	144.70	9.65

* NIST gives an extremely sharp peaks for water at supercritical temperature and pressure

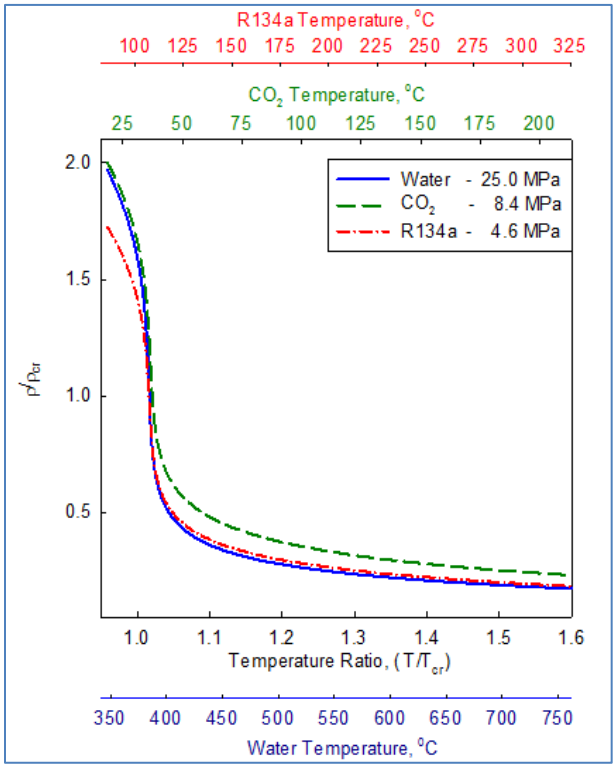

Figure 2-22: Density/Density$_{Critical}$ vs. Temperature Ratio for water, CO_2 and R134a

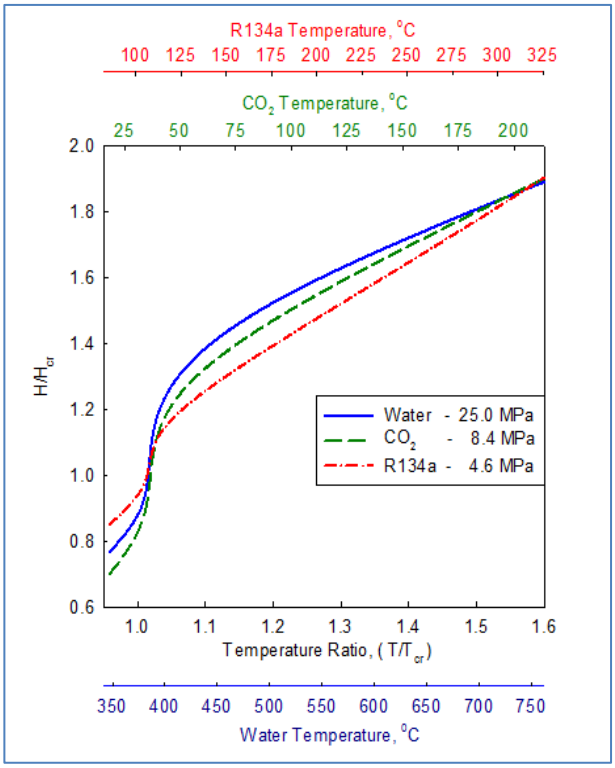

Figure 2-23: Enthalpy/Enthalpy$_{Critical}$ vs. Temperature Ratio for water, CO_2 and R134a

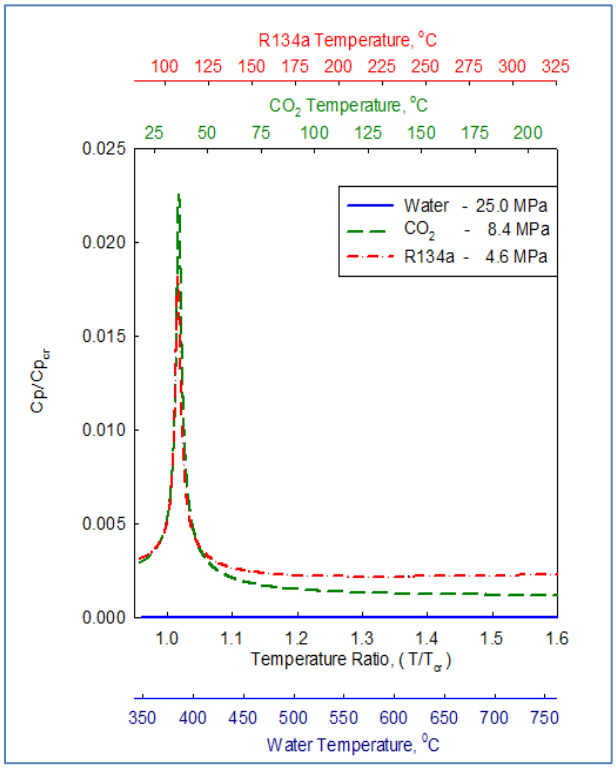

Figure 2-24: Cp/Cp_{cr} vs. Temperature Ratio for water, CO_2 and R134a

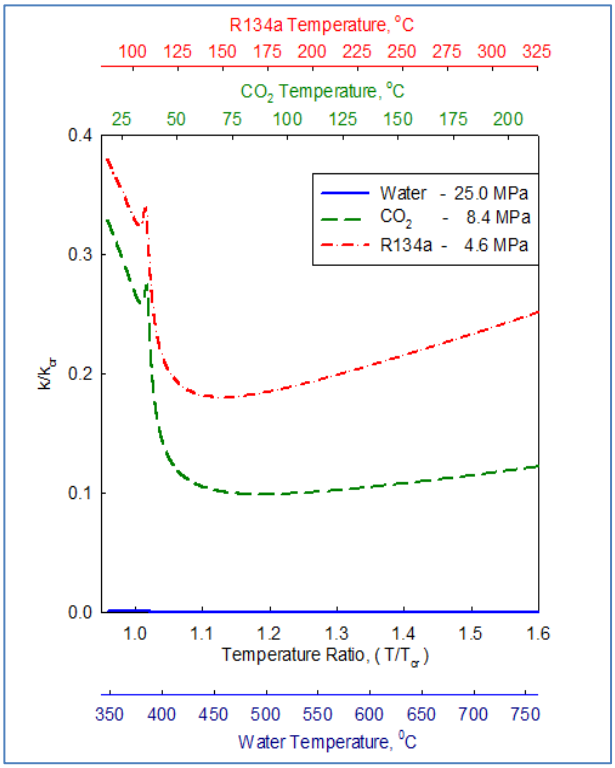

Figure 2-25: k/k_{cr} vs. Temperature Ratio for water, CO_2 and R134a

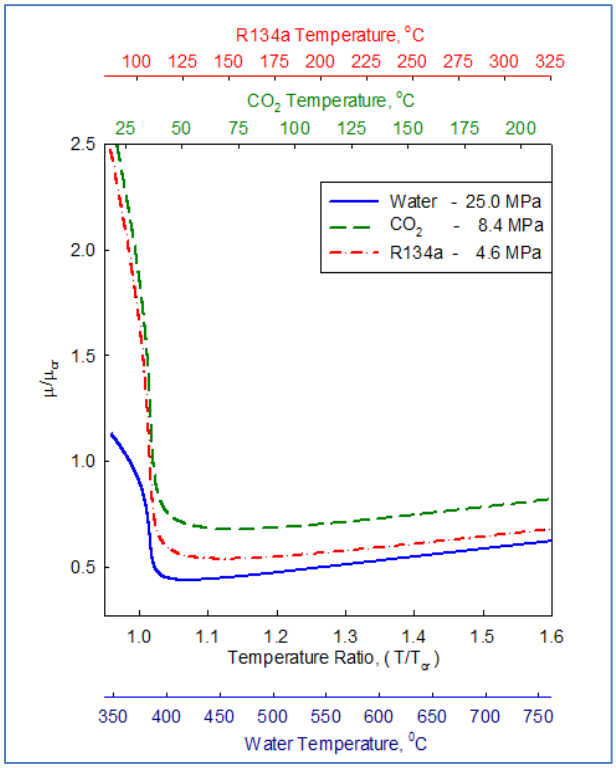

Figure 2-26: Dynamic-Viscosity/Dynamic-Viscosity$_{critical}$ vs. Temperature Ratio for water, CO_2 and R134a

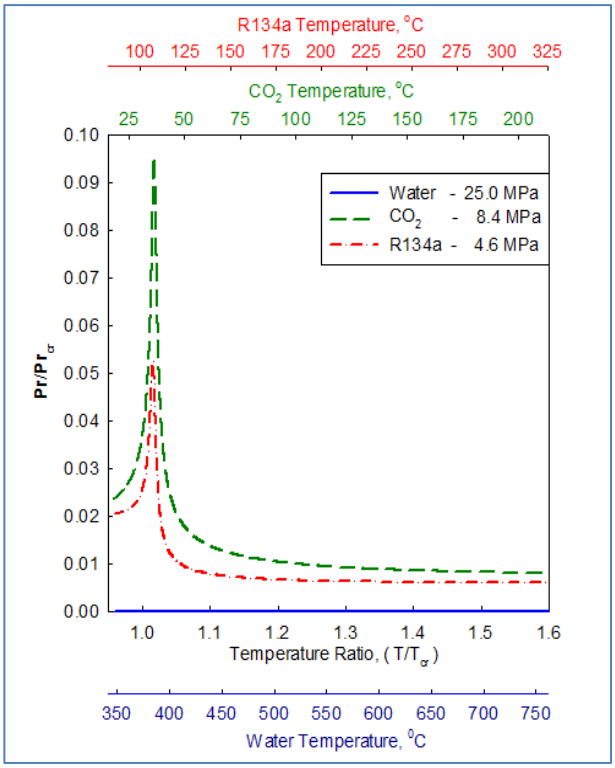

Figure 2-27: Pr/Pr$_{cr}$ vs. Temperature Ratio for water, CO_2 and R134a

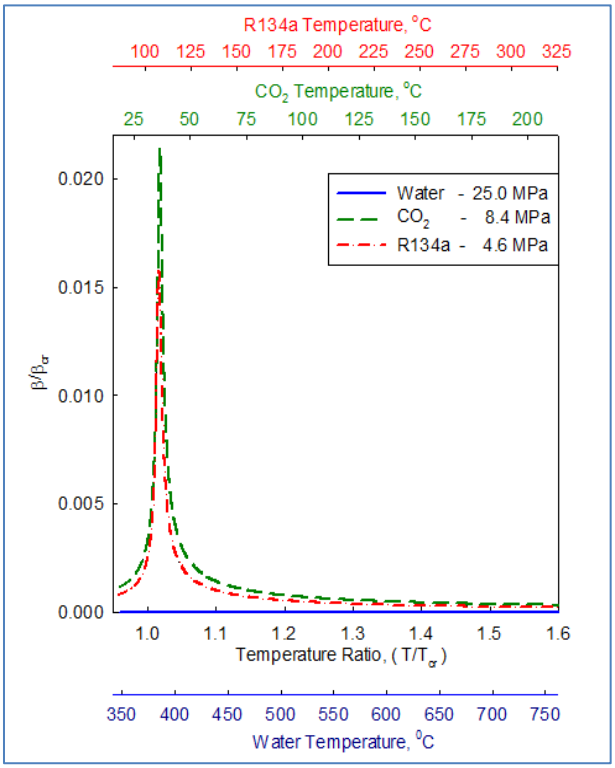

Figure 2-28: Volume-Expansivity/Volume-Expansivity$_{cr}$ vs. Temperature Ratio for water, CO_2 and R134a

Second approach comprised of plotting ratio of property/property$_{pseudo\text{-}critical}$ with varying Temperature Ratios (T/T_{cr}), where property$_{pseudo\text{-}critical}$ is the value at the pseudocritical point (defined by a peak in c_p) for the respective fluid. The resulting graphs are shown in Figure 2-29 to Figure 2-35.

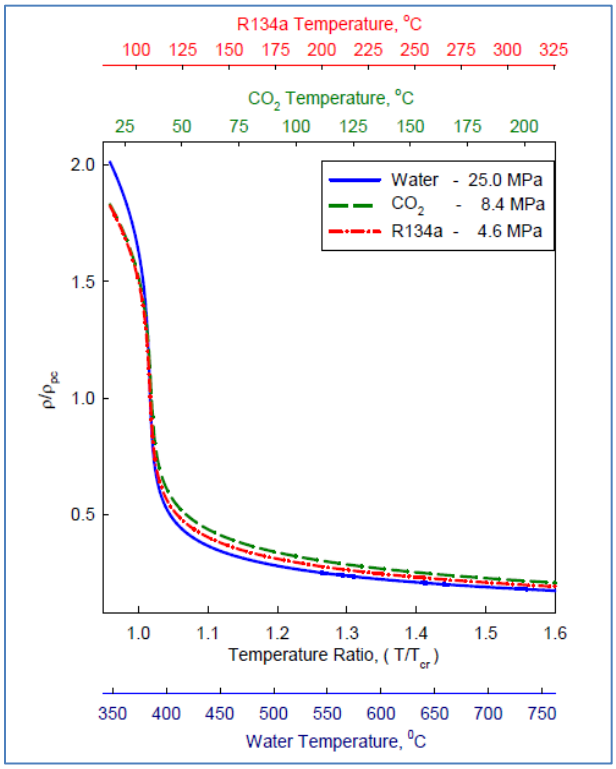

Figure 2-29: Density/Density$_{pc}$ vs. Temperature Ratio for water, CO_2 and R134a

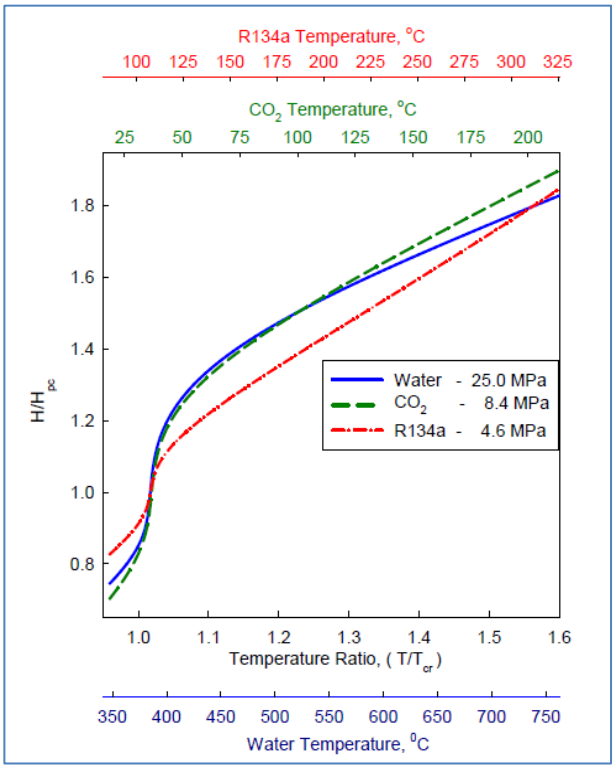

Figure 2-30: Enthalpy/Ehthalpy$_{pc}$ vs. Temperature Ratio for water, CO_2 and R134a

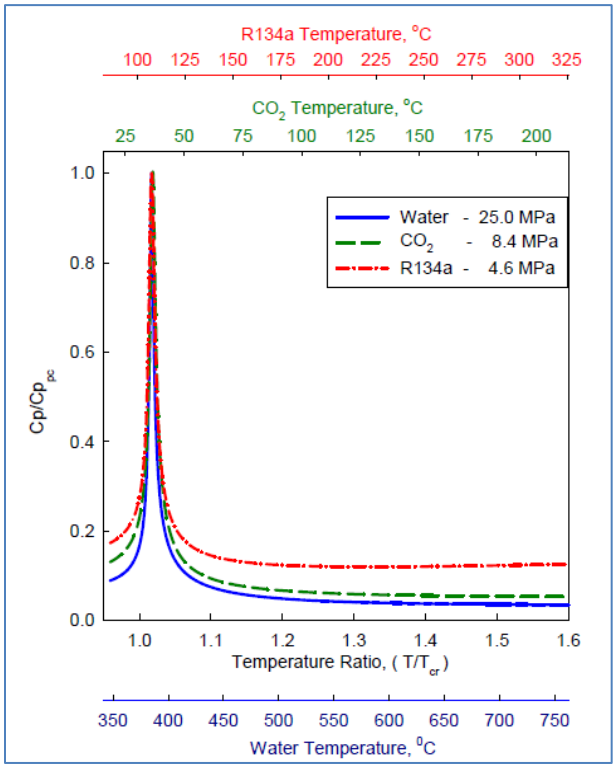

Figure 2-31: Cp/Cp_{pc} vs. Temperature Ratio for water, CO_2 and R134a

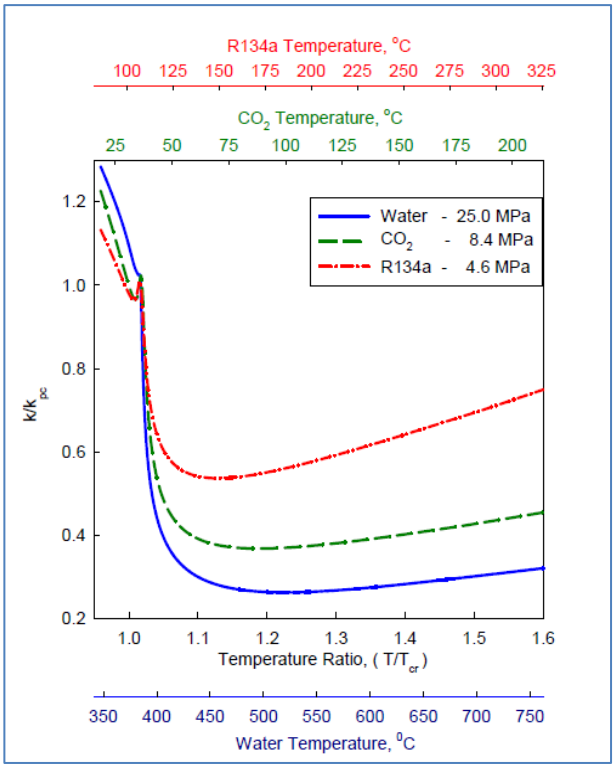

Figure 2-32: k/k_{pc} vs. Temperature Ratio for water, CO_2 and R134a

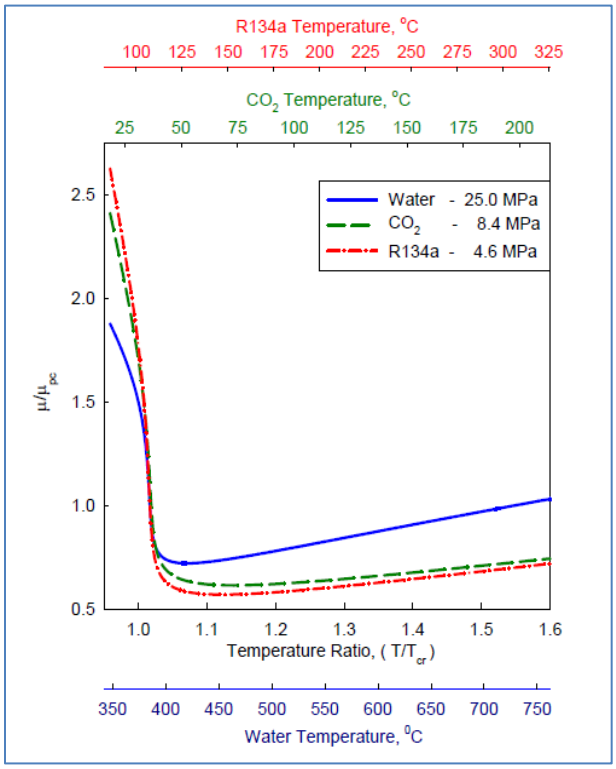

Figure 2-33: Dynamic-Viscosity/Dynamic-Viscosity$_{pc}$ vs. Temperature Ratio for water, CO_2 and R134a

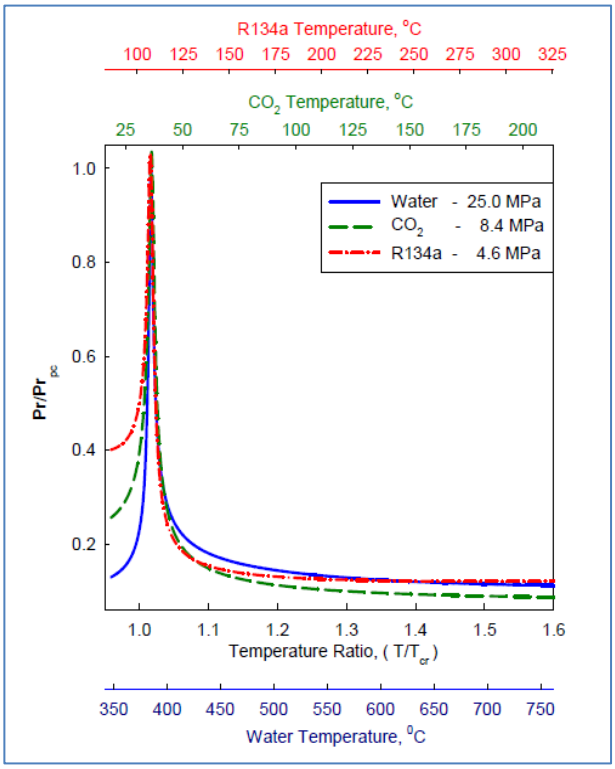

Figure 2-34: Pr/Pr_{pc} vs. Temperature Ratio for water, CO_2 and R134a

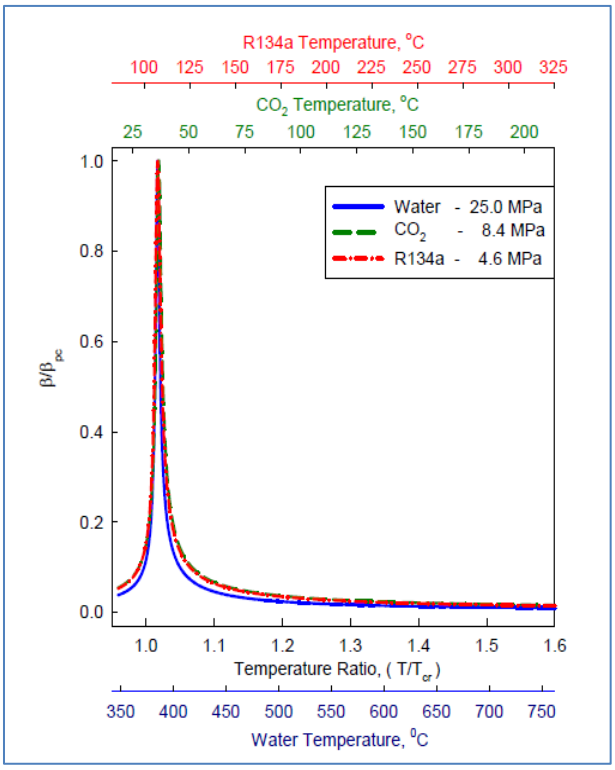

Figure 2-35: Volume-Expansivity/Volume-Expansivity$_{pc}$ vs. Temperature Ratio for water, CO_2 and R134a

In general, an analysis of the graphs in Figure 2-15 to Figure 2-35 shows that property profiles for all 3 fluids are quite similar. However, none of these approaches allowed combining data into a single profile for each property. It seems that the 3rd approach (ratio of a value of property/property$_{pc}$ vs. reduced temperature), i.e., Figure 2-29 to Figure 2-35 allowed to combine some property profiles quite close within some reduced-pressure ranges; for example, volume expansivity (Figure 2-35) within the whole range; density and Prandtl number (Figure 2-29 and Figure 2-34) in the pseudocritical point and beyond (i.e., for a gas-like fluid region).

2.8 Transition of fluids from Sub-Critical regions to Super-Critical regions

In general, crossing the pseudocritical line from left to right (see Figure 2-1) is quite similar as crossing the saturation line from liquid into vapour. The major difference in crossing these two lines is that all changes (even drastic variations) in thermophysical properties at supercritical pressures are gradual and continuous, and take place within a certain temperature range (see Figure 2-9 and Figure 2-14). The transition from single phase liquid to single phase gas does not involve a distinct phase change under these conditions. Phenomena such as dryout (or critical

heat flux) are therefore not relevant (Pioro, 2011). On the contrary, at subcritical pressures we have properties discontinuation on the saturation line: one value for liquid and another for vapour (see Figure 2-36). Therefore, supercritical fluids behave as single-phase substances.

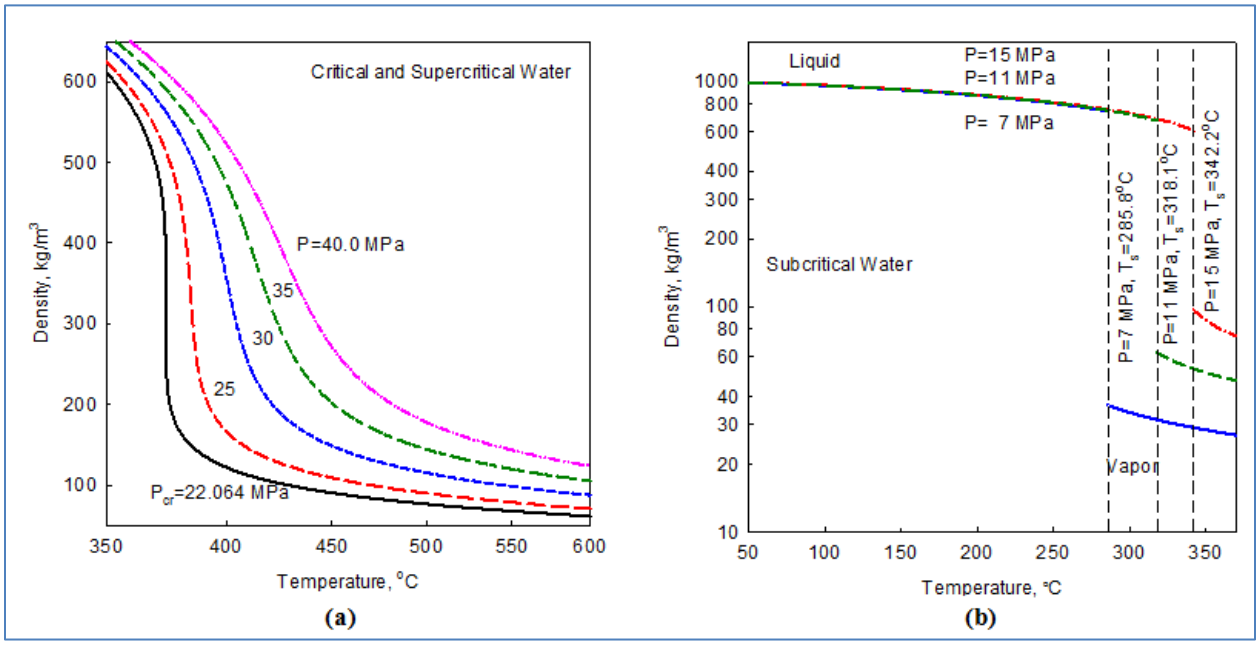

Figure 2-36: Density vs. Temperature: (a) Water at critical and supercritical pressures; (b) Water at subcritical pressures (Pioro et. al., 2011)

At critical and supercritical pressures, a fluid is considered as a single-phase substance in spite of the fact that all thermophysical properties undergo significant changes within the critical and pseudocritical regions (see Figure 2-9 and Figure 2-14). Near the critical point, these changes are dramatic. In the vicinity of pseudocritical points with an increase in pressure these changes become less pronounced.

Also, it can be seen that properties such as density and dynamic viscosity undergo significant drops (near the critical point this drop is almost vertical) within a very narrow temperature range, while the specific enthalpy undergo a sharp increase. The specific heat, thermal conductivity and Prandtl number have peaks near the critical and pseudocritical points. Magnitudes of these peaks decrease very quickly with an increase in pressure. Also, "peaks" transform into "humps" profiles at pressures beyond the critical pressure. At pressures approximately above 300 MPa for water a peak (here it is better to say "a hump") in specific heat almost disappears. Therefore, such term as a pseudocritical point does not exist anymore. The same applies to the

pseudocritical line. It should be noted that peaks in the thermal conductivity and volume expansivity may not correspond to the pseudocritical temperature (Pioro and Duffey, 2007).

2.9 Experimental setup to show transitions of CO_2 through sub-critical to super-critical states

In order to visually see the transition of a fluid through sub-critical to supercritical regions, an experiment was conducted by the Faculty of Science at UOIT (Donald McGillivray). The experiment was performed using CO_2 fluids in a spherical chamber, which was then subjected to a continuous increase in temperature and pressure. A camera was placed to record pictures as CO_2 transitions through various states. The results are shown in Figure 2-37 and Figure 2-38.

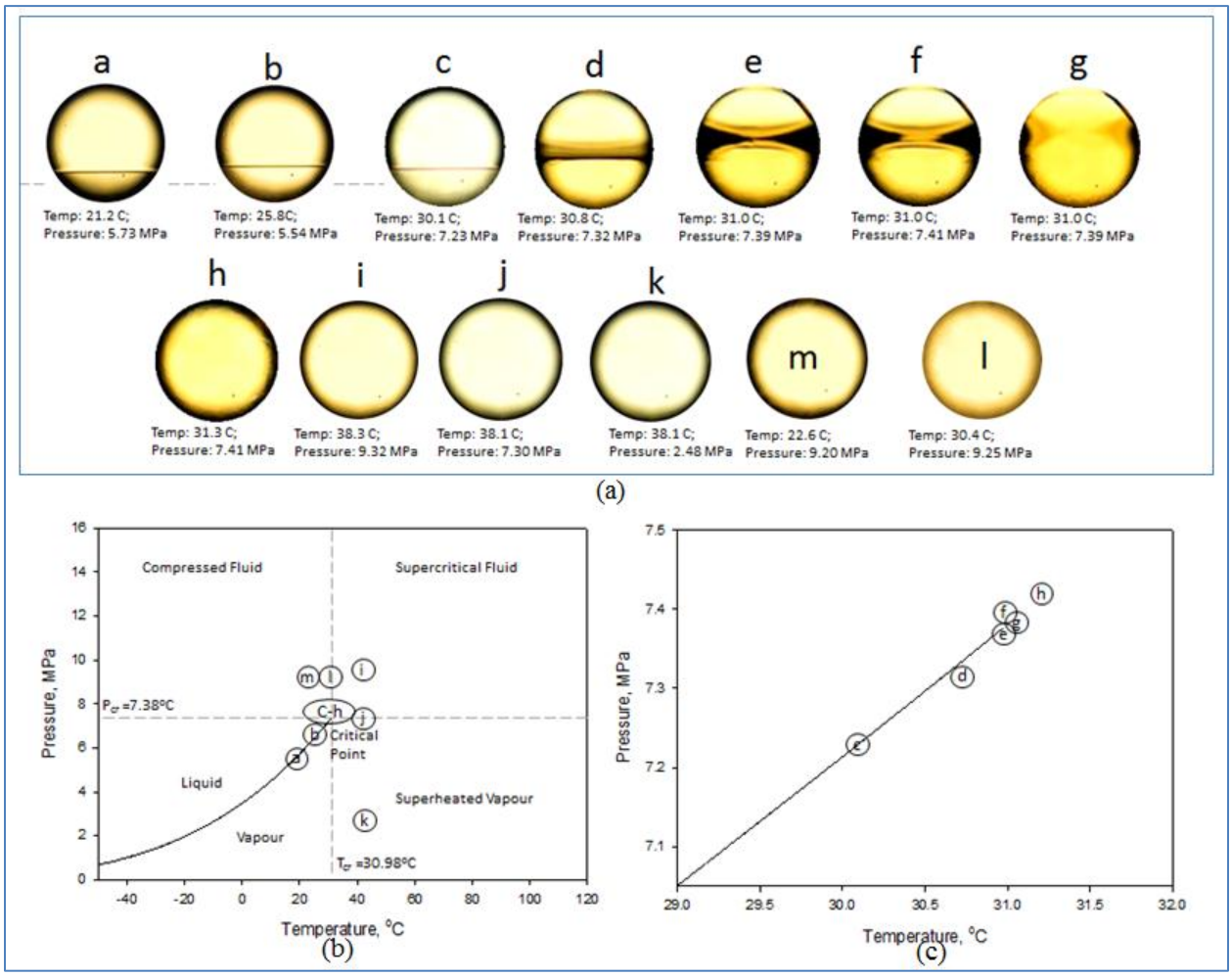

Figure 2-37: Transition of CO_2 through critical point - (a) pictures at various stages; (b) corresponding stages in pressure-temperature diagram of CO_2; (c) pressure profiles (Gupta et. al, 2013)

In Figure 2-37a (pictures a-e); the CO_2 fluid is having a clear two phase boundary (meniscus) which begins to diminish (picture f-g) and eventually forming a single phase supercritical fluid (pictures h-m), as the temperature and pressure is increased to supercritical region. At this point, the meniscus can no longer be seen and a single homogenous phase called the "supercritical fluid" occurs.

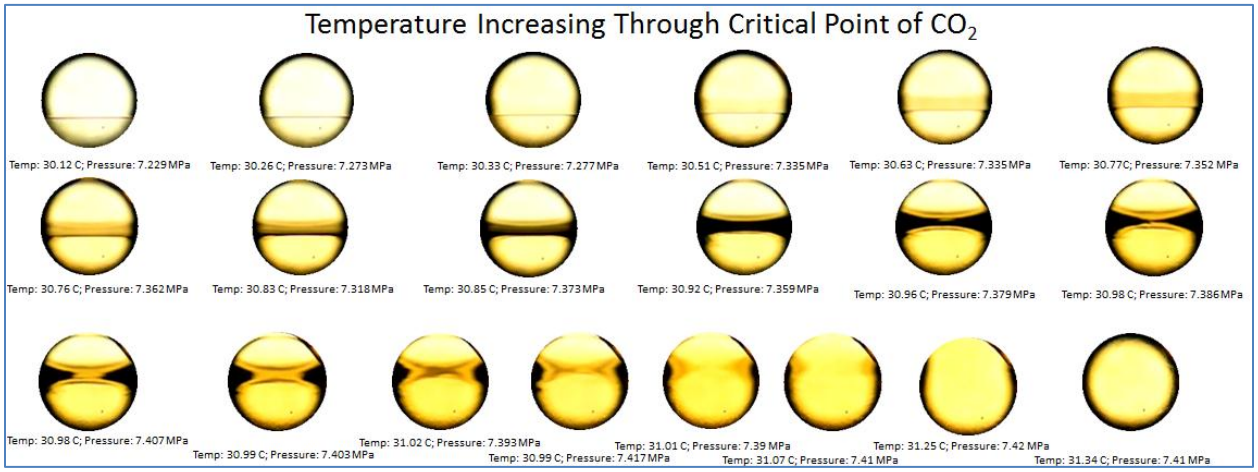

Figure 2-38: Pictures of CO_2 as Temperature and Pressure is increased in Test Chamber

2.10 EXISTING CORRELATIONS FOR FORCED-CONVECTIVE HEAT TRANSFER IN BARE TUBES

Currently, there is just one SCW heat-transfer correlation for fuel bundles developed by Dyadyakin and Popov (1977). This correlation was obtained in a 7-element helically-finned bundle (see Figure 2-39). However, heat-transfer correlations for bundles are usually quite sensitive to a particular bundle design. Therefore, this correlation cannot be applied to other bundle geometries.

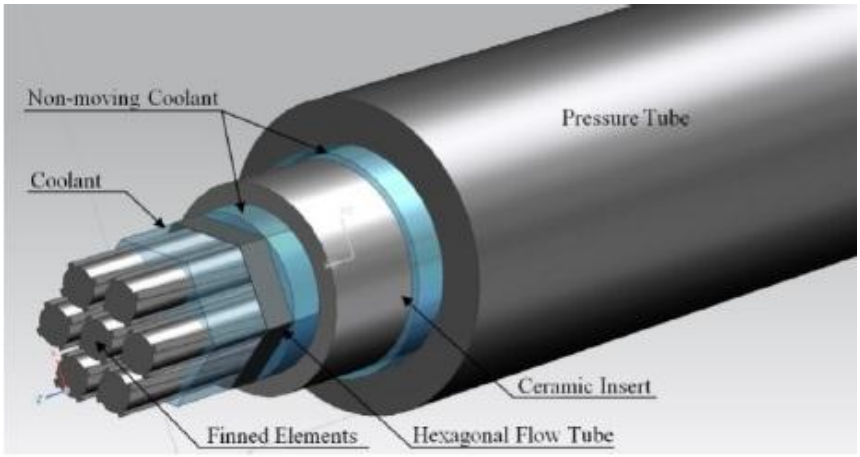

Figure 2-39: Test Section with bundle used by Dyadyakin and Popov (1977)

To overcome this problem, wide-range heat-transfer correlations based on bare-tube data can be developed as a preliminary, but still conservative approach. This approach is based on the fact that HTCs in bare tubes are generally lower than those in bundle geometries, where heat transfer is enhanced with appendages (grids, endplates, bearing pads, spacers, button, fins/ribs etc.). Extending prediction methods developed with tube or small bundle subassembly data is necessary in the conceptual design phase due to the high cost and long preparation time in testing large assemblies or full-scale bundles at relevant conditions.

A number of empirical generalized correlations have been proposed to calculate the HTC in forced convection for various fluids including water at supercritical pressures. However, differences in calculated HTC values can be up to several hundred percent (Pioro and Duffey, 2007).

2.10.1 HTC Correlations for Water

The most widely used heat-transfer correlation at subcritical pressures for forced convection is the Dittus-Boelter correlation, developed in 1930. McAdams (1942) corrected and proposed the use of the Dittus-Boelter correlation in the following form for forced-convective heat transfer in turbulent flows at subcritical pressures (this statement is based on the study by Winterton, 1998).

Equation 2-5: Dittus-Boelter (1930) Correlation

$$\mathbf{Nu_b} = 0.0243\mathbf{Re_b^{0.8}Pr_b^{0.4}}$$

Equation 2-5 was originally obtained for application in car radiators. Therefore, this correlation neither had the entrance-effect term nor the heat-flux effect, which can be quite essential in bare tubes/bundle geometry in power-engineering applications. In spite of that, Equation 2-5 is widely used for heat-transfer calculations in gases and liquids at various conditions. According to Schnurr et al. (1976) the correlation showed good agreement with experimental data of supercritical water flowing inside circular tubes at pressures of 31 MPa and low heat fluxes. However, Equation 2-5 gave unrealistic results in some flow conditions, especially near the critical and pseudocritical points (because it is sensitive to property variations in that region). This classical correlation was used as a base for many modified supercritical heat-transfer correlations.

Bishop et al. (1964) conducted experiments for supercritical water flowing inside tubes and annuli. The tests were conducted at pressures from 22.8-27.6 MPa, bulk fluid temperature of 228°C-527°C, mass flux 651-3662 kg/m^{2}s and heat flux 0.31-3.46 MW/m^2. The data gathered was generalized and resulted in the following correlation which has a ±15% fit.

Equation 2-6: Bishop et al. (1964) Correlation

$$\mathbf{Nu_x} = 0.0069\mathbf{Re_b^{0.9}}\,\overline{\boldsymbol{Pr}}_{\boldsymbol{b}}^{\mathbf{0.66}}\left(\frac{\rho_w}{\rho_b}\right)^{0.43}\left(1+\frac{2.4\mathbf{D}}{x}\right)$$

In Equation 2-6, *x* is the axial location along the heated length and the last term of the equations is the entrance region term. This term accounted for the geometry of the inlet and outlet of the test section and for the purposes of this report will be removed for the data analysis.

Swenson et al. (1965) investigated local forced-convection HTCs in supercritical water flowing inside smooth tubes. They found conventional correlations did not work well because of the instability of thermophysical properties near the pseudocritical point. They suggested the following correlation in which the majority of the thermopysical properties are based on wall temperature.

Equation 2-7: Swenson et al. (1965) Correlation

$$\mathbf{Nu_w} = 0.00459\mathbf{Re_w^{0.923}}\,\overline{\mathbf{Pr}}_{\mathbf{w}}^{\mathbf{0.613}}\left(\frac{\rho_w}{\rho_b}\right)^{0.231}$$

Equation 2-7 was obtained within pressures ranging from 22.8 - 41.4 MPa, mass flow rate of 542-2150 kg.m^{2}s, T_w of 93°C-649°C and T_b of 75-576°C:

Jackson (2002) modified the Krasnoshchekov et al (1967) original correlation for forced-convection heat transfer at supercritical pressures for water and carbon dioxide to employ the Dittus-Boelter form for $\mathbf{Nu_0}$.

Equation 2-8: Jackson et al. (2002) Correlation

$$\mathbf{Nu} = 0.0183\mathbf{Re}_b^{0.82}\mathbf{Pr}_b^{0.5}\left(\frac{\rho_w}{\rho_b}\right)^{0.3}\left(\frac{\bar{\bar{c}}_p}{c_{pb}}\right)^n$$

Where n is:

$n = 0.4$ For $T_b < T_w < T_{pc}$ and for $1.2 \cdot T_{pc} < T_b < T_w$

$n = 0.4 + 0.2\left(\frac{T_w}{T_{pc}} + 1\right)$ For $T_b < T_{pc} < T_w$;

and

$n = 0.4 + 0.2\left(\frac{T_w}{T_{pc}} + 1\right)\left[1 - 5\left(\frac{T_b}{T_{pc}} - 1\right)\right]$ For $T_{pc} < T_b < 1.2 \cdot T_{pc}$ and $T_b < T_w$

It should be noted that all heat-transfer correlations presented in this paper are intended only for the NHT and IHT regime calculations. Further analysis and HTC correlations involving DHT, q_{dht} is subjected to future investigations.

A preliminary empirical correlation (Equation 2-9) was proposed for calculating the minimum heat flux at which the DHT regime appears (Mokry et al, 2010a; 2010b):

Equation 2-9: q_{dht} Equation for water

$q_{dht} = -58.97 + 0.745\,G$, kW/m^2

2.10.2 HTC Correlations for CO_2 and Other Fluids

Krasnoshchekov and Protopopov (1959, 1960) proposed the following correlation for forced convective heat transfer in water and carbon dioxide at supercritical pressures:

Equation 2-10: Krasnoshchekov and Protopopov Correlation

$$\mathbf{Nu} = \mathbf{Nu_0}\left(\frac{\mu_b}{\mu_w}\right)^{0.11}\left(\frac{k}{k}\right)^{-0.33}\left(\frac{\bar{c}}{c_{pb}}\right)^{0.35}$$

Where according to Petukhov and Kirillov (1958), $\mathbf{Nu_0}$ is obtained as following.

$$\mathbf{Nu_0} = \frac{\frac{\xi}{8}\mathbf{Re_b}\overline{\mathbf{Pr}}}{12.7\sqrt{\frac{\xi}{8}}\left(\overline{\mathbf{Pr}}^{\frac{2}{3}} - 1\right) + 1.07}$$

$$\xi = \frac{1}{(1.82\log_{10}\mathbf{Re_b} - 1.64)^2}$$

Bringer and Smith (1957) conducted experiments with supercritical CO_2 flowing inside a tube and correlated their data as follows:

Equation 2-11: Bringer and Smith (1957) Correlation

$$\mathbf{Nu_x} = 0.0375\mathbf{Re_x^{0.77}Pr_w^{0.55}}$$

Gorban' et al. (1990) investigated heat transfer to Freon-12 flowing at subcritical and supercritical pressures inside a circular tube (D = 10 mm and L = 1 m). The range of investigated parameters was as follows: P = 1.08 and 4.46 MPa, G = 500 – 2000 kg/m^{2}s, tin = 20 – 140ºC and q = 6 – 290 kW/m^2. They proposed the following correlation:

Equation 2-12: Gorban' et al. (1990) Correlation

$$\mathbf{Nu_b} = 0.0094\mathbf{Re_b^{0.86}Pr_b^{-0.15}}$$

Many other similar correlations were developed at various flow conditions. Table 2-5 presents a brief summary of some of the different **Nu**-type correlations proposed for calculating HTC. Refer to Pioro and Duffey (2007) for a more thorough discussion and comparison of various HTC correlations.

Table 2-5: Summary of some important HTC correlation.

Author	Correlation	Operating Parameters
Dittus-Boelter (1930)	$\mathbf{Nu_b} = 0.0243\ \mathbf{Re_b^{0.8} Pr_b^{0.4}}$	Subcritical Pressures
Bringer and Smith (1957)	$\mathbf{Nu_x} = 0.0266\ \mathbf{Re_x^{0.77} Pr_b^{0.55}}\ (for\ Water)$ $\mathbf{Nu_x} = 0.0375\ \mathbf{Re_x^{0.77} Pr_b^{0.55}}\ (for\ CO_2)$ $t_x = t_b\ If\ (t_{pc} - t_b)/(t_w - t_b) < 0$ $t_x = t_{pc}\ If\ 0 \le (t_{pc} - t_b)/(t_w - t_b) \le 1$ $t_x = t_w\ If\ (t_{pc} - t_b)/(t_w - t_b) > 1$	SCW (*P=34.5* MPa*)*
Krasnoshchekov and Protopopov (1960)	$\mathbf{Nu} = \mathbf{Nu_0}\left(\frac{\mu_b}{\mu_w}\right)^{0.11}\left(\frac{k}{k}\right)^{-0.33}\left(\frac{\bar{c}}{c_{pb}}\right)^{0.35}$ $\mathbf{Nu_0} = \frac{\frac{\xi}{8}\mathbf{Re_b}\overline{\mathbf{Pr}}}{12.7\sqrt{\frac{\xi}{8}}\left(\overline{\mathbf{Pr}}^{\frac{2}{3}} - 1\right) + 1.07}$ $\xi = \frac{1}{(1.82\log_{10}\mathbf{Re_b} - 1.64)^2}$	*P*=22.3-32 MPa (water) *P*=8.3 MPa (CO_2)
Bishop et al. (1964)	$\mathbf{Nu_b} = 0.0069\ \mathbf{Re_b^{0.9}}\ \overline{\mathbf{Pr_b}}^{\mathbf{0.66}}\left(\frac{\rho_w}{\rho_b}\right)^{0.43}$	*P:* 22.8-27.6 MPa T_b=282 -527°C *G*=651-3662 kg/m^{2}s *q*=0.31-3.46 MW/m^2
Swenson et al. (1965)	$\mathbf{Nu_w} = 0.00459\ \mathbf{Re_w^{0.923}}\overline{\mathbf{Pr_w}}^{\mathbf{0.613}}\left(\frac{\rho_w}{\rho_b}\right)^{0.231}$	*P:* 22.8-41.4 MPa T_b=75-576°C T_w=93-649°C *G*=542-2150 kg/m^{2}s
Gorban' et al. (1990)	$\mathbf{Nu_b} = 0.0059\ \mathbf{Re_b^{0.90} Pr_b^{-0.12}}\ (for\ water)$ $\mathbf{Nu_b} = 0.0094\ \mathbf{Re_b^{0.86} Pr_b^{-0.15}}\ (for\ R-12)$	$T_b > T_{cr}$
Jackson (2002)	$\mathbf{Nu_b} = 0.0183\ \mathbf{Re_b^{0.82} Pr_b^{0.5}}\left(\frac{\rho_w}{\rho_b}\right)^{0.3}\left(\frac{\bar{\bar{c}}_p}{c_{pb}}\right)^n$ $n = 0.4$ For $T_b < T_w < T_{pc}$ and $1.2 \cdot T_{pc} < T_b < T_w$ $n = 0.4 + 0.2\left(\frac{T_w}{T_{pc}} + 1\right)$ For $T_b < T_{pc} < T_w$; $n = 0.4 + 0.2\left(\frac{T_w}{T_{pc}} + 1\right)\left[1 - 5\left(\frac{T_b}{T_{pc}} - 1\right)\right]$ For $T_{pc} < T_b < 1.2 \cdot T_{pc}$ and $T_b < T_w$	Supercritical pressures

Author	Correlation	Operating Parameters
Sarah Mokry et al. (2009)	$\mathbf{Nu_b} = 0.0061\ \mathbf{Re_b^{0.904}}\ \overline{\mathbf{Pr}}_\mathbf{b}^{-0.684}\ \left(\frac{\rho_w}{\rho_b}\right)^{0.564}$ (developed for SC H_2O)	Supercritical Ranges
Gupta et al. (2011) (see Section 4.7 later for more details)	$\mathbf{Nu_w} = 0.0033\ \mathbf{Re_w^{0.94}}\ \overline{\mathbf{Pr}}_\mathbf{w}^{-0.76}\left(\frac{\mu_w}{\mu_b}\right)^{0.4}\left(\frac{\rho_w}{\rho_b}\right)^{0.156}$ (developed for SC H_2O)	Supercritical Ranges

2.11 Limitations of Existing Correlations

There have been many other correlations which have been developed with varying conditions. The majority of the empirical correlations as detailed in section 2.10, were proposed during the era of 1960s and 1970s, when experimental techniques were not as advanced as they are today. Also, thermophysical properties of fluids have been updated since that time. For example, a peak in thermal conductivity of water in critical and pseudocritical points, within a range of pressures from 22.1 to 25 MPa, was not officially recognized until the 1990s (Pioro and Duffey, 2007).

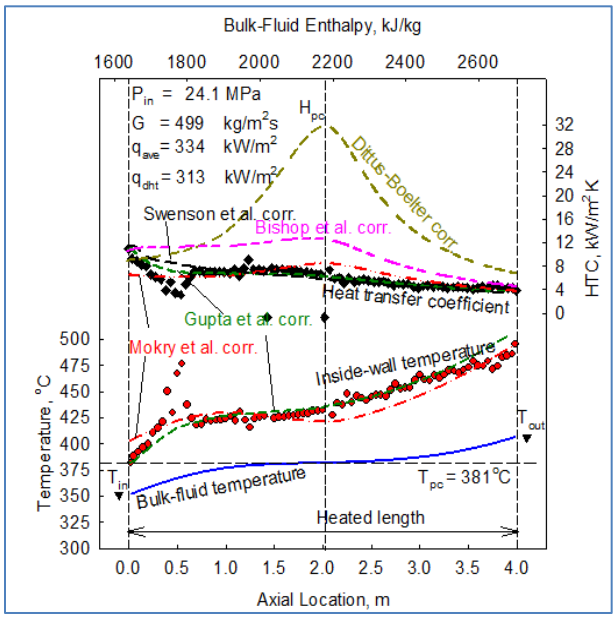

Figure 2-40: Comparison of HTC values calculated through various correlations with experimental data of 4-m circular tube (D=10mm): P_{in}~ 24 MPa and G = 500 kg/m^{2}s.

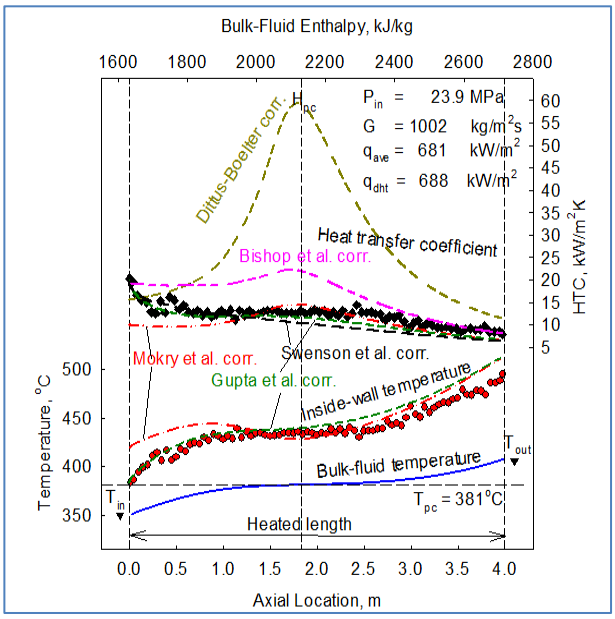

Figure 2-41: Comparison of HTC values calculated through various correlations with experimental data of 4-m circular tube (D=10mm): P_{in}~ 24 MPa and G = 1000 kg/m^{2}s.

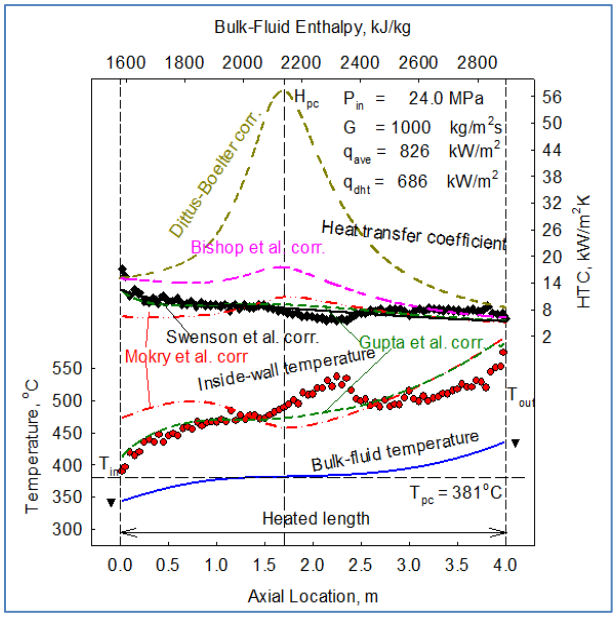

Figure 2-42: Comparison of HTC values calculated through various correlations with experimental data of 4-m circular tube (D=10mm): P_{in}~ 24 MPa and G = 1000 kg/m^{2}s.

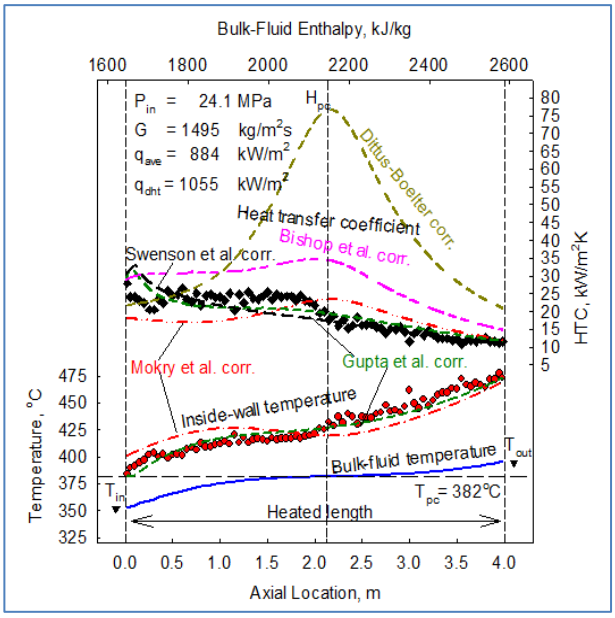

Figure 2-43: Comparison of HTC values calculated through various correlations with experimental data of 4-m circular tube (D=10mm): P_{in}~ 24 MPa and G = 1500 kg/m^{2}s.

The combination of these factors explains why most of these correlations do not achieve the desired level of accuracy for current experimental data. Figure 2-40 to Figure 2-43 shows comparison of HTC values calculated through few common correlations with the Kirillov's et al. (2005) experimental data obtained in water flowing in a 4 (four) metre long bare tube. It should be noted that differences in calculated HTC values can be up to several hundred percent, especially, within the pseudocritical range.

Similar errors are also noticed with CO_2 datasets. Figure 2-44 and Figure 2-45 shows a comparison of HTC values calculated through various correlations for SC CO_2 data obtained at Chalk River Laboratories (CRL) AECL. Thus, it was decided to develop a new or an updated correlation, based on a new set of heat-transfer data and the latest thermophysical properties of water using NIST (2007).

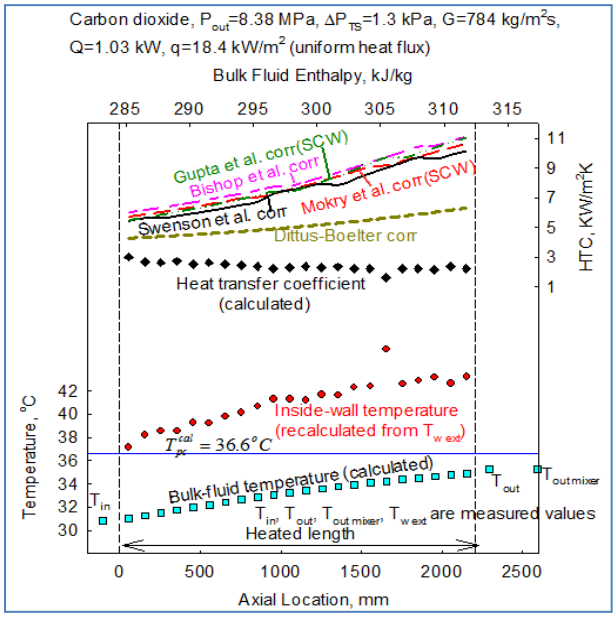

Figure 2-44: Comparison of HTC values calculated through various correlations with experimental CRL data (SC CO_2) - vertical bare tube (D=8 mm): P_{in} ~ 8.38 MPa and G ~ 784 kg/m^{2}s

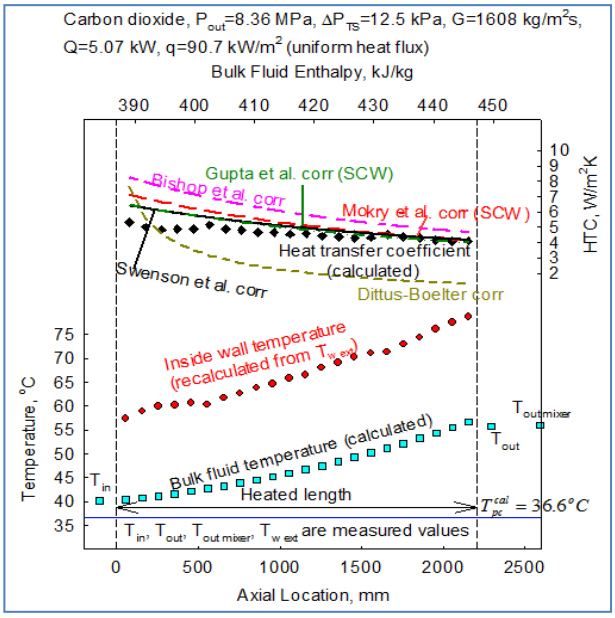

Figure 2-45: Comparison of HTC values calculated through various correlations with experimental CRL data (SC CO_2) - vertical bare tube (D=8 mm): P_{in} ~ 8.36 MPa and G ~ 1608 kg/m^{2}s.

CHAPTER 3 METHODOLOGY DESCRIPTION

3.1 Considerations for Methodology Selection

There are multiple techniques that can be applied to analyse the heat transfer problems ranging from numerical solutions to purely empirical correlations. Extensive computer modelling techniques such as CFD is also gaining vast popularity to analyze a heat transfer problems in a given set of boundary conditions and geometry. Specialized commercial thermal hydraulic codes such as thermal hydraulic network analysis (CATHENA) are also extensively used in the industry applications.

Each of the techniques and methods discussed above have their own pros and cons and the selection of the methodology boils down to system complexity, nature of application and the desired level of accuracy requirements. Use of numerical solutions is often not feasible due to various complexities associated with supercritical heat transfer; especially within the pesudocritical regions (recall the previous discussions in CHAPTER 2). Thus, numerical solutions are typically limited to small fraction of possible flows that are both geometrically and physically simple. Computer modelling techniques on the other hard require extensive use of computational power and are often less accessible and costly. Furthermore, mature modelling like CFD is yet to report consistent success in prediction of the supercritical heat transfer data.

The focus of this thesis was to develop a simplistic 1-D Heat Transfer Correlation that can be used for quick preliminary calculations without the need for specialized computer modelling software that require extensive training and resources. For this reason, time tested approach of dimensional analysis was considered adequate to achieve the desired outcome. Dimensional analysis is simplistic, yet a very powerful tool that can enable us to simplify the relationships of heat transfer parameters through the use of dimensionless groups. Empirical correlations can then be developed by coupling them with experimental data points and used to describe the correlations between these groups.

3.2 Dimensional Analysis

A dimensional analysis can be performed, to obtain a general empirical form of a correlation for HTC calculations. It is well known that HTC is not an independent variable, and that HTC

values are affected by mass flux, inner diameter, heat flux, thermophysical property variations, etc. Therefore, a set of the most important variables, which affect the HTC, were identified based on theoretical and experimental HTC studies at supercritical pressures. Table 3-1 lists parameters identified as essential for the analysis of heat-transfer processes for forced convection at supercritical conditions.

Table 3-1: Primary parameters affecting Heat Transfer process.

Variable	Description	Formula	SI units	Dimensions (M, L, T, K)	Physical Significance
HTC	Heat transfer coefficient	$h = \frac{k}{D_h} Nu$ $h = \frac{q}{\Delta T}$	W/m^2K	$MT^{-3}K^{-1}$	The proportionality coefficient between the heat flux and the thermodynamic driving force for the flow of heat (i.e., the temperature difference, ΔT):
D_h	Hydraulic diameter of tube	$D_h = \frac{4A}{P}$	m	L	Basic variable that defines the geometry in the flow channel and also impacts various flow variables dimensionless parameters such as Nu, Re,
k_b	Thermal conductivity of fluid at T_b	$q_x = -k\frac{dT}{dx}$ (Fourier's Law)	W/m/K	$MLT^{-3}K^{-1}$	Basic property of a material that defines its ability to conduct heat. It is a temperature dependant property.
k_w	Thermal conductivity of fluid at T_w		W/m/K	$MLT^{-3}K^{-1}$	
ρ_b	Density of fluid at T_b	$\rho = \frac{m}{V}$	kg/m^3	ML^{-3}	Basic property of a substance that defines how tightly molecules are packed in a given volume. It varies with temperature and pressure.
ρ_w	Density of fluid at T_w		kg/m^3	ML^{-3}	
μ_b	Dynamic Viscosity of fluid at T_b	$\tau = \mu \frac{\partial u}{\partial y}$ where, $\tau = \frac{F}{A}$ $\partial u/\partial y$ represents local shear velocity	Pa·s	$ML^{-1}T^{-1}$	Basic property of a fluid that provides a measure of its resistance to gradual deformation by shear stress or tensile stress. At molecular level liquid's viscosity depends on the size and shape of its particles and the forces of attractions between the particles.
μ_w	Dynamic Viscosity of fluid at T_w		Pa·s	$ML^{-1}T^{-1}$	

Variable	Description	Formula	SI units	Dimensions (M, L, T, K)	Physical Significance
c_p	Specific heat	$c_p = \frac{Q}{\Delta T . m}$	J/kg K	$L^2T^{-2}K^{-1}$	It represents the measurable quantity of heat energy required to change the unit mass of substance by 1K.
$\bar{c_p}$	Averaged Specific Heat (defined for annual flow)	$\bar{c_p} = \frac{H_w - H_b}{T_W - T_b}$	J/kg K	$L^2T^{-2}K^{-1}$	Averaged Specific Heat values have been used in Nu equations to account for the thermophysical properties variations within the pseudocritical region.
V	Characteristic Velocity	$V = \frac{dx}{dt}$	m/s	LT^{-1}	Fundamental parameter that measures the rate of change of fluid particles.
ε	Surface Roughness	–	m	L	It is a measure of texture of a flow surface. It is an important parameter as it affects the velocity profiles of fluids near the wall and friction factors.
Nu	Nusselt number	$\mathbf{Nu} = \frac{hL}{k}$ Where: L is characteristic length	–	–	Nusselt number (Nu) represents the ratio of convective to conductive heat transfer across the heat transfer surface (boundary). The magnitude of Nu is characteristic of a slug/laminar flow (when Nu ~1) and turbulent flow (when Nu ~ 100-1000).
Pr	Prandtl number	$\mathbf{Pr} = \frac{c_p \mu}{k} = \frac{v}{\alpha}$	–	–	Prandtl number (Pr) represents the ratio of momentum diffusivity (kinematic viscosity) to thermal diffusivity. It is dependent only on the fluid state and determines the relative thickness of the momentum and thermal boundary layers.
$\overline{\mathbf{Pr}}$	Ave. Prandtl number	$\overline{\mathbf{Pr_x}} = \frac{\bar{c_p} \mu_x}{k_x}$	–	–	Averaged Pr values have been used in Nu equations to account for the thermophysical properties variations within the pseudocritical region.

Variable	Description	Formula	SI units	Dimensions (M, L, T, K)	Physical Significance
Re	Reynolds number	$\mathbf{Re_x} = G\frac{D_h}{\mu}$ Where: G = mass flux	–	–	Reynolds number defines the ratio of intertial forces to viscous forces and consequently quantifies the relative importance of these two types of forces for given flow conditions.

The Buckingham *Π*-Theorem for dimensional analysis (Munson et al., 2005) was used to produce the following expression for HTC as a function of the identified heat-transfer parameters.

$$\text{HTC} = f\,(D, k_b, k_w, \rho_w, \rho_b, \mu_w, \mu_b, c_p, V)$$

Through a consideration of the primary dimensions - mass (M), length (L), time (T) and temperature (K), six unique dimensionless *Π*-terms were determined (see Table 3-2).

Table 3-2: Description of Dimensionless Terms.

Π-terms	Dimensionless group	Name
Π_1	$\frac{HTC\ D}{k_x}$ $\frac{\text{HTC.D}}{\text{k}_\text{b}}$	Nusselt number, $\mathbf{Nu_x}$
Π_2	$\frac{\rho\ V\ D}{\mu_x}$	Reynolds number, $\mathbf{Re_x}$
Π_3	$\frac{c_p\ \mu_x}{k_x}$	Prandtl number, $\mathbf{Pr_x}$
Π_4	$\frac{k_w}{k_b}$	Thermal conductivity ratio
Π_5	$\frac{\mu_w}{\mu_b}$	Viscosity ratio
Π_6	$\frac{\rho_w}{\rho_b}$	Density ratio

The resulting relationship based on this analysis is as follows:

$$\Pi_1 = f(\Pi_2, \Pi_3, \Pi_4, \Pi_5, \Pi_6)$$

Equation 3-1: Model Equation for the Empirical Correlation

$$\mathbf{Nu_x} = C\mathbf{Re_x^{n_1}Pr_x^{n_2}}\left(\frac{k_w}{k_b}\right)^{n_3}\left(\frac{\mu_w}{\mu_b}\right)^{n_4}\left(\frac{\rho_w}{\rho_b}\right)^{n_5}$$

3.3 Role of Characteristic Temperature in HTC Correlations

There are two characteristic parameters to consider in the development of correlation:

1) Characteristic length; and

2) Characteristic temperature, at which the majority of thermophysical properties have to be determined.

The characteristic length in **Nu** and **Re** can be a tube diameter or hydraulic-equivalent diameter. It is a more complicated case to determine the characteristic temperature. In general, the conventional correlations like Dittus-Bolter, Bishop et al., Jackson etc. use bulk-fluid temperature. However, at high heat fluxes fluid near the tube wall will have a temperature close to the wall temperature, which might be significantly different from the bulk-fluid temperature. Therefore, another approach can be used based on the wall temperature as the characteristic temperature (example Swenson et al. correlation). Also, there can be some interim approaches, for example, the film-temperature approach, i.e., using the arithmetic average temperature between the wall and bulk-fluid temperatures. In this report, all three approaches were considered for developing a new correlation.

3.4 Data Reduction Techniques

Experimentally obtained data cannot be used straightforwardly to determine the values of the coefficients of the model equation using curve fitting techniques (as described in subsequent sections). Before such techniques are employed, data reduction is often warranted to remove outliers from the base dataset. These outliers often are results of defective thermocouple readings. First and last points of most experimental runs might also be needed to be removed as they would be affected by test-section clamps. In addition, DHT regimes from the dataset might also have to be removed based on visual inspections of the plotted data. All these points would

lie outside the generic trends and can significantly skew the linear regression values, hence introducing significant errors in the correlation.

It must be mentioned here that Data Reduction of DHT points is again subjected to visual bias. In removal of these data, one must be very meticulous to ensure that there are justifications for removing particular points.

3.5 Manual Iterations to Determine Coefficients of Model Equation

In general, the coefficients of the model Equation 3-1 can be found by graphical and statistical techniques. The experimental dataset, with removed outliers and points in the DHT and IHT regimes, was compiled into a MS Excel Spreadsheet. Curve fitting techniques are employed to fit experimental data (with removed points) to the dimensionless parameters identified in the model equation; and coefficients can be determined from scatter plots using linear regression on a log-log scale.

For example, for simplification purposes Nusselt's can be assumed as a function of Reynold's number.

$$\boldsymbol{Nu_x} = C[\boldsymbol{Re_x^{n1}}]$$

$$\Rightarrow Log\ (\boldsymbol{Nu_x}) = Log\ (C\ \boldsymbol{Re_x^{n1}})$$

$$\Rightarrow Log\ (\boldsymbol{Nu_x}) = Log\ C + n1\ Log\ (\boldsymbol{Re_x})$$

The above equation is in the form of linear equation (y=mx+c, where *m* is the slope and *c* is the 'y intercept'). Thus, if we plot log (**Nu**) on y-axis vs. log (**Re**) on x-axis, the slope of the linear trendline of the plot shall give the preliminary coefficients (n_1) for Re.

Similar plots can then be made for $\log\left(\frac{\mathbf{Nu}}{\mathbf{Re}^{n_1}}\right)$ $vs.$ $\log(\mathbf{Pr})$ etc. and the iterations can be repeated to arrive at preliminary exponents for the model Equation 3-1.

3.6 Curve Fitting Using Sigma Plot Dynamic Fit Wizard

Nonlinear curve fitting is an iterative process that may converge to find a best possible solution. It begins with a guess of the parameters, checks to see how well the equation fits, and then continues to make better guesses until the differences between the residual sum of squares no

longer decreases significantly. Sigma plot (2011) Dynamic Fit Wizard automates the search for initial parameter values that lead to convergence to the best possible solution for the model equation. Thus, to finalize the coefficients found using manual iteration methods, the complete set of primary data and the preliminary equation can be fed into the SigmaPlot Dynamic Fit Wizard which would fine tune the coefficients to provide the best possible accuracy.

3.7 Error Analysis Techniques

Error analysis forms a vital part of testing the validity of the developed correlation. In general, there are many statistical techniques that can be applied to calculate parameters like mean errors, Root Mean Square (RMS) error etc.

For the purpose of this project, the following equations were used to calculate errors associated with the developed correlations.

Equation 3-2: Percentage (%) Error

$$Error = \frac{X_{calculated} - X_{exp}}{X_{exp}}$$

Equation 3-3: Mean Error

$$Mean\ error = \frac{\sum_{i=1}^{n} Error_i}{n} * 100\ \%$$

Equation 3-4: RMS Error

$$RMS\ error = \sqrt{\frac{\sum_{i=1}^{n} {Error_i}^2}{n}} \times 100\%$$

Note that RMS, as calculated from the above equation, represents the relative deviation of experimental value from the calculated value.

3.8 Testing Facilities and Experimental Considerations

As discussed previously in CHAPTER 2, heat transfer analysis and HTC calculations at SuperCritical conditions can be complex. From SCWR design and safety analysis point of view; there is not enough qualified data available that takes into account the various geometries, power profiles, and flow conditions used in SCWR designs. As noted in the literature surveys by Pioro and Duffey (2007), most experimental data were obtained using with tubular test sections.

Hence the correlations are only strictly applicable for tubes and cannot be extended for use in sub-channel applications.

Nevertheless, tube data can provide a fundamental understanding of supercritical heat transfer phenomena and help in the development of basic 1-D HTC correlations. Use of first principle techniques is often not feasible due to various unknown parameters in forced convective flows and traditionally, empirical curve-fitting techniques have been employed to predict HTC values in a given set of geometrical and operational constraints. These curve-fitting empirical models require a vast set of experimental data for SCFs obtained with tubes under supercritical pressure conditions for the development and validation of heat-transfer correlations.

Several heat-transfer databases for supercritical water and other SCFs flow are available through various experiments conducted around the world. However, measurements can be negatively impacted by a wide variety of parameters such as improper insulations of test sections, impurities in the test fluid, lack of precisions on the measuring instruments, lack of well-defined experimental process controls etc. Thus careful considerations are required to obtain accurate experimental datasets with meticulous quality control procedures to limit the uncertainty in test measurements. In most of the published data and reports; the information about experimental uncertainties and test procedures are limited.

It must be stressed that the accuracy of the empirical correlations relies almost entirely on the accuracy of the test datasets. For the purpose of this report, experimental sets in water and CO_2 were selected for Kirilov SKD-1 loop (see 0) and AECL loop (see CHAPTER 5) since detailed information on test sections, experimental uncertainties etc. was available. Improved correlations can be derived using more extensive databases combined from various sources that can provide better prediction accuracy and more appropriate parametric trends.

Eventually, to extend the use of these correlations to sub-channel applications, there would be a need to device specific experiment setups that will take into account SCWR bundle geometries, axial and radial power profiles in bundles (uniform and non-uniform with various flux shapes), spacing devices (spacer grids, wrap-around wires that typically increase turbulence in the flow geometry), flow directions (upwards and downwards) and various transient analysis for postulated accident scenarios.

CHAPTER 4 SC WATER DATASET AND DEVELOPED CORRELATIONS

As described in CHAPTER 3; in order to find the coefficients in the model equations we need to correlate it to an experimentally obtained dataset. Careful selection of the base dataset is the key for developing a reliable curve fit.

The experimental data used in the current thesis was obtained at Supercritical Test Facility of the State Scientific Center of Russian Federation – Institute for Physics and Power Engineering (Obninsk, Russia)[17]. This set of data was obtained within operating conditions close to those of SCWRs, including the hydraulic-equivalent diameter (D_{hy}) (Kirillov et al., 2005).

4.1 Test Facility – SKD-1 Loop

The Supercritical-Pressure Test Facility SKD-1 loop (see Figure 4-1) was used to obtain experimental data for water. It is a high pressure and temperature loop made up entirely of stainless steel components. The SKD-1 is capable of operating at pressures as high as 28 MPa, an outlet temperature of 500°C and power up to 0.6 MW. High pressure N_2 gas was used to achieve the desired pressurization.

Distilled and de-ionized water acts as the coolant for the loop. The water is sent through the loop with a pump and passes through a flow meter, a preheater, a test section, mixing cooler and main coolers before reaching the pump again.

[17] Experiments were formed in Obninsk, Russia by Kirillov et al., and raw data was made available for the present analysis.

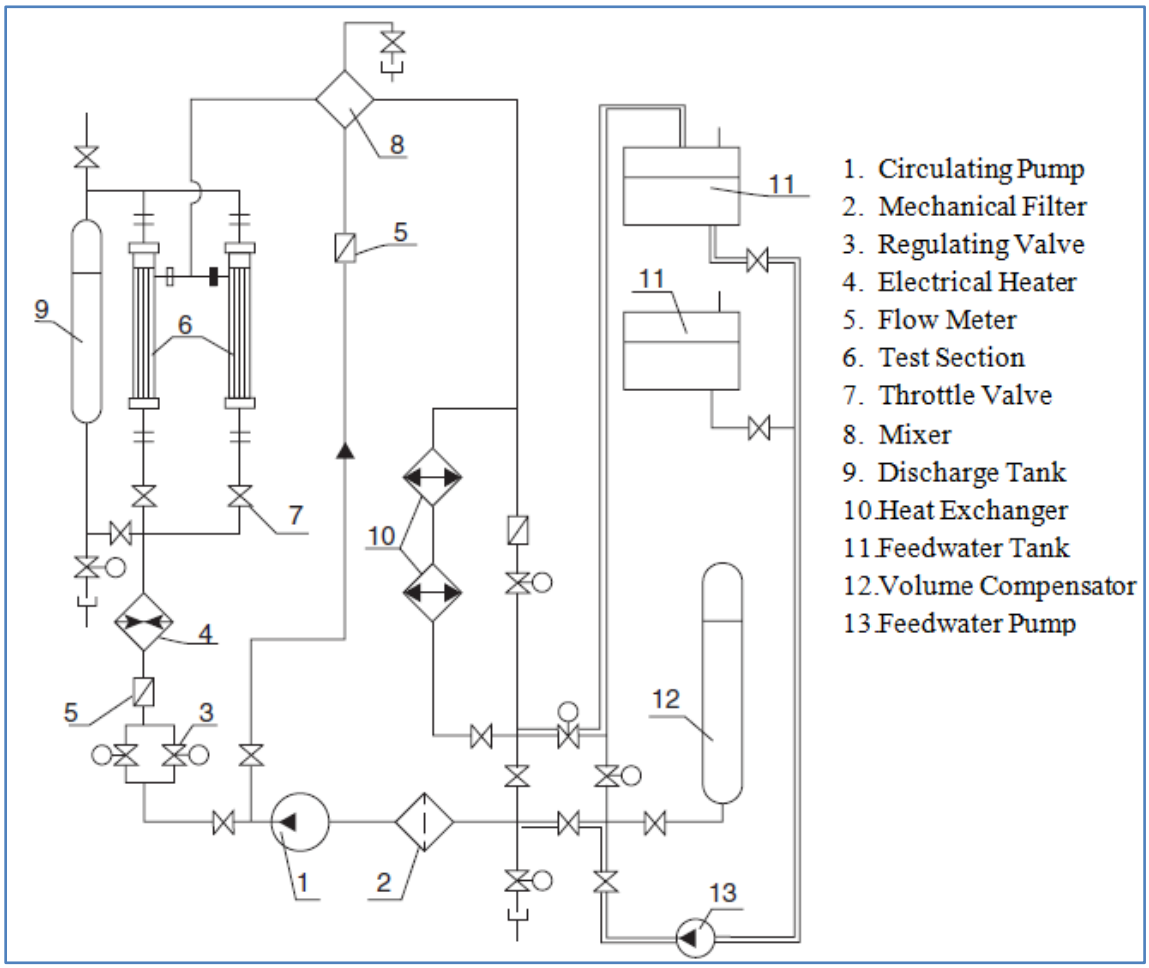

Figure 4-1: Supercritical-Pressure Test Facility SKD-1 Loop Schematic (adapted from Pioro and Duffey, 2007)

4.2 Test Section- Vertical Stainless Steel Circular Tube

The test section is a vertical stainless steel smooth circular tube. The dimensions of the section are 10 mm ID, 2 mm wall thickness, and a surface roughness $R_a = 0.63 - 0.8\,\mu m$. The diameter of the test section is close to proposed hydraulic-equivalent diameter of a SCWR fuel bundle. There are two heated lengths that are used to perform the tests; their length's being 1 meter long and a 4 meter long.

It should be noted that the experimental dataset for the 1 meter long test section was insufficient as the number of points was very limited. As a result only the 4 meter test section experimental data was used to develop the correlation.

4.3 Experimental Procedure

The test-section was heated by the application of an alternating current through the tube. The specified operating parameters (pressure, mass flux and water temperature at the tube inlet) were set at the test section. The experimental dataset was recorded by a Data Acquisition System (DAS) when the desired flow conditions and power level had been reached and stabilized. Next, a new power level and/or new set of flow conditions were setup. The data points were recorded over one minute in five-second intervals.

The test matrix covered in the experiments is listed in Table 4-1. These test matrix values are close to the operating conditions of SCWRs (pressure of 24 – 25 MPa, inlet temperature of up to 350ºC, outlet temperature of up to 625ºC, mass flux within 800 – 1500 kg/m^{2}s and heat flux of up to 1000 – 1200 kW/m^2). The experimental runs were carried out under steady-state operating conditions, at forced water circulation, with vertical upward flow in the test section.

Table 4-1: Dataset Test Matrix for Water (adapted from Pioro and Duffey, 2007)

P (MPa)	T_{in} (°C)	T_{out} (°C)	T_w (°C)	q (kW/m^2)	G (kg/m^{2}s)
24	320 – 350	380 – 406	<700	70 – 1250	200; 500; 1000; 1500;

The heat-loss tests, conducted at the beginning of the experimental program, were used to determine the heat-loss characteristics of the test section. Heat loss was estimated by comparing the electrical heat input against the actual heat transfer to water. The test results showed that heat-loss from the test section was minor, within 3% of the electrical heat input. The values of power used in the heat-transfer calculations were adjusted for this heat loss.

4.4 Instrumentation and Test Matrix

The following test-section parameters were measured or calculated during the experimental runs:

- Test-section current and voltage were used to calculate the power;
- Pressure at the test-section inlet
- Temperatures at the test-section inlet and outlet. These temperatures were measured using ungrounded sheathed thermocouples (K-type) inserted into the fluid stream. The thermocouples were installed just downstream of the mixing chambers, which were used

to minimize non-uniformity in the cross-sectional temperature distribution. These thermocouples were calibrated in situ

- Outside wall temperatures at equal intervals (50 mm) along the test section. Eighty-one thermocouples, attached to the 4-m-long test section, were contact welded onto the outside wall surface. These thermocouples were isolated by glass cord and were calibrated in situ
- Water mass-flow rate was calculated based on the measured pressure drop over a small orifice plate, which was monitored with a differential-pressure cell
- Ambient temperature

4.5 Uncertainty in Test Data

Table 4-2 displays the uncertainty in the Test Data in the SKD-1 Loop mainly arising from instrumentation limitations.

Table 4-2: Uncertainty in Instrumentation of SKD-1 Loop (Gupta et. al., 2010).

Parameter	Maximum Uncertainty
Test-section power	±1.0%
Inlet pressure	±0.25%
Wall temperature	±3.0%
Mass-flow rate	±1.5%
Heat loss	≤3.0%

4.6 Data Reduction

The dataset includes 89 experimental runs, with 81 data points per run for a total of over 7,200 points collected. Abnormalities, such as defective thermocouple readings were removed from the dataset. Data points in the Deteriorated Heat-Transfer (DHT) regions were also removed from the dataset (based on visual inspections of plotted data) because the correlation was developed to model the normal heat transfer regime. The DHT region does not fall under the normal heat transfer region and is a topic for future investigation, outside of the scope of this project.

Also, the very first and last points of most test runs were removed. Temperatures at these outlying points were likely affected by test-section clamps, which were at a lower temperature

than the heated part of tube. Overall, approximately 87% of the experimental data was used to develop the correlation.

Figure 4-2 and Figure 4-3 show sample of the points that were removed as part of data reduction (Mokry et al, 2009).

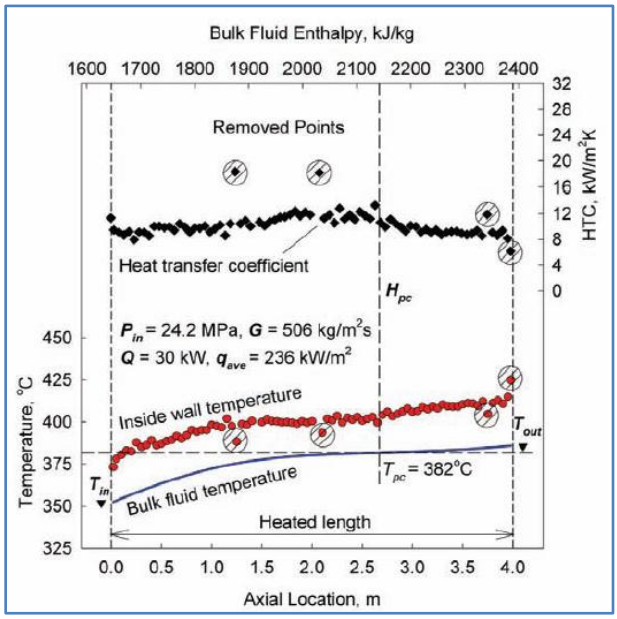

Figure 4-2: Sample Experimental Run with Removed Outliers (Gupta et. al, 2010)

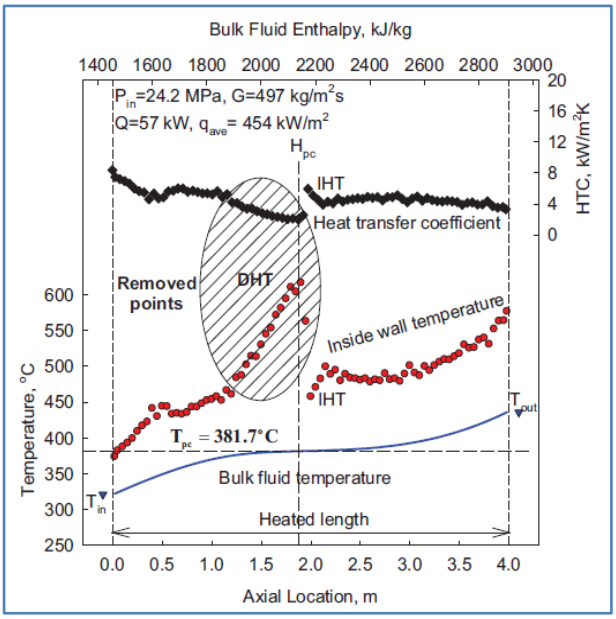

Figure 4-3: Sample Experimental Run with Removed Points in the DHT and IHT regimes (Gupta et. al, 2010)

4.7 Development of HTC Correlations for Water

The methodology outlined in Section 4.2 and the Test Section data was used to develop new correlations for water. Three different approaches – (1) Wall Approach; (2) Bulk Approach; and (3) Film Approach was used to develop new correlations using Equation 3-1, as the starting point.

4.7.1 Wall-Fluid Temperature Approach

In this approach, the thermophysical properties are calculated using T_w. This approach was used by Swenson et al. and has proved to be more effective for calculating HTC values at supercritical conditions.

4.7.1.1 Determination of preliminary correlation

In order to determine the coefficients in the general form proposed by Equation 3-1, manual iterations were performed. The experimental dataset, with removed outliers and points in the DHT regime, was used to calculate the required parameters through the NIST (2007) [10] software. Scatter plots were then created and analysed using linear regression on a log–log scale.

1st Manual Iterations

Manual iteration Step 1: $\mathbf{Nu_w}$ **vs.** $\mathbf{Re_w}$

Figure 4-4 shows a resulting scatter plot for this step. The slope of the linear-regression line (0.96) gives the preliminary exponent for the $\mathbf{Re_w}$ term. The R^2 value indicates a dependency of the parameters

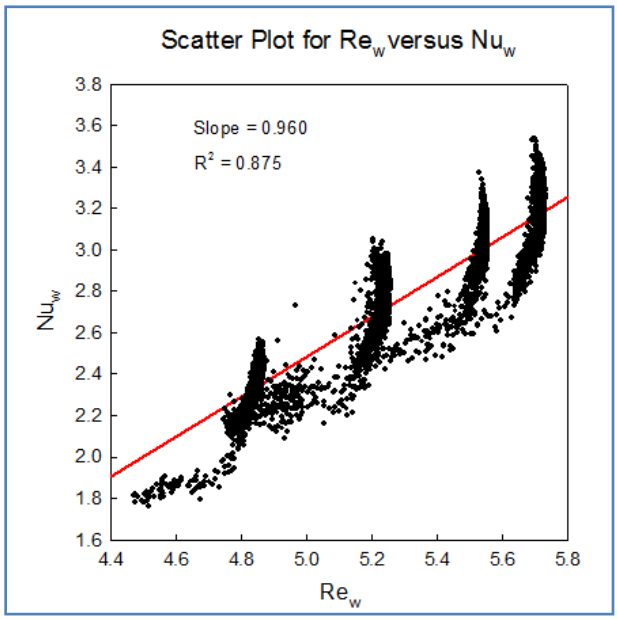

Figure 4-4: Log (Nu_w) vs Log (Re_w) for Water

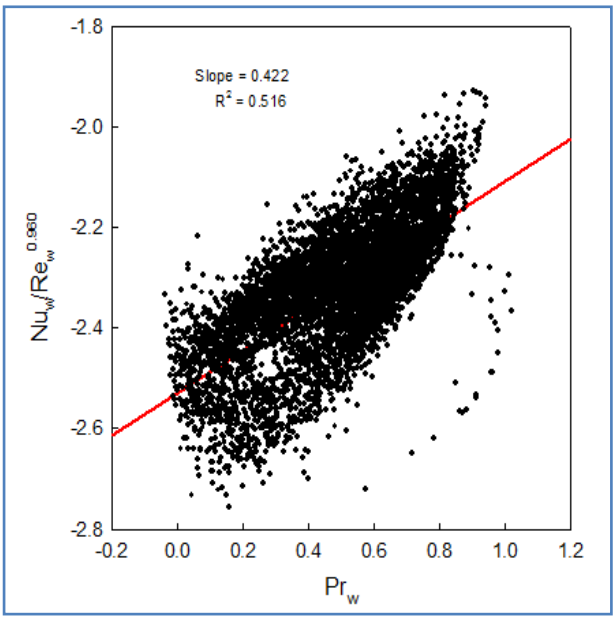

Figure 4-5: Determination of Exponent of Prandlt Number

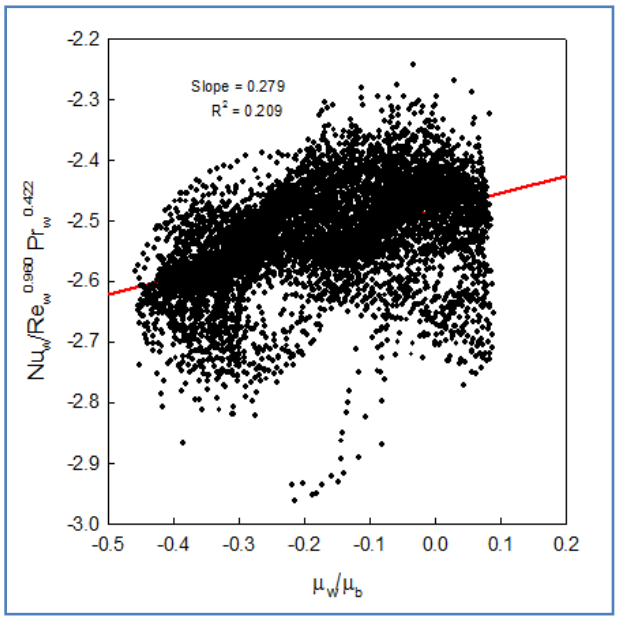

Figure 4-6: Determination of Exponents for ratio of viscosity

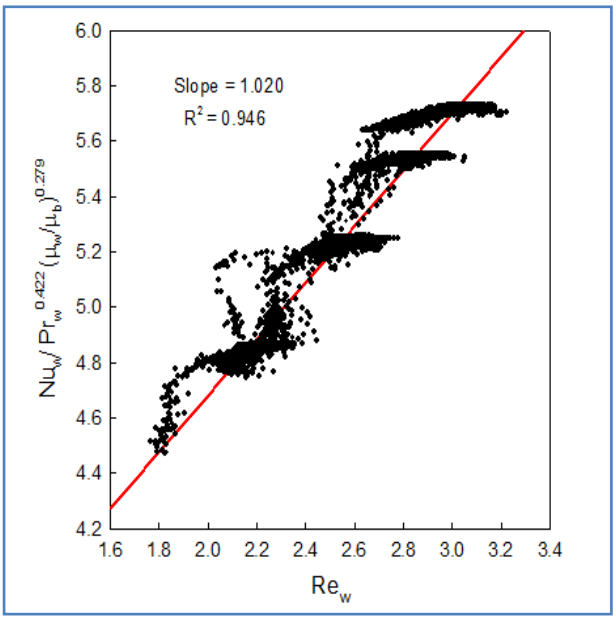

Figure 4-7: Determination of Reynolds Number

Manual iteration Step 2:

$$\frac{\mathbf{Nu_w}}{\mathbf{Re_w^{0.96}}} \textbf{ vs. } \overline{\mathbf{Pr_w}}$$

From Figure 4-5, a preliminary exponent for $\overline{\mathbf{Pr_w}}$ was taken to be 0.422.

Manual iteration Step 3:

$$\frac{\mathbf{Nu_w}}{\mathbf{Re_w^{0.96}}\ \overline{\mathbf{Pr_w}}^{0.422}} \textbf{ vs. } \frac{\boldsymbol{\mu_w}}{\boldsymbol{\mu_b}}$$

Similar iterations were performed, with the ρ_w/ρ_b and k_w/k_b terms.

2nd Manual Iterations

The manual iterations were repeated with the preliminary exponents from first iterations until they converged to steady values.

Step 1:

$$\frac{\mathbf{Nu_w}}{\overline{\mathbf{Pr_w}}^{0.422}\left(\frac{\mu_w}{\mu_b}\right)^{0.279}} \text{ vs. } \mathbf{Re_w}$$

We can see that the R^2 in Figure 4-7 (0.946) has considerable improved from the one in Figure 4-4 (0.875). Thus, increasing a number of iterations corresponds to an increase in accuracy.

Step 2:

$$\frac{\mathbf{Nu_w}}{\mathbf{Re_w}^{0.96}\left(\frac{\mu_w}{\mu_b}\right)^{0.279}} \text{ vs. } \overline{\mathbf{Pr_w}}$$

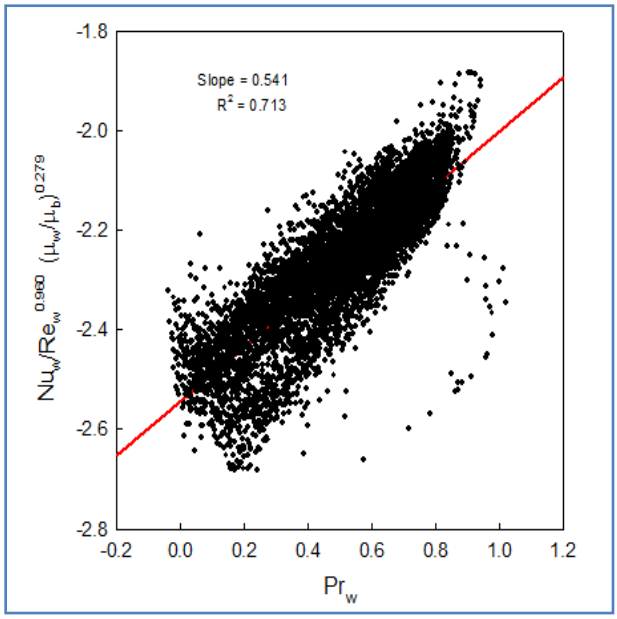

Figure 4-8: Determination of refined averaged Prandtl number exponent

Similarly, further iterations were performed on the remaining parameters each time refining the exponents and an improvement in R^2 value.

Through subsequent iterations, it was determined that ρ_w/ρ_b has a noticeable dependency (slope ≈ 0.15), while k_w/k_b has a slope close to 0 indicating that it has almost no effect on the **Nu** term. Hence, k_w/k_b was not considered in the final correlation.

4.7.1.2 Finalizing Correlation

The coefficients *C*, n_1, n_2, etc. determined using the manual iterations were then further refined. Some restraints were applied to the values of the exponents, and the complete set of primary data was coupled with the preliminary correlation using the SigmaPlot Dynamic Fit Wizard. This process fine-tuned the exponents to have maximum *R*-squared values. The final correlation is as follows (Gupta et al., 2011):

Equation 4-1: Finalized Water HT Correlation- Wall Temperature approach (Gupta et. al, 2011)

$$\mathbf{Nu_w} = 0.0033\ \mathbf{Re_w^{0.941}}\ \overline{\mathbf{Pr}}_{\mathbf{w}}^{0.764} \left(\frac{\mu_w}{\mu_b}\right)^{0.398} \left(\frac{\rho_w}{\rho_b}\right)^{0.156}$$

Equation 4-1 has an uncertainty of about ±25% for HTC values and about ±15% for calculated wall temperature (see Figure 4-9 and Figure 4-10). Note that for the empirical correlations ±25% for HTC values is acceptable since they are used for preliminary calculations only and the errors are within the range of experimental uncertainty.

4.7.1.3 Verifying the New Correlation

Figure 4-9 and Figure 4-10 show scatter plots of the experimental values for HTC & wall temperature versus the calculated values using Equation 4-1 (Gupta et al., 2011).

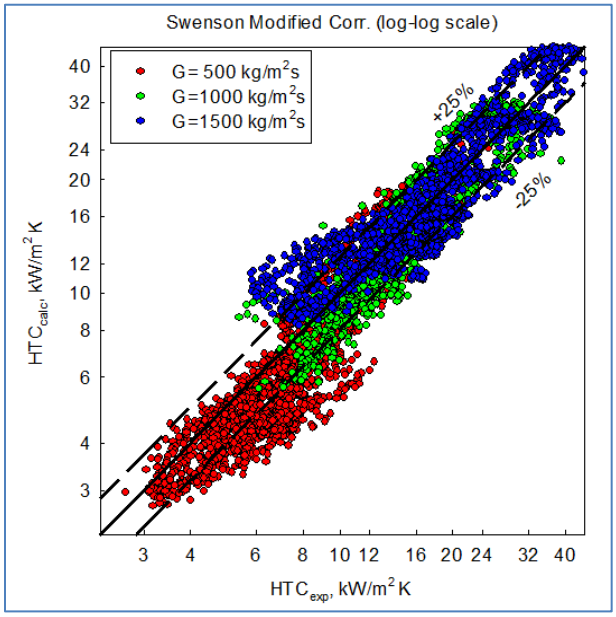

Figure 4-9: Comparison of data fit for HTC values using proposed correlation (Gupta et. al, 2011)

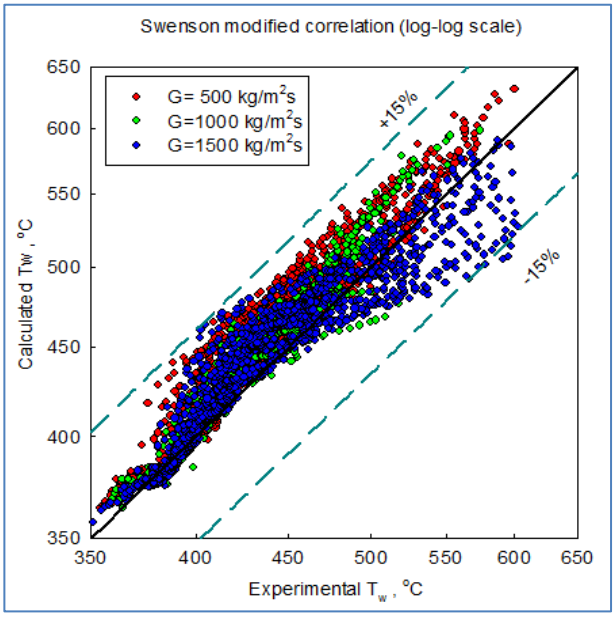

Figure 4-10: Comparison of data fit for Tw values using proposed correlation (Gupta et. al, 2011)

Figure 4-11, Figure 4-12 and Figure 4-13 below provide some additional comparison of experimental data with the results predicted by Equation 4-1 for three different mass and heat fluxes.

Figure 4-14 shows a comparison between experimentally obtained HTCs and wall-temperature values and those calculated with FLUENT CFD code produced by Vanyukova et al. (2009) and the proposed correlation Equation 4-1.

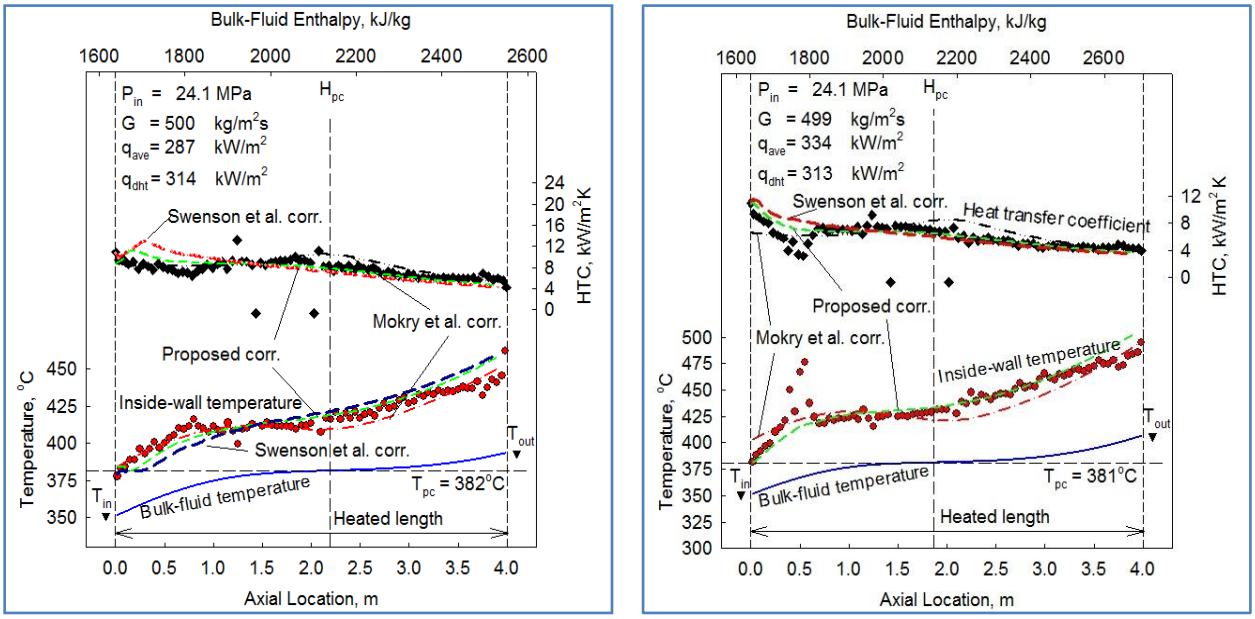

Figure 4-11: HTC variations at various heat fluxes along 4-m circular tube (D=10 mm): P_{in}=24.0 MPa and G=500 kg/m^{2}s (Gupta et. al, 2011)

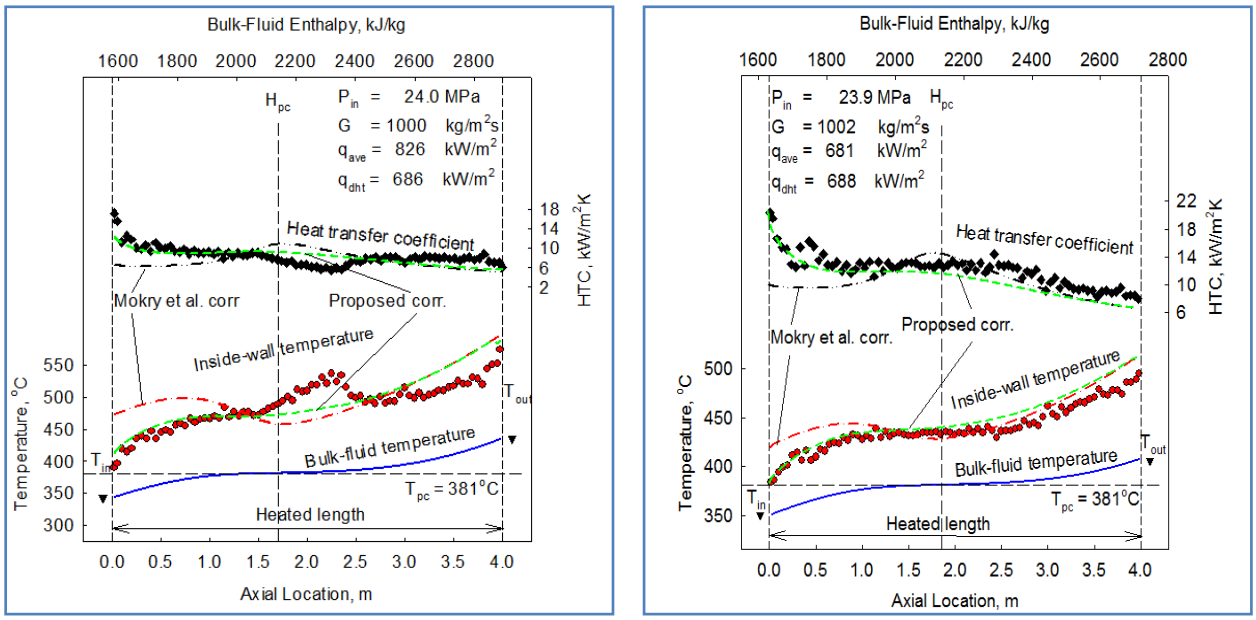

Figure 4-12: HTC variations at various heat fluxes along 4-m circular tube (D=10 mm): P_{in}=24 MPa and G=1000 kg/m^{2}s (Gupta et. al, 2011)

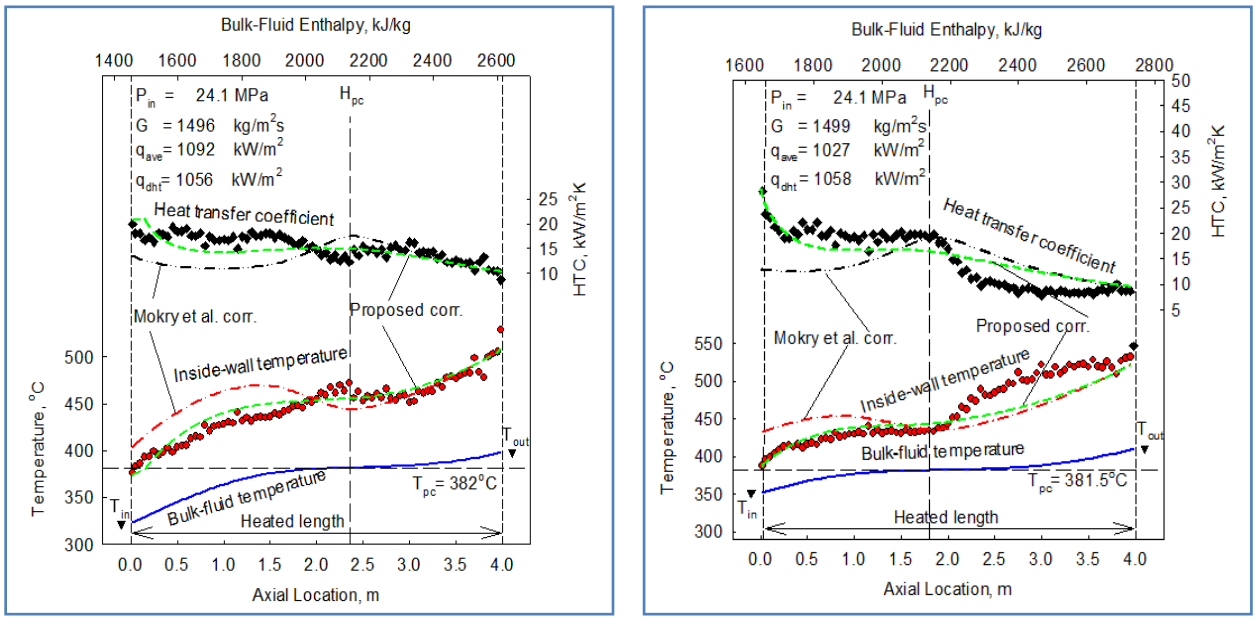

Figure 4-13: HTC variations at various heat fluxes along 4-m circular tube (D=10 mm): P_{in}=24 MPa and G=1500 kg/m^{2}s (Gupta et. al, 2011)

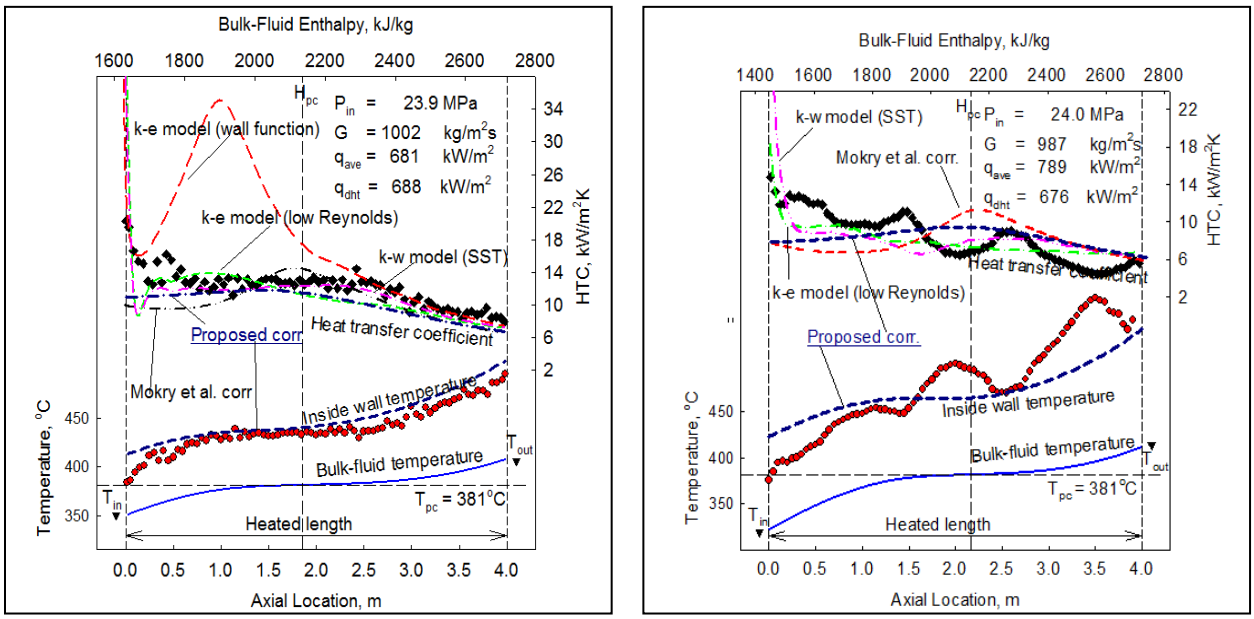

Figure 4-14: Comparison of values calculated with Equation 4-1 and FLUENT CFD- code with experimental data along 4-m circular tube (D=10 mm): P_{in}=24 MPa and G=1000 kg/m^{2}s. (Gupta et. al, 2011)

4.7.1.4 Entrance Effect

To make the proposed correlation even more accurate, a term accounting for the entrance-region effect can be added to Equation 4-1. This entrance-region effect was modeled by an exponentially decreasing term (see Equation 4-2):

Equation 4-2: Proposed Water Correlation with entrance effect (Gupta et. al, 2011)

$$\mathbf{Nu_w} = 0.0033\ \mathbf{Re_w^{0.941}}\ \overline{\mathbf{Pr_w}}^{0.764} \left(\frac{\mu_w}{\mu_b}\right)^{0.398} \left(\frac{\rho_w}{\rho_b}\right)^{0.156} \left[1 + exp\left(-\frac{x}{24D}\right)\right]^{0.3}$$

Where, x is the axial location and D is the diameter.

Equation 4-2 has an uncertainty of about ±25% for HTC and ±10% for calculated wall temperature (see Figure 4-15 and Figure 4-16), which is by far the most accurate prediction of the experimental data.

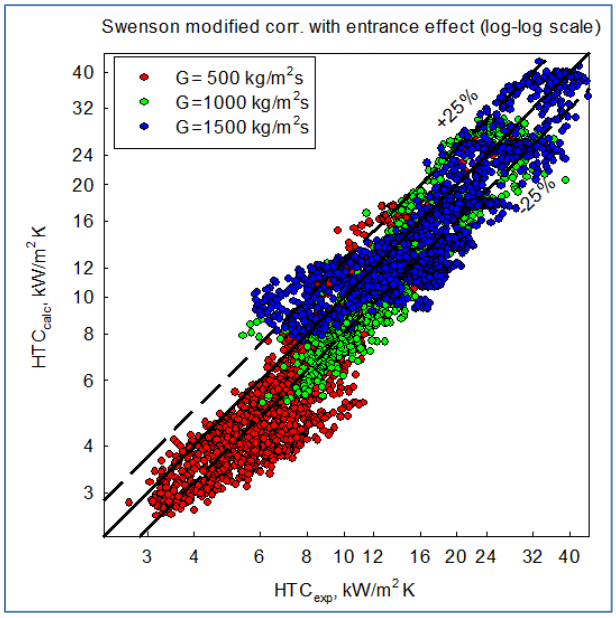

Figure 4-15: Comparison of data fit for HTC values using proposed correlation with entrance effect

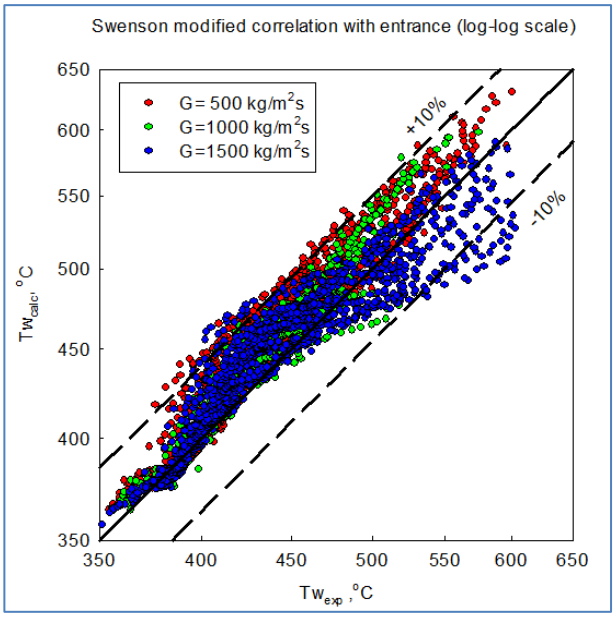

Figure 4-16: Comparison of data fit for *Tw* values using proposed correlation with entrance effect

4.7.2 Bulk-Fluid Temperature Approach

Recently, Mokry et al. (2009) used the Bishop et al. correlation as a starting point to come up with the following updated correlation that uses bulk-fluid temperature as characteristic temperature:

Equation 4-3: Mokry et al. 2009 Correlation (Bulk Temperature approach)

$$\mathbf{Nu_b} = 0.0061\ \mathbf{Re_b^{0.904}}\overline{\mathbf{Pr_b}}^{0.684}\left(\frac{\rho_w}{\rho_b}\right)^{0.564}$$

Equation 4-3 was also based on experimental dataset obtained by Kirillov et al. (2005) (as described previously throughout Section 4.1). It showed the best fit within the majority of the examined operating conditions with an uncertainty of about ±25% for HTC values and about ±15% for the calculated wall temperatures.

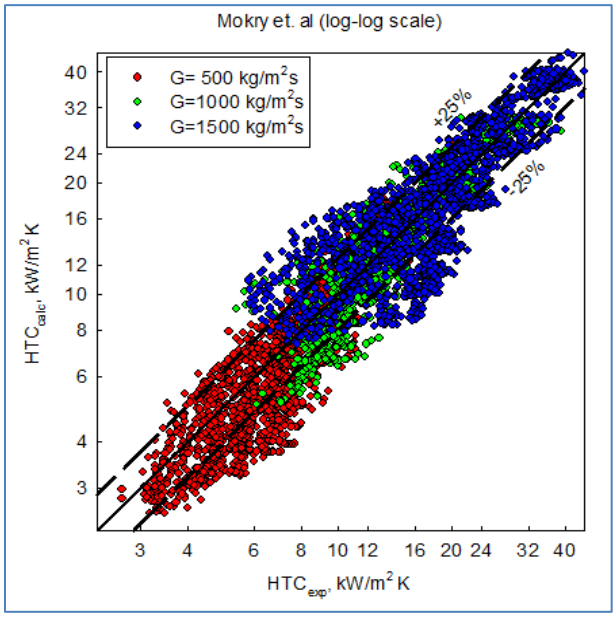

Figure 4-17: Comparison data fit for HTC values using Mokry Correlation

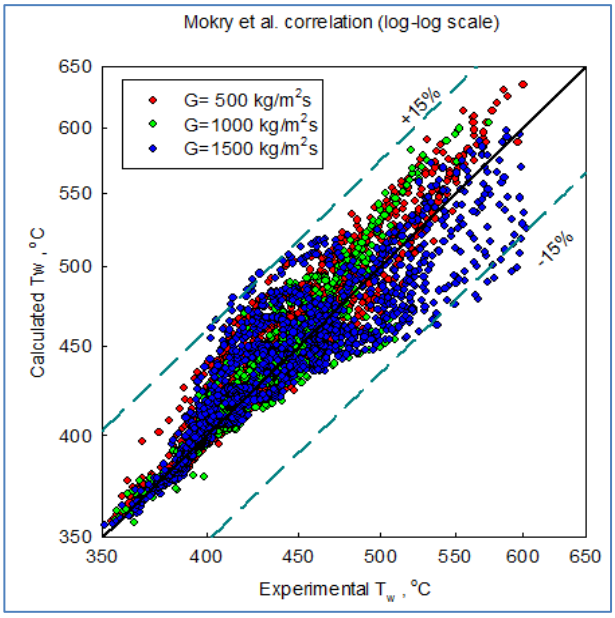

Figure 4-18: Comparison of data fit for T_w values using Mokry et al. correlation

The spread of the data in Figure 4-9 and Figure 4-10 (using Equation 4-1), is similar to the Figure 4-17 and Figure 4-18 (using Equation 4-3), indicating that both correlation have similar prediction capabilities. However, wall temperature approach seems to give slightly better results in terms of RMS and mean errors (as shown in Section 5.8).

4.7.3 Film-Fluid Temperature Approach

Methodology described in CHAPTER 3 was used to develop a new correlation based on the film temperature:

Equation 4-4: SC-Water Film-Temperature Correlation (Gupta et. al, 2011)

$$\mathbf{Nu_f} = 0.0041\ \mathbf{Re_f^{0.9284}}\ \overline{\mathbf{Pr_f}}^{0.7516} \left(\frac{\rho_w}{\rho_b}\right)^{0.2585} \left(\frac{\mu_w}{\mu_b}\right)^{0.3452}$$

Equation 4-4 showed an uncertainty of ±30% for HTC values and about ±15% for calculated wall temperatures.

4.8 Error Analysis for Water Correlations

All the points from 4 m Kirilov data were fed into the MATLAB code to determine the values predicted by the new correlation and compared with the experimental results.

Equations (Equation 3-2 to Equation 3-4) described in section 3.7 were used to calculate mean and HTC errors. Table 4-3 lists errors in the Mokry et al (2009), Swenson et al. (1965) correlations and the proposed correlation (Equation 4-2) for HTC values. In addition to show overall errors, the table also shows individual errors separated based on mass flux. A case excluding G = 200 kg/m^{2}s is also shown, as lower mass flux tends to give higher experimental uncertainty and it is likely that lower mass fluxes will not be used in SCWR.

Table 4-3: Errors in HTC values (In bold are the minimum values).

Correlations	**Mokry et al. (Bulk-fluid Temp. Approach)**		**Swenson et al.**		**Sahil et al. (Wall-fluid Temp. Approach)**		**Sahil et al. (Film Temp Approach)**	
Errors, %	**Mean**	**RMS**	**Mean**	**RMS**	**Mean**	**RMS**	**Mean**	**RMS**
Overall Data	3.3	32.0	**0.0**	27.3	– 0.7	**25.6**	1.5	29.9
G = 500 kg/m^{2}s	– 4.7	20.3	– 6.9	25.2	– 8.7	**19.9**	– 6.5	22.2
G =1000 kg/m^{2}s	– 1.2	18.3	– 0.9	24.5	– 1.4	**16.6**	**– 0.0**	18.8
G =1500 kg/m^{2}s	1.3	26.6	**3.9**	21.9	5.6	**21.5**	4.1	22.7
G = 200 kg/m^{2}s	14.4	47.0	3.5	**33.8**	**1.6**	35.4	7.2	43.2
Excluding G = 200 kg/m^{2}s	– 1.6	22.3	– 1.5	23.9	– 1.7	**19.7**	**– 1.0**	21.6

Table 4-4 lists errors in the Mokry et al., Swenson et al. correlations and the proposed correlation (Equation 4-2) for T_w values.

Table 4-4: Errors in wall temperature [18]values (in Bold are the minimum values).

Correlations	Mokry et. al.		Swenson et al.		Mod Swenson with entrance		Film Temp Corr.	
Errors, %	**Mean**	**RMS**	**Mean**	**RMS**	**Mean**	**RMS**	**Mean**	**RMS**
Overall Data	**0.6**	2.8	0.7	**2.3**	**0.7**	**2.3**	0.7	2.5
G = 500 kg/m^{2}s	**1.0**	2.3	1.2	2.4	1.2	**2.1**	1.1	2.1
G =1000 kg/m^{2}s	0.5	1.8	0.5	1.8	**0.3**	**1.3**	0.4	1.4
G =1500 kg/m^{2}s	**0.2**	3.0	0.3	**1.9**	0.5	2.2	**-0.2**	2.4
G = 200 kg/m^{2}s	**0.8**	3.5	1.2	**2.6**	1.3	2.9	1.3	3.3
Excluding G = 200 kg/m^{2}s	0.6	2.5	0.5	2.1	**0.4**	**1.2**	0.5	2.0

4.9 Independent Verification of Water Correlations

A recent study was conducted by Zahlan et al. (2010) in order to develop a heat-transfer look-up table for critical/supercritical pressures. For this study a large supercritical water databank has been compiled at the University of Ottawa. This databank covers a wide range of near-critical and supercritical heat-transfer conditions and was used for the assessment of existing HTC correlations. In their conclusions, Zahlan et al. stated that the Mokry et al. (2009) correlation showed the best prediction for the data within the supercritical region (see Table 4-5). The proposed correlation based on T_w also showed quite close results to those of Mokry correlation. Thus, both Mokry et al.(2009) and the proposed correlation can be used for calculations of HTCs in vertical bare tubes.

[18] T_w errors calculated as 1) Error = $\frac{Tw_{Cal}-Tw_{Exp}}{Tw_{Exp}(K)}$, 2) Mean Error= $\frac{\sum_{i=1}^{n} Error_i}{n}$ and 3) RMS error = $\sqrt{\frac{\sum_{i=1}^{n} Error_i^2}{n}}$

Table 4-5: Overall average and RMS errors in three supercritical sub-regions (Zahlan et al., 2011).

Correlation*	Liquid-like region		Gas-like region		Critical or pseudocritical regions	
	Error, %					
	Average	RMS	Avg.	RMS	Average	RMS
Bishop et al. (1964)	5	28	5	20	23	31
Swenson et al. (1965)	**1**	31	-16	21	4	23
Krasnochekov et al. (1967)	18	40	-30	32	24	65
Watts and Chou (1982), NHT	6	30	-6	21	11	28
Watts and Chou (1982), DHT	2	**26**	9	24	17	30
Griem (1996)	2	28	11	28	9	35
Koshizuka and Oka (2000)	26	47	27	54	39	83
Jackson (2002)	15	36	15	32	30	49
Mokry et al. (Equation 4-3)	-5	**26**	-9	**18**	**-1**	**17**
Kuang et al. (2008)	-6	27	10	24	-3	26
Cheng et al. (2009)	4	30	**2**	28	21	85
Gupta et al. (Equation 4-1)	-26	33	-12	20	**-1**	**18**

In bold – minimum values. * All these correlations can be found in Zahlan et al. (2011).

CHAPTER 5 SC CO_2 DATASET AND DEVELOPED CORRELATIONS

One of the enabling objectives of the study was to apply newly developed SC Water correlations for SC CO_2 data (recall the discussions of using SC CO_2 as a modelling fluid in Section 1.8). However, when SC Water correlations were directly applied to SC CO_2 data large errors were noticed (see Figure 2-44). It was concluded that due to the differences in thermophysical properties of water and CO_2 (recall discussions in Section 2.7); correlations cannot be directly applied between different fluids. Further studies are warranted to analyze modelling correction factors that may perhaps allow the use of SC Water correlations in other fluids. However, in the present study this attempt was unsuccessful and thus it was decided to develop correlations specifically for SC CO_2.

A large set of experimental data was obtained from Fuel Channel Thermalhydrauliccs (FCT) laboratory located at Chalk River (CRL)[19]. The experimental dataset was obtained at the MR-1 test facility (see Figure 5-1) at the CRL lab, which is a former steam/water high pressure and high-temperature pump loop adapted for use with supercritical CO_2 (Pioro and Duffey, 2007).

Its operating range is within high pressures up to 10.3 MPa and temperatures as high as 310°C. Carbon dioxide is charged into the loop with 99.9% purity and 0.8 ppm content of hydrocarbons.

5.1 Test Facility – AECL MR-1 Loop

The MR-1 loop (see Figure 5-1) is a high-temperature and high-pressure pumped loop. CO_2 (99.9% purity, content of hydrocarbons 0.8 ppm) passes through various sections of the loop starting at the centrifugal pump. The pump is fitted with a special seal and barrier-fluid cooling because CO_2 has poor lubricity so it cannot serve this function for the pump as it runs through the pump. The test section is powered by a 350 kW (175 V × 2000 A).

Fluid passes from the pump through an orifice flow meter, a 25 kW preheater, a test section, a cooler and back to the pump. The loop is pressurised by heating the CO_2 in a vessel with electrical heaters.

[19] Note experiments were previously performed and raw data was available in the form of excel files.

Heat is removed downstream of the test section using helicoil coolers and main loop heat exchangers in the discharge circuit of the pump using river water as a heat sink.

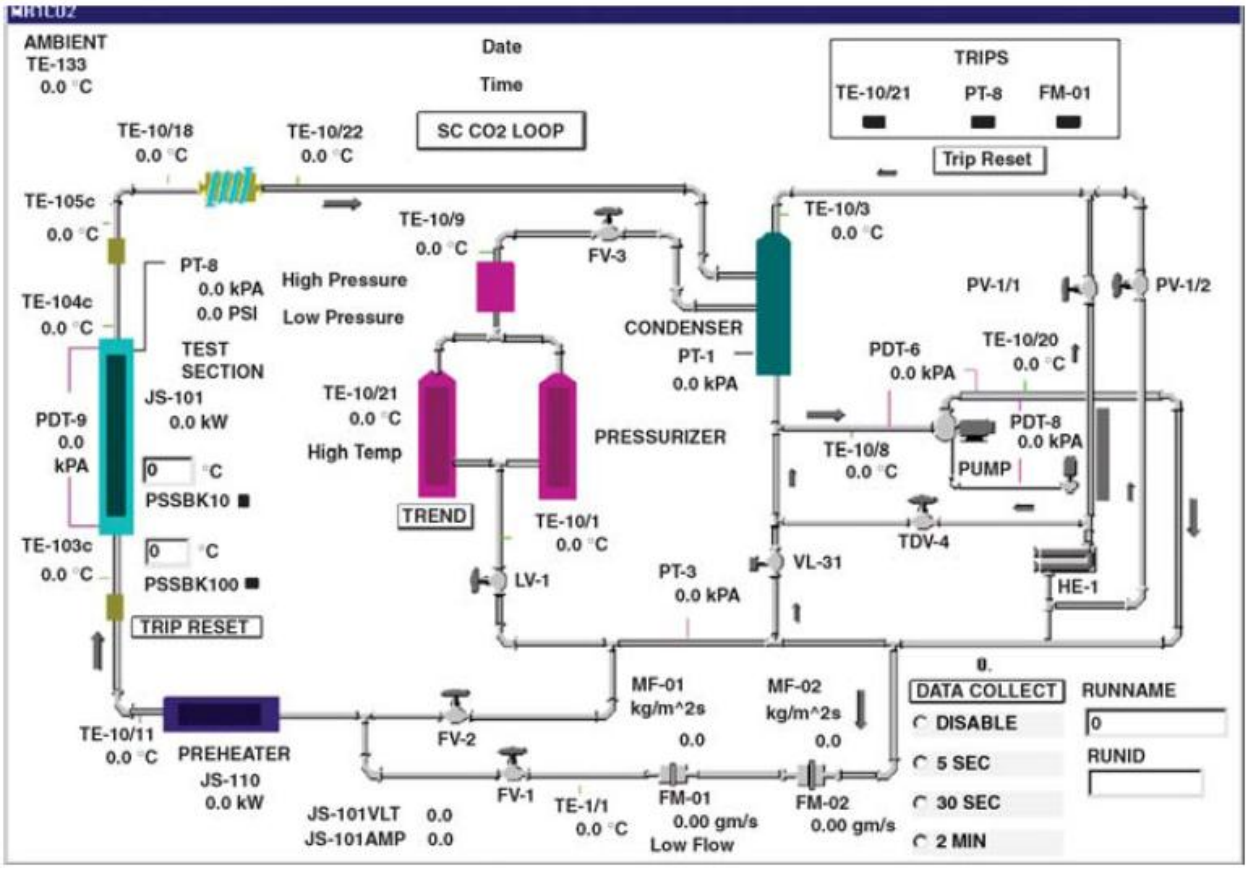

Figure 5-1: Fuel Channel Thermalhydraulics MR-1 Loop Schematic (Pioro and Duffey, 2007)

5.2 Test Section- Vertical Stainless Steel Circular Tube

The test section, shown in Figure 5-2, is made up of 2.4 m long Inconel 600 tube with an inner diameter (ID) of 8 mm, an outer diameter of 10 and 2.208 m of heated lenght. The diameter is close to the equivalent-hydraulic diameter of a typical subchannel in the CANFLEX® fuel bundle that is proposed for use in the SCW CANDU design. Direct electrical current passes through the tube wall that heats the fluid from the inlet to the outlet power terminals with the use of copper clamps. The test section and mixing chambers are wrapped with thermal insulation to minimize heat loss. The test section is attached with structural supports to a post to maintain its vertical orientation.

® CANFLEX is a registered trademark of AECL and the Korea Atomic Energy Research Institute (KAERI).

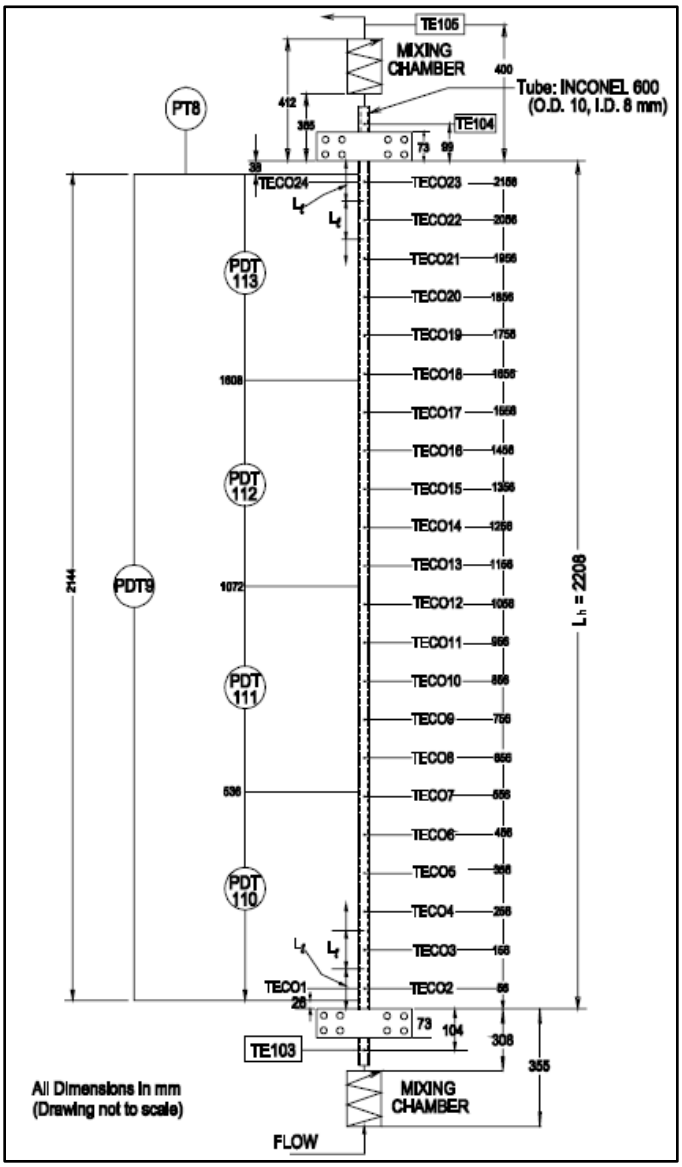

Figure 5-2: Test Section of MR-1 Loop Schematic (Pioro and Duffey, 2007)

5.3 Experimental Procedure

The experimental data were recorded by DAS when the desired flow conditions and power level was reached and stabilized. Stable conditions mean no visible variations in parameters with time. After that a new power level or/and new flow conditions were set up. The data was recorded during 1 minute in 5 seconds intervals.

Table 5-1: Data Matrix for CO_2 (adapted from Pioro and Duffey, 2007).

P (MPa)	T_{in} (°C)	T_{out} (°C)	T_w (°C)	q (kW/m^2)	G (kg/m^{2}s)
7.57 – 8.8	20 – 40	29 – 136	29 – 224	9.3 – 616.6	706 – 3169

5.4 Instrumentation and Test Section

The following test-section parameters were measured or calculated during the experiments (See Figure 5-2)

- Test-section current (based on the measured voltage drop across a calibrated shunt) and voltage. These parameters were used to calculate the power.
- Pressure at the test-section outlet.
- Four pressure drops over equal lengths (536 mm) along the test section.
- Temperatures at the test-section inlet and outlet. These temperatures were measured using 1/16″ K-type ungrounded sheathed thermocouples inserted into the fluid stream. The thermocouples were installed just downstream of the mixing chambers. The mixing chambers were used to minimize non-uniformity in the cross-sectional temperature distribution. The thermocouples were calibrated *in situ* within the temperature range of 0-100°C.
- Wall temperatures at equal intervals (100 mm) along the test section. Twenty-four fast response K-type thermocouples with self-adhesive fibreglass backing were attached to the tube outer wall and were wrapped with Teflon tape and fibreglass string to achieve proper contact with the wall. The temperature trip for the external wall temperature was set at 250°C. Thermocouples TEC02 to TEC023 were located at one side of the test section. Thermocouples TEC01 and TEC024 were located at the same° axial locations as thermocouples TEC02 and TEC023, but 180° apart. All fast-response thermocouples were calibrated *in situ* within the range of 0-100°C prior to use.
- CO2 mass-flow rate. Loop mass-flow rate was calculated based on the measured pressure drop over a small orifice plate, which was monitored with a differential-pressure (DP) cell.
- Ambient temperature.

5.5 Uncertainty in Instrumentation and Test Data

Table 5-2 displays the uncertainty in the instrumentation in the MR-1 Loop.

Table 5-2: Uncertainty of measured and calculated parameters in MR-1 Loop (Pioro and Duffey, 2007).

Parameter	Uncertainty
Test Section Power	±0.46% for P = 3 kW ±0.30% for P = 35 kW
Absolute Pressure	±0.2%
Differential-Pressure Cells	$\pm 30.1\% \; for \; \Delta p_{min} = 5$ kPa $\pm 2.2\% \; for \; \Delta p_{max} = 70$ kPa
Average Heat Flux	±0.53% for $q_{ave\ min}$ =53.7 kW ±0.39% for $q_{ave\ max}$ =626.2 kW
Temperatures	±0.3°C within 0-100°C ±2.2°C beyond 100°C
Mass Flow rates	±12.5% at t=19°C and p=8.36 MPa for m_{min}= 46 g/s (G=902 kg/m^{2}s) ±1.6% at t=19°C and p=8.36 MPa for m_{max}= 155 g/s (G=3039 kg/m^{2}s)
Electrical Resistivity	±0.20% for L=2461mm
Thermophysical Properties (near pseudocritical point)	$\Delta\rho = \pm 7\%; \Delta H = \pm 2.5\%;$ $\Delta c_p = \pm 4.5\%; \; \Delta k = \pm 2\%;$ $\Delta\mu = \pm 7\%;$

5.6 Data Reduction

The objective of this part of the study was to develop an updated CO_2 heat-transfer correlation for the IHT and NHT regime. Therefore, data points in the DHT regions were removed from the dataset (please see Figure 5-3). The DHT region is subject to future investigations. Abnormalities, such as defective thermocouple readings were also removed from the dataset. Overall, approximately 88% of the experimental data were used to develop the correlation.

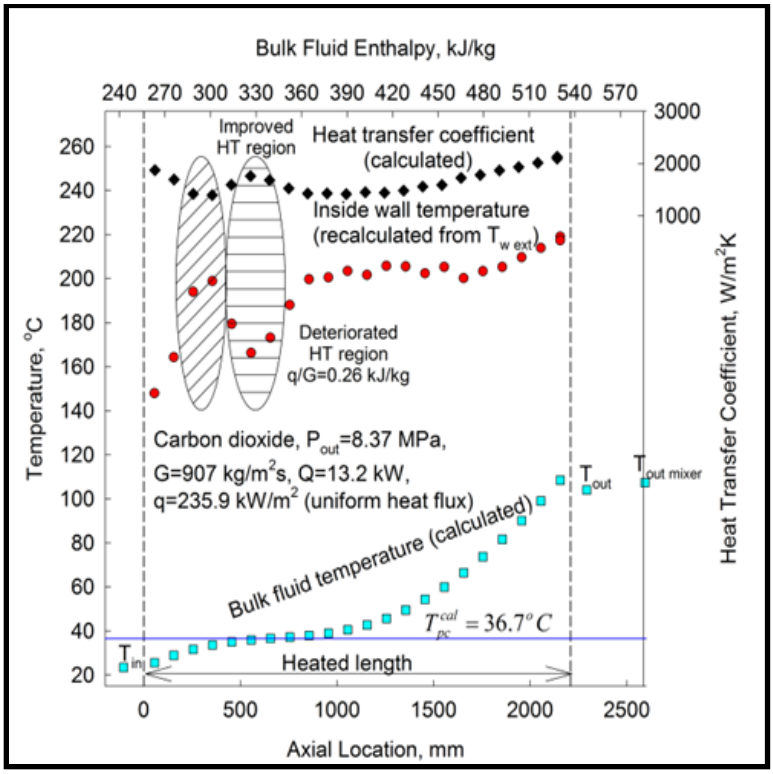

Figure 5-3: Example of data reduction for DHT regimes removed from dataset (Gupta et. al, 2012)

5.7 Development of HTC Correlations for Carbon Dioxide

The new correlations developed for SCW (Mokry et al., 2009 and Gupta et al., 2011), which show good results for SCW data, cannot be directly applied to SC CO_2, as the thermophysical properties of the two fluids differ significantly (refer to discussions in Section 2.7). Therefore, new empirical heat-transfer correlations based on bare-tube CO_2 data and latest thermophysical properties were developed.

Please refer to Section 4.7 for approach to developing correlation for water, as the same methodology was used for the development of the correlations for carbon dioxide.

5.7.1 Wall-Temperature Approach

A new wall-temperature approach correlation was also found using the same approach and is presented in Equation 5-1

Equation 5-1: SC CO_2 Correlation using Wall Temperature Approach (Gupta et. al, 2012)

$$\mathbf{Nu_w} = 0.0038\mathbf{Re_w^{0.957}Pr_w^{-0.139}}\left(\frac{\rho_w}{\rho_b}\right)^{0.836}\left(\frac{k_w}{k_b}\right)^{-0.754}\left(\frac{\mu_w}{\mu_w}\right)^{-0.222}$$

Preliminary error analysis shows that the proposed wall-temperature correlation better predicts the experimental dataset.

The spread of the data was roughly ±30% and ±20% for HTC and wall temperatures. These values can be seen in Figure 5-4, Figure 5-5 and Figure 5-6 where the comparison between calculated HTC vs. experimental HTC is displayed for various parameters. Figure 5-7, Figure 5-8 and Figure 5-9 display wall temperatures. They are arranged in different ranges of mass flux, pressure and heat flux respectively.

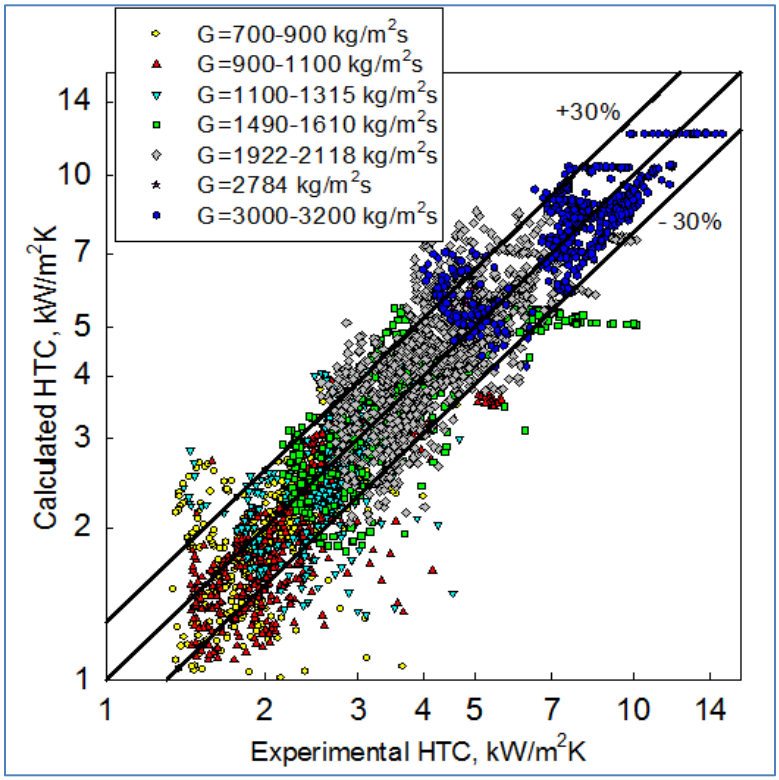

Figure 5-4: Calculated vs. Experimental HTC for Various Mass Fluxes

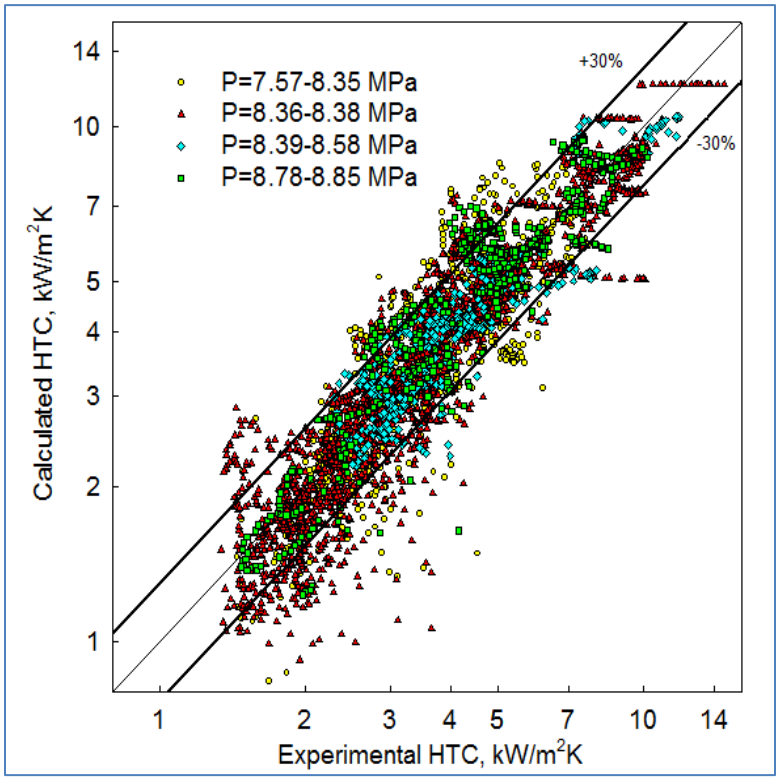

Figure 5-5: Calculated vs. Experimental HTC for Various Pressures

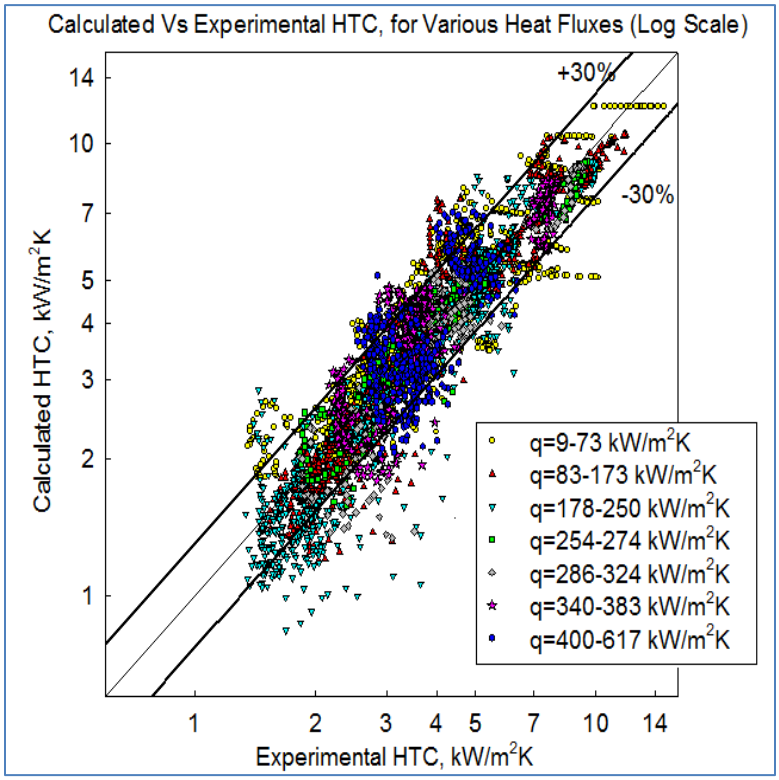

Figure 5-6: Calculated vs. Experimental HTC for Various Heat Fluxes

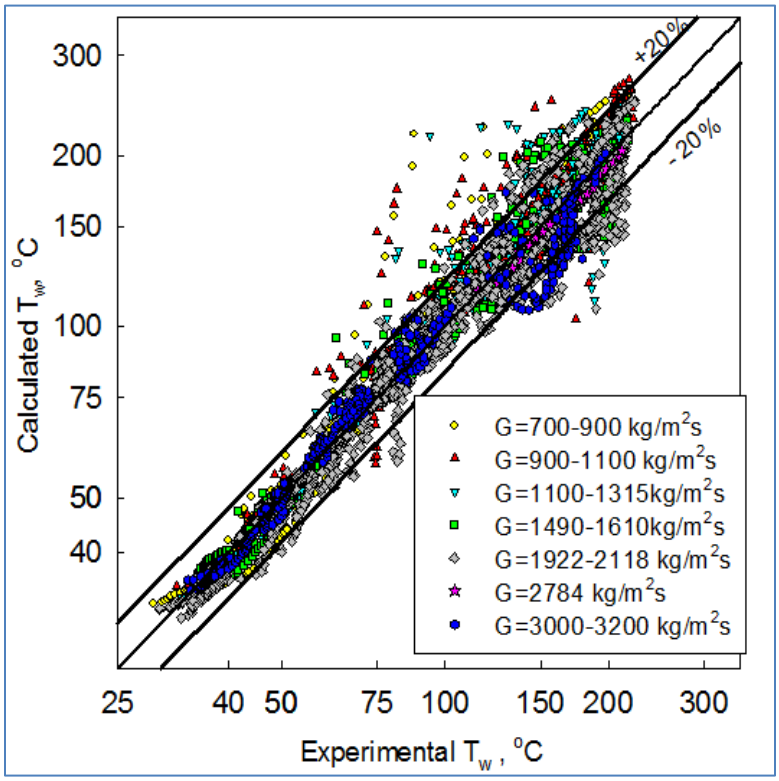

Figure 5-7: Calculated vs. Experimental T_w for Various Mass Fluxes

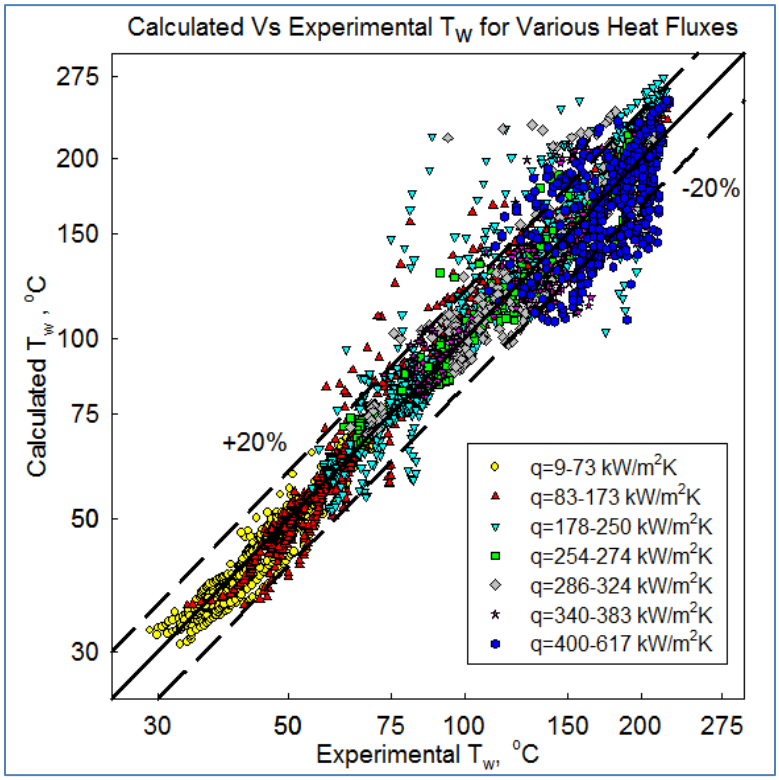

Figure 5-8: Calculated vs. Experimental T_w for Various Heat Flux

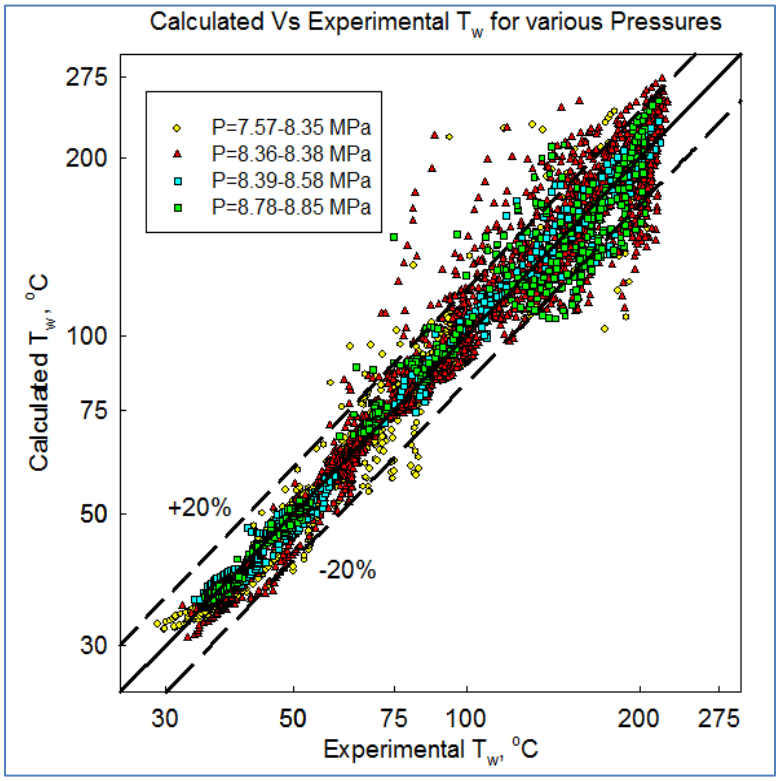

Figure 5-9: Calculated vs. Experimental T_w for Various Pressures

5.7.2 Bulk-Temperature Approach

The initial bulk temperature correlation (Equation 5-2) based on the CO_2 data was first proposed by Mokry et al. (2011) for supercritical carbon dioxide.

Equation 5-2: Bulk Correlation for CO_2 (Mokry et al.2011)

$$\mathbf{Nu_b} = 0.0121\mathbf{Re_b}^{0.86}\overline{\mathbf{Pr}}_{\mathbf{b}}^{0.23}\left(\frac{\rho_w}{\rho_b}\right)^{0.59}$$

Figure 5-10 shows a scatter plot of the calculated **Nu** versus the experimental **Nu** from Equation 5-2.

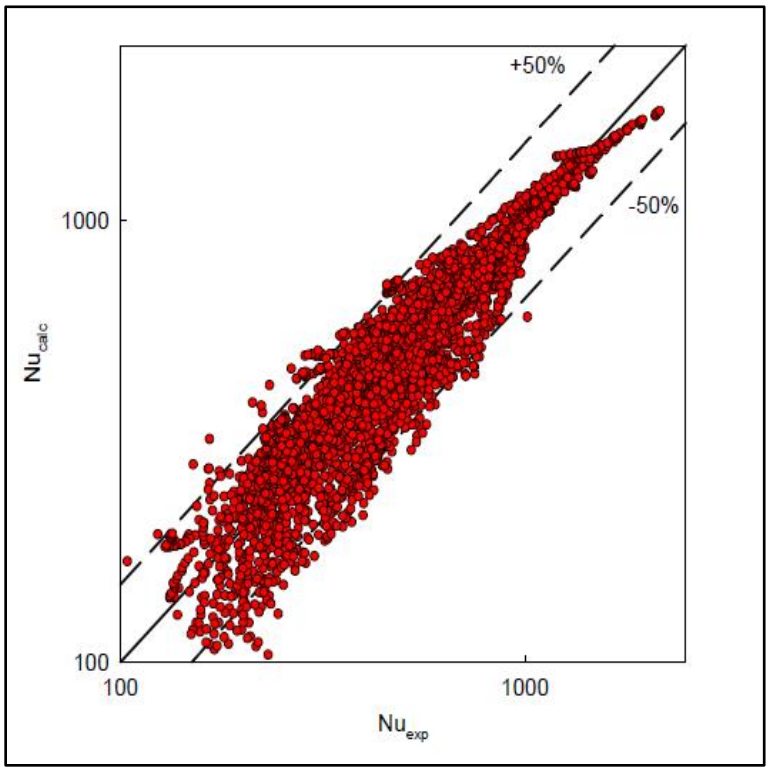

Figure 5-10: Calculated Nu versus Experimental Nu for using Mokry et al. SC CO_2 correlation

As Figure 5-10 shows, the correlation has a fairly high inaccuracy with data spread over ±50% around experimental values. A more thorough analysis of the experimental data was suggested for this correlation given the results produced.

Thus, it was decided to develop a new bulk-temperature correlation for the dataset using the methodology described in section CHAPTER 3 and the model Equation 3-1. The resulting correlation is as follows:

Equation 5-3: SC CO_2 Correlation using Bulk Temperature Approach (Gupta et. al, 2012)

$$\mathbf{Nu_b} = 0.0094\ \mathbf{Re_b^{0.892}}\ \overline{\mathbf{Pr_b}}^{-0.141} \left(\frac{\rho_w}{\rho_b}\right)^{0.926} \left(\frac{k_w}{k_b}\right)^{0.216} \left(\frac{\mu_w}{\mu_b}\right)^{-1.128}$$

5.7.3 Film-Temperature Approach

The film-temperature approach correlation is shown in Equation 5-4. It is interesting to note that using the film temperature approach, the reduced dataset showed no dependence on Prandtl number.

Equation 5-4: SC CO_2 Correlation using Film Temperature Approach (Gupta et. al, 2012)

$$\mathbf{Nu_f} = 0.0043\,\mathbf{Re_f^{0.935}}\left(\frac{\rho_w}{\rho_b}\right)^{0.572}\left(\frac{k_w}{k_b}\right)^{-0.524}$$

5.8 Error Analysis for Carbon Dioxide Correlations

Error analysis was conducted in the same manner as in the water error analysis. Table 5-3 presents the errors associated with the reduced dataset calculated using equations proposed in section 5.7. On analyzing values from Table 5-3, it is seen that correlation based on wall approach predicts the reference dataset with the least RMS error. It can also be seen that the HTC errors associated with correlations developed for SC water are huge, which further reiterates that these correlations cannot be directly applied towards SC CO_2.

Table 5-3: Mean and RMS Errors in predicted HTC and T_w values for SC CO_2.

Mean and RMS Errors in predicted HTC and T_w values				
	HTC		**T_w[20]**	
	Mean Error%	**RMS % (relative deviation)**	**Mean Error%**	**RMS % (relative deviation)**
Mokry et al. corr. for SC CO_2 (Bulk Fluid Approach) - Equation 5-2	5.1	32.2	1.5	8.8
Proposed new correlation (Bulk Approach) - Equation 5-3	0.9	22.4	1.3	7.4
Proposed new correlation (Wall Approach) - Equation 5-1	0.8	**20.3**	0.8	4.5
Proposed new correlation (Film Approach) - Equation 5-4	**0.2**	21.7	0.9	**4.3**
Swenson et. al (1965) Corr.	89.3	131.6	– 3.7	4.9
Mokry et. al (2009) Corr.	68.2	123.0	**0.3**	7.2
Gupta et. al (2011) Corr.	77.6	129.8	– 2.2	**4.2**

[20] T_w Errors were calculated as formula 1) Error = $\frac{Tw_{Cal}-Tw_{Exp}}{Tw_{Exp}(K)}$,

2) Mean Error= $\frac{\sum_{i=1}^{n} Error_i}{n}$ and 3) RMS error = $\sqrt{\frac{\sum_{i=1}^{n} Error_i^{\,2}}{n}}$

Figure 5-11 to Figure 5-15 presents the results of the new correlation against specific test runs with varying flow parameters.

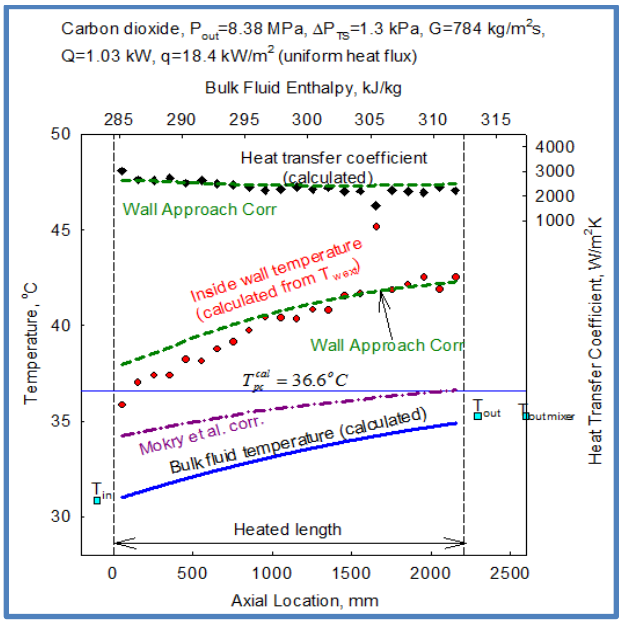

Figure 5-11: Specific Test Run Results; *P*=8.38 MPa, *G*= 784 kg/m^{2}s, *Q*=1.03 kW and *q* = 18.4 kW/m^2 (Gupta et. al, 2012)

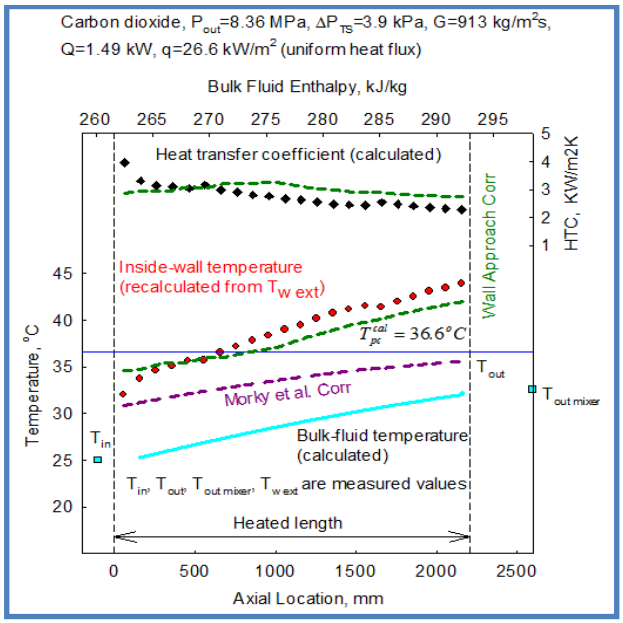

Figure 5-12: Specific Test Run, *P*=8.36 MPa, *G* =913 kg/m^{2}s. *Q*=1.49 kW and *q*=26.6 kW/m^2 (Gupta et. al, 2012)

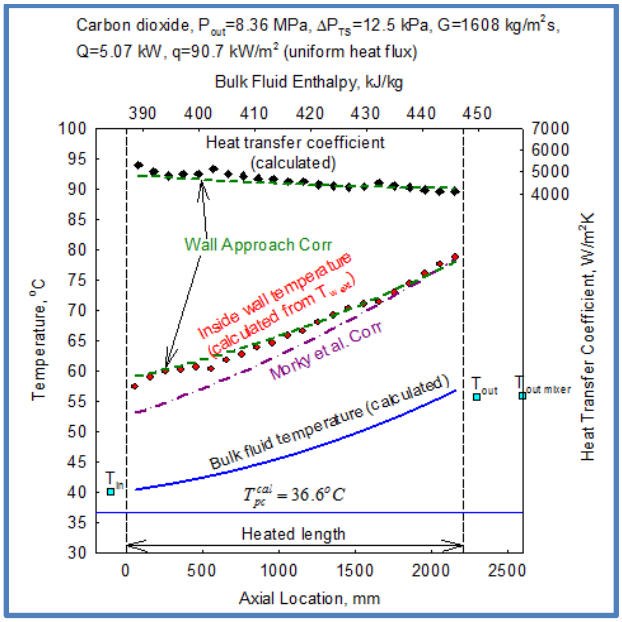

Figure 5-13: Specific Test Run, *P*=8.36 MPa, *G* =1608 kg/m^{2}s. *Q*=5.07 kW and *q*=90.7 kW/m^2 (Gupta et. al, 2012)

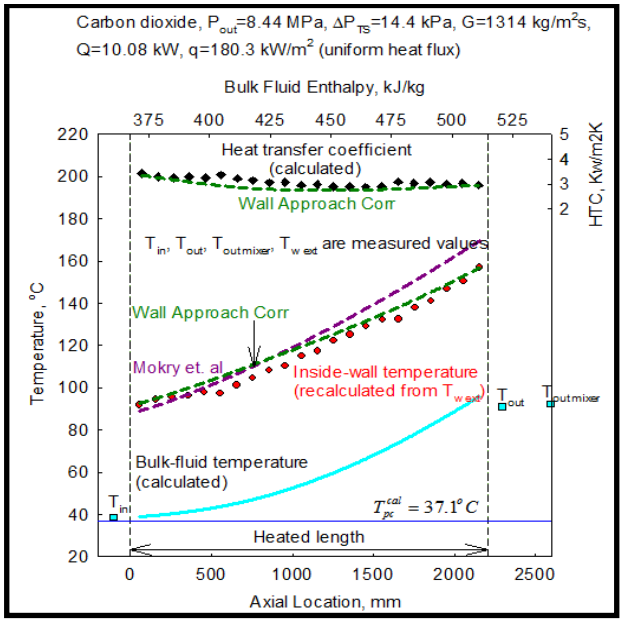

Figure 5-14: Specific Test Run, *P*=8.44 MPa, *G* =1314 kg/m^{2}s. *Q*=10.08 kW and *q*=180.3 kW/m^2

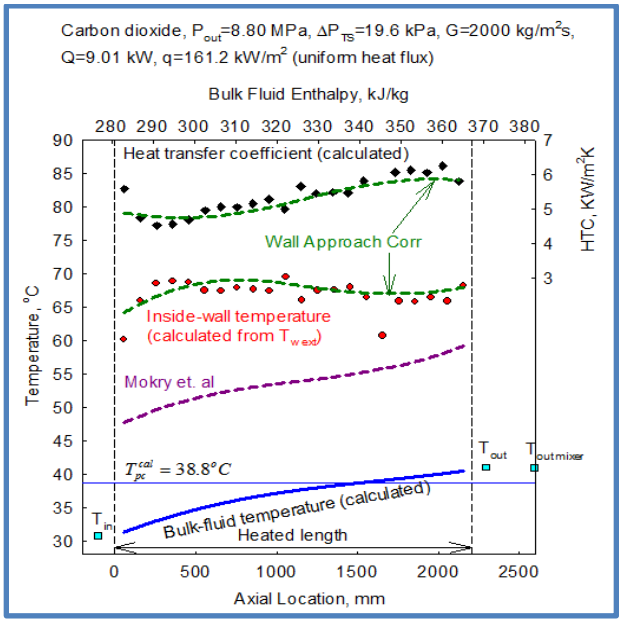

Figure 5-15: Specific Test Run, *P*=8.80 MPa, *G* =2000 kg/m^{2}s. *Q*=9.01 kW and *q*=161.2 kW/m^2 (Gupta et. al, 2012)

5.9 Comparison with Other CO_2 Datasets

Literature survey was conducted to filter for papers that contained $SCCO_2$ data-points. Datasets collected from He et. al (2005) , Kim et al. (2005) and Koppel (1960) were considered An Excel

dataset was compiled by digitizing the graphs from these papers using UN-SCAN-IT Graph Digitizing Software (Silk Scientific Inc.).

It must be noted that error analysis presented in subsequent sections are the results obtained from digitized datasets. In addition to experimental uncertainties associated with instrumentations and testing, they also contain an inherent imprecision of digitizing the data-points from UN-SCAN-IT. Statistically they also represent a much smaller dataset. Hence the absolute values of the errors should be considered relevant only for comparison purposes. AECL dataset on the other hand was obtained directly from Data Acquisition Software (DAS) in raw form and experimental uncertainties were carefully controlled and well documented (refer to section 5.4). Nevertheless, the results can show relative trends and can be a valid tool for comparative analysis.

5.9.1 Kim et. al. dataset (2005)

Kim et. al. (2005) dataset consisted of points collected in an upward flow of $SCCO_2$ operating at the constant pressure of 8MPa. Refer to Table 5-4 for test-matrix parameters and Figure 5 for schematic of test loop.

Table 5-4: Test-Matrix Parameters – Kim et al., 2005.

Flow Orientation	Upwards
Flow Geometry	Vertical tubes with circular, triangular and square cross-sections
Pressure (P)	8 MPa
Bulk Temperatures (T_b)	15 – 32 °C
Wall Temperatures (T_w)	27 – 100 °C
Heat Flux (q)	3 – 180 kW/m^2
Mass velocity (G)	209 - 1230 kg/m^{2}s
Reynolds numbers (Re)	3 x 10^4 – 1.4 x 10^5
Entrance region	600 mm
Heated region	1200 mm
Hydrodynamic Diameter (D_{hy})	7.8 mm (circular tube) 9.8 mm (triangular tube) 7.9 mm (square tube)

Only circular tube geometry was considered for error analysis in this report. The final compiled dataset consisted of 451 points. HTC and T_w values were calculated based on various existing and the new proposed correlations using MATLAB codes. These calculated values were then compared to experimental data. Table 5-5 lists Mean and RMS errors in HTC and T_w for Kim et al. dataset.

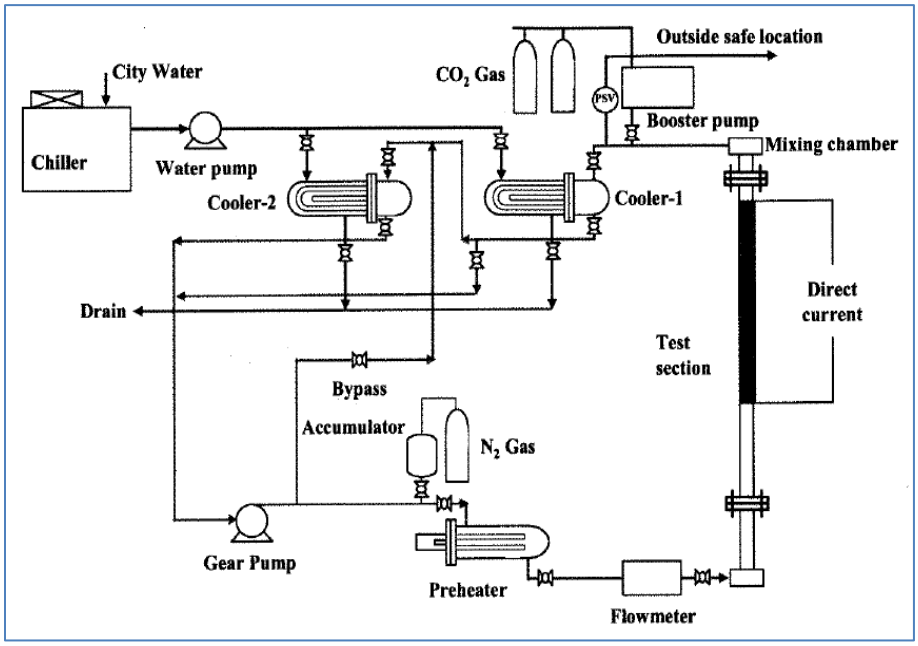

Figure 5-16: Schematic of Test Loop – Kim et. al (2005)

Table 5-5: Mean and RMS errors for HTC values- Kim et al. dataset (Gupta et. al, 2012).

	Errors in *HTC*		Errors in T_w	
	Mean Error%	**RMS % (relative deviation)**	**Mean Error%**	**RMS % (relative deviation)**
Dittus-Boelter (1930)	88	131	– 3.5	6.1
Swenson et al. (1965) Corr.	28	80	3.1	12.2
Jackson et al. (2002)	57	144	11	28.1
Mokry et. al (2009) SCW Corr.	– 13	55	12.4	27.3
Mokry et al. (2009) $SCCO_2$ Corr.	– 53	56	16.5	24.4
Gupta et al. (2011) SCW Corr.	– 17	50	8.5	16.4
Bulk Approach- Equation 5-3	– 40	47	12.1	21.4
Film Approach- Equation 5-4	– 44	51	14.3	23.2
Wall Approach- Equation 5-1	– 45	51	16.8	31.3

5.9.2 He et. al. dataset (2005)

He et. al. (2005) dataset consisted of points collected in an upward flow of $SCCO_2$ in a vertical tube of 0.948 mm diameter. Refer to Table 5-6 for test-matrix parameters.

Table 5-6: Test-Matrix Parameters – He et al. dataset.

Flow Orientation	Upwards
Flow Geometry	Vertical tube
Pressure (P)	8.4 – 9.6 MPa
Bulk Temperatures (T_b)	32 – 52 °C
Wall Temperatures (T_w)	28 – 80 °C
Heat Flux (q)	30 – 70 kW/m^2
Mass velocity (G)	540 - 665 kg/m^2s
Reynolds numbers (Re)	9×10^3 – 2.5×10^4
Heated region	0.05 m
Hydrodynamic Diameter (D_{hy})	0.95 mm (circular tube)

The final compiled dataset consisted of 108 points. Table 5-7 lists Mean and RMS errors in HTC and T_w for He et al. dataset.

Table 5-7: Mean and RMS errors for HTC values- He et al. dataset (Gupta et. al, 2012).

	Errors in *HTC*		**Errors in T_w**	
	Mean Error%	**RMS % (relative deviation)**	**Mean Error%**	**RMS % (relative deviation)**
Dittus-Boelter (1930)	58	75	– 1.3	1.7
Swenson et al. (1965) Corr.	10	21	-0.2	0.6
Jackson et al. (2002)	45	53	– 1.0	1.1
Mokry et. al (2009) SCW Corr.	18	29	– 0.3	0.7
Mokry et al. (2009) $SCCO_2$ Corr.	– 23	40	1.6	2.8
Gupta et al. (2011) SCW Corr.	– 3	23	0.6	1.3
Bulk Approach- Equation 5-3	– 34	43	2.2	2.8
Film Approach- Equation 5-4	– 45	48	3.1	3.6
Wall Approach- Equation 5-1	– 49	53	3.8	4.4

5.9.3 Koppel et. al. dataset (1960)

Koppel et. al. (1960) dataset consisted of points collected in a horizontal flow of $SCCO_2$ in an Inconel. Refer to Table 5-8 for test-matrix parameters. Figure 5-17 and Figure 5-18 shows schematics of the test loop.

Table 5-8: Test-Matrix Parameters – Koppel (1960) dataset.

Flow Orientation	Horizontal
Flow Geometry	Inconel Tube
Pressure (P)	7.2 – 8.3 MPa
Bulk Temperatures (T_b)	30 – 48 °C
Wall Temperatures (T_w)	74 – 132 °C
Heat Flux (q)	100 – 225 kW/m^2
Mass velocity (G)	450 – 870 kg/m^{2}s
Reynolds numbers (Re)	4.3 x 10^4 – 2.2 x 10^5
Heated region	0.45 m
Hydrodynamic Diameter (D_{hy})	5.1 mm (circular tube)

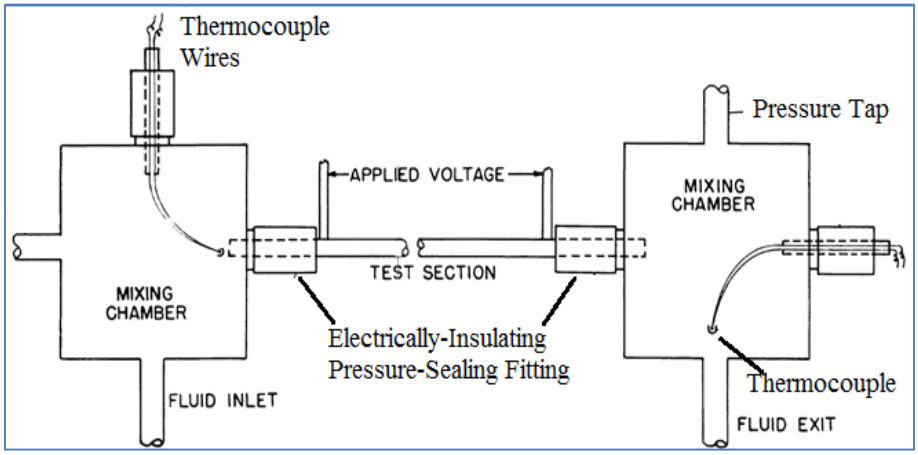

Figure 5-17: Test Section Details – Koppel et. al (1960) (adapted)

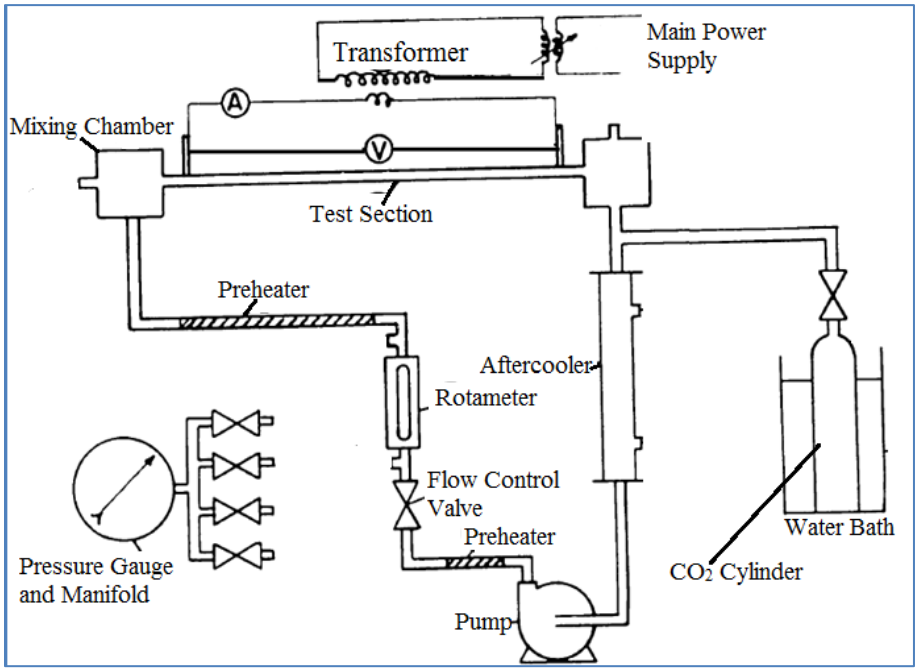

Figure 5-18: Schematic of Test Loop – Koppel et. al (1960) (adapted)

The final compiled dataset that was analyzed consisted of 43 points. Table 5-9 lists Mean and RMS errors in HTC and T_w for He et al. dataset. It is to be noted that these results for Koppel et. al. may not be statistically relevant since only 43 points were digitized. Nevertheless, the results still hold value in terms of comparing various HTC correlations.

Table 5-9: Mean and RMS errors for HTC values- He et al. dataset (Gupta et. al, 2012).

	Errors in *HTC*		**Errors in T_w**	
	Mean Error%	**RMS % (relative deviation)**	**Mean Error%**	**RMS % (relative deviation)**
Dittus-Boelter (1930)	352	477	– 10.8	11.4
Swenson et al. (1965) Corr.	– 32	34	8.5	9.3
Jackson et al. (2002)	–70	72	58.9	71.5
Mokry et. al (2009) SCW Corr.	– 45	47	16	17.6
Mokry et al. (2009) $SCCO_2$ Corr.	– 20	35	7.2	11.7
Gupta et al. (2011) SCW Corr.	– 41	43	12.3	12.9
Bulk Approach- Equation 5-3	– 27	43	11.7	16.3
Film Approach- Equation 5-4	– 45	47	15.6	17.1
Wall Approach- Equation 5-1	– 43	48	17.3	20.7

CHAPTER 6 DISCUSSIONS, SUMMARY AND CONCLUDING REMARKS

6.1 Theoretical Comparison of HTC Profiles in CO_2 and Water

From the discussions of the previous sections (especially Section 2.7), one can see that while the behaviour of supercritical fluids (in our case water and CO_2) is similar, yet at the same time it is difficult to come up with a correlation for HTC that applies to both fluids. These difficulties arise from the vast difference in absolute values of the thermo-physical parameters for water and CO_2. Also, due to the difference of thermo-physical parameters, the effectiveness of CO_2 and water as a heat transfer fluid can significantly vary. Thus, an important aspect that should be investigated is the comparison of HTC values between that of water and CO_2 at different flow conditions. In general, water has a much higher performance as a heat transfer fluid than CO_2, but to investigate deeper into this aspect, HTC profiles of CO_2 and Water were compared over a wide range of flow conditions. The profiles are shown in Figure 6-1 to Figure 6-3 below. To generate these profiles, Mokry et. al correlation (Equation 4-3) was used for water and the new correlation developed for CO_2 using wall approach (Equation 5-1) was used for CO_2 profiles.

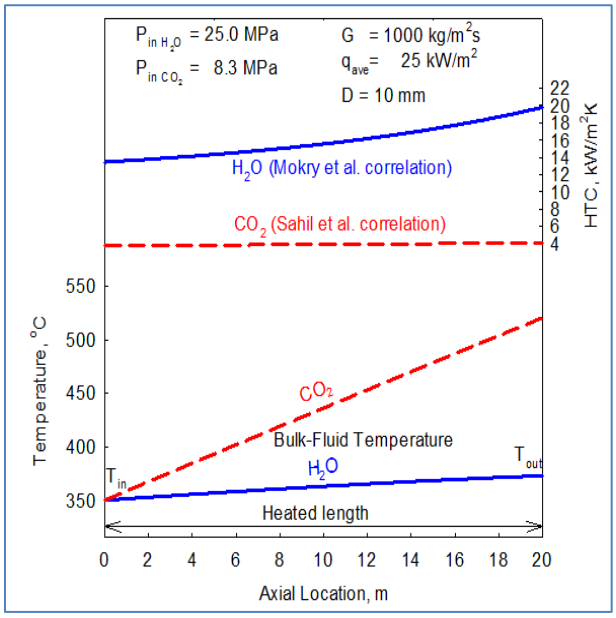

(a)

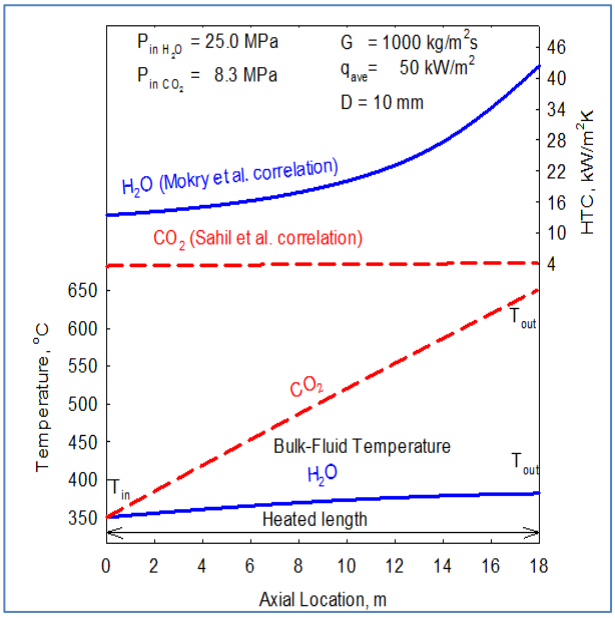

(b)

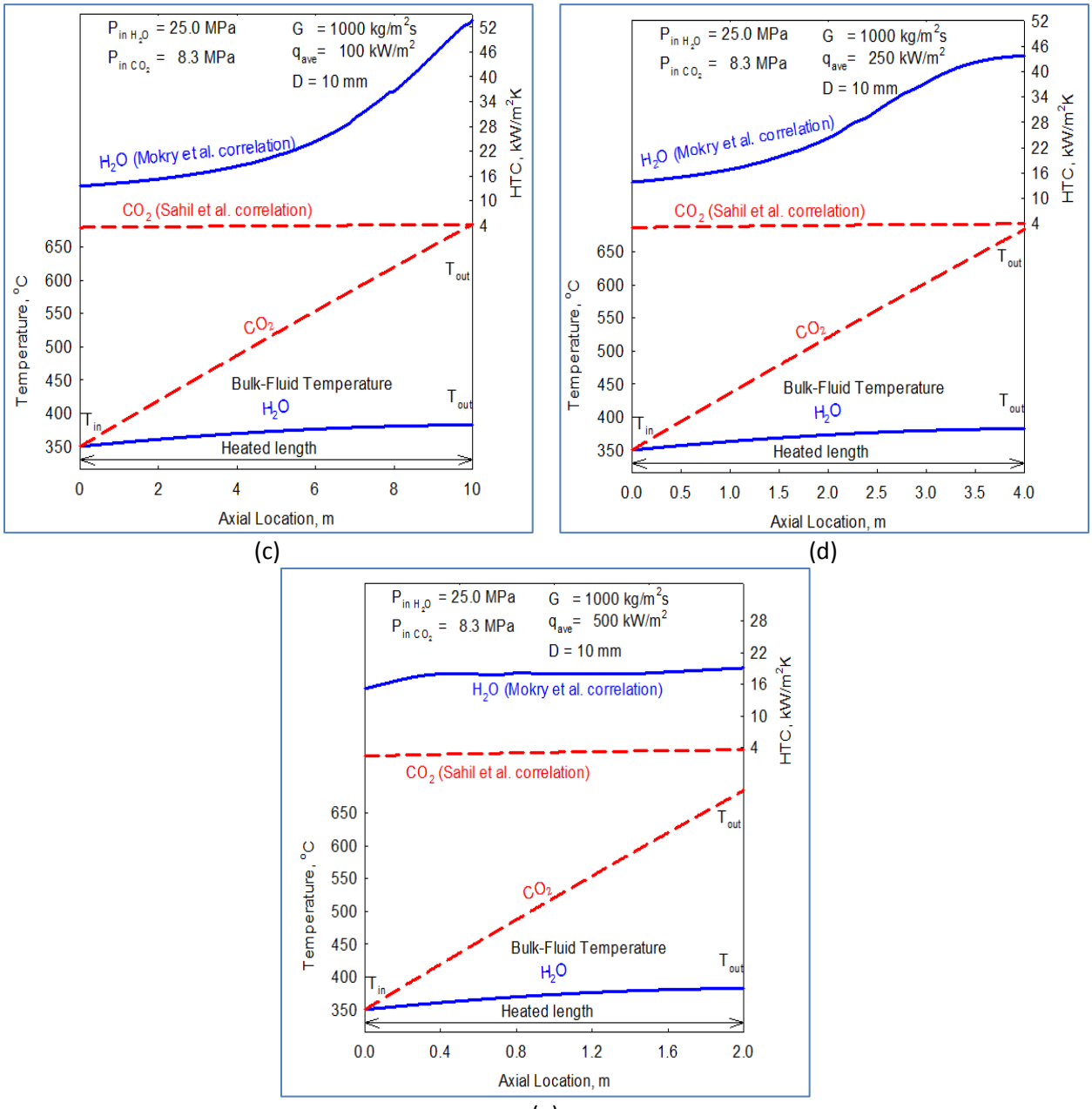

Figure 6-1: CO_2 and Water comparison for G =1000 kg/m^{2}s; D =10 mm (a) q_{ave}= 25 kW/m^2 (b) q_{ave}= 50 kW/m^2 (c) q_{ave}= 100 kW/m^2 (d) q_{ave}= 250 kW/m^2 (e) q_{ave}= 500 kW/m^2

As expected, it can be seen that the HTC values for water is much higher than CO_2 values. This also means that for HX applications of SC fluids, a CO_2 HX would have to be much longer than water HX to achieve the same heat transfer exchange.

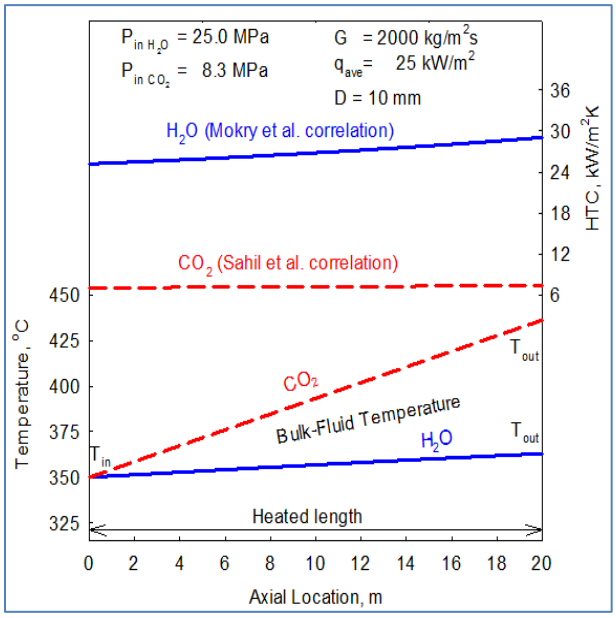
$P_{in\ H_2O}$ = 25.0 MPa
$P_{in\ CO_2}$ = 8.3 MPa
G = 2000 kg/m^{2}s
q_{ave} = 25 kW/m^2
D = 10 mm
H_2O (Mokry et al. correlation)
CO_2 (Sahil et al. correlation)
CO_2
Bulk-Fluid Temperature
H_2O
T_{in}
T_{out}
Heated length
Temperature, °C
HTC, kW/m^{2}K
Axial Location, m

(a)

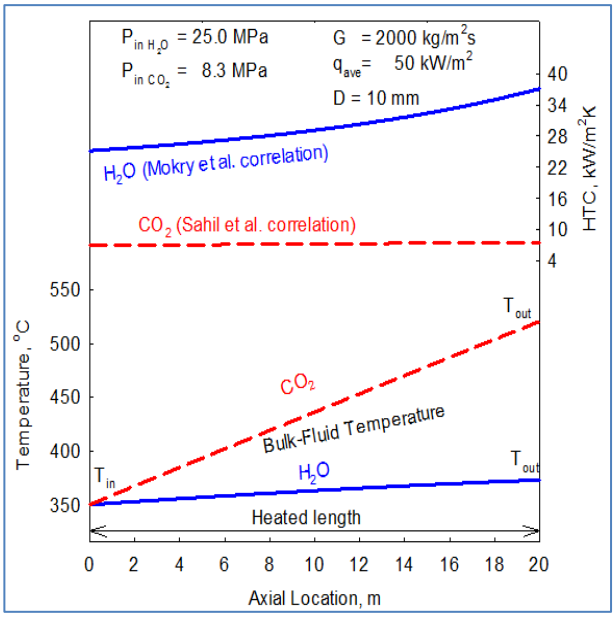
$P_{in\ H_2O}$ = 25.0 MPa
$P_{in\ CO_2}$ = 8.3 MPa
G = 2000 kg/m^{2}s
q_{ave} = 50 kW/m^2
D = 10 mm
H_2O (Mokry et al. correlation)
CO_2 (Sahil et al. correlation)
CO_2
Bulk-Fluid Temperature
H_2O
T_{in}
T_{out}
Heated length
Temperature, °C
HTC, kW/m^{2}K
Axial Location, m

(b)

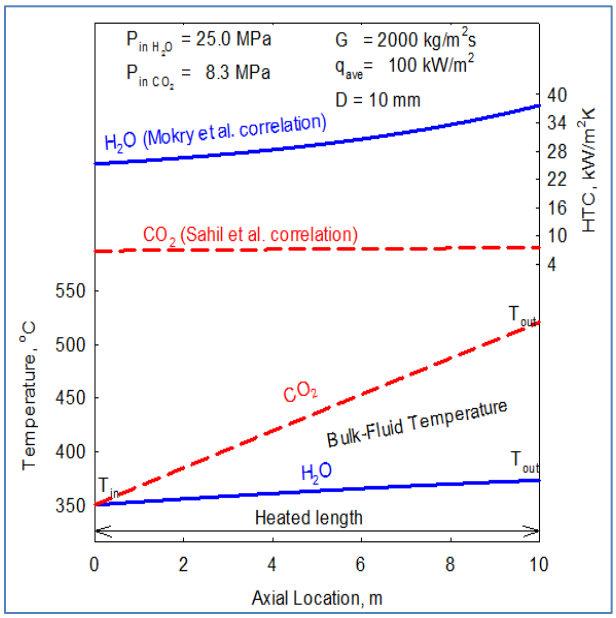
$P_{in\ H_2O}$ = 25.0 MPa
$P_{in\ CO_2}$ = 8.3 MPa
G = 2000 kg/m^{2}s
q_{ave} = 100 kW/m^2
D = 10 mm
H_2O (Mokry et al. correlation)
CO_2 (Sahil et al. correlation)
CO_2
Bulk-Fluid Temperature
H_2O
T_{in}
T_{out}
Heated length
Temperature, °C
HTC, kW/m^{2}K
Axial Location, m

(c)

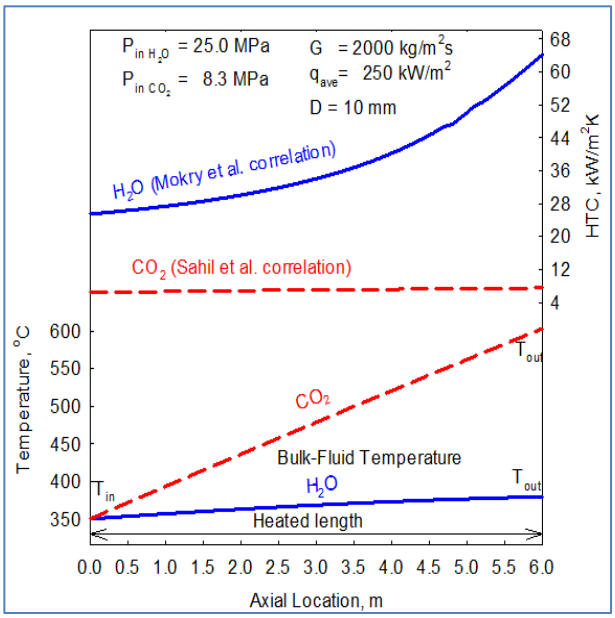
$P_{in\ H_2O}$ = 25.0 MPa
$P_{in\ CO_2}$ = 8.3 MPa
G = 2000 kg/m^{2}s
q_{ave} = 250 kW/m^2
D = 10 mm
H_2O (Mokry et al. correlation)
CO_2 (Sahil et al. correlation)
CO_2
Bulk-Fluid Temperature
H_2O
T_{in}
T_{out}
Heated length
Temperature, °C
HTC, kW/m^{2}K
Axial Location, m

(d)

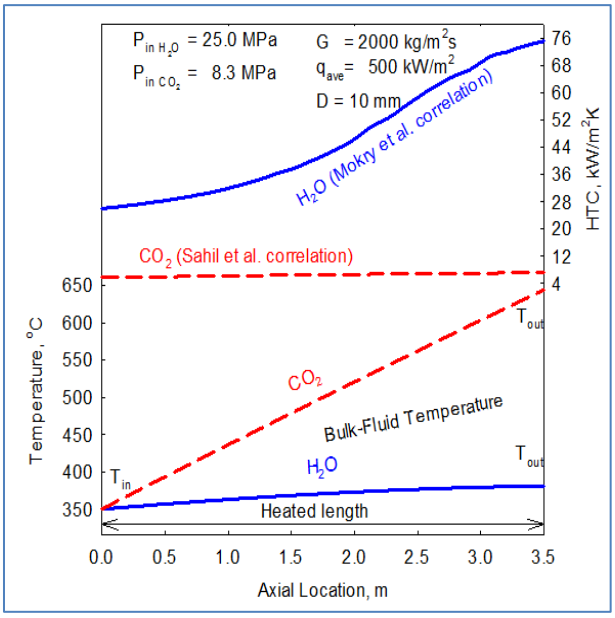

(e)

Figure 6-2: CO_2 and Water comparison for G =2000 kg/m^{2}s; D =10 mm (a) q_{ave}= 25 kW/m^2 (b) q_{ave}= 50 kW/m^2 (c) q_{ave}= 100 kW/m^2 (d) q_{ave}= 250 kW/m^2 (e) q_{ave}= 500 kW/m^2

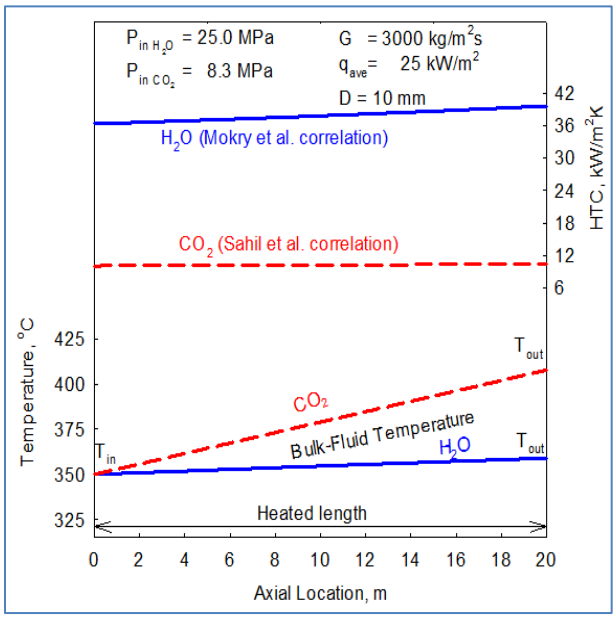

(a)

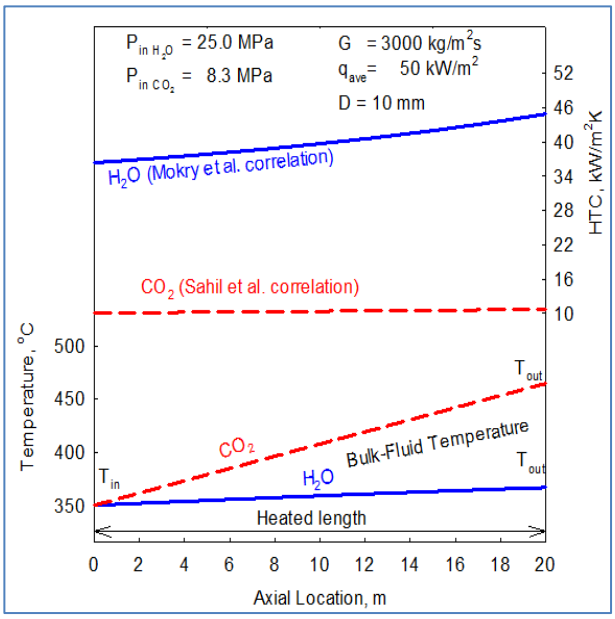

(b)

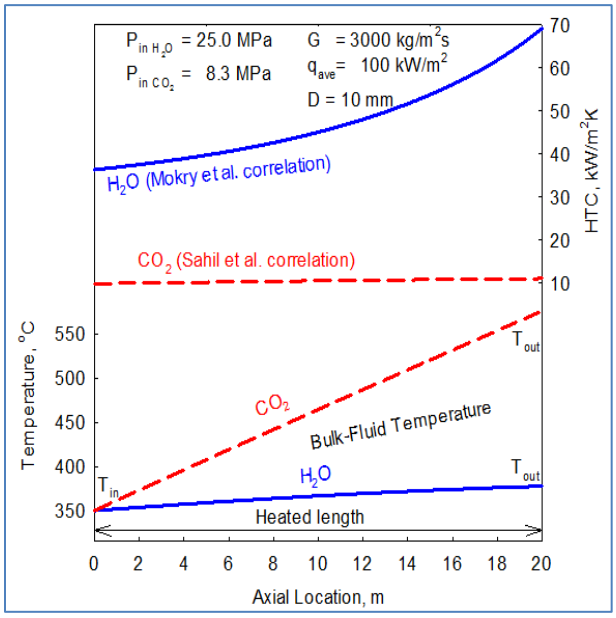

(c)

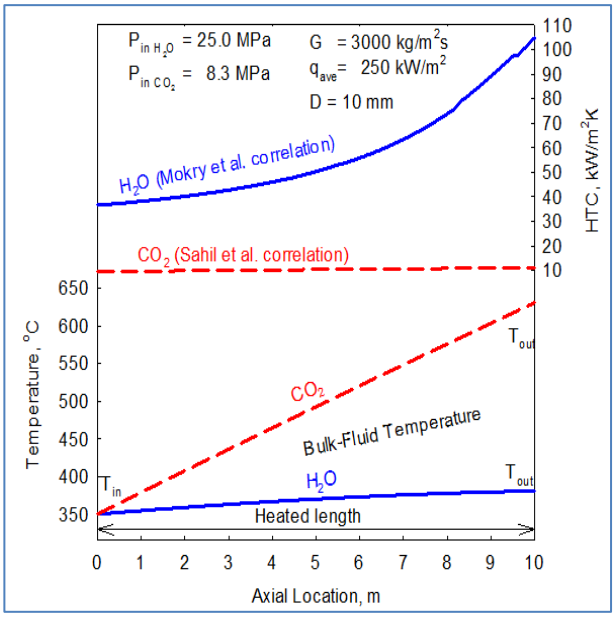

(d)

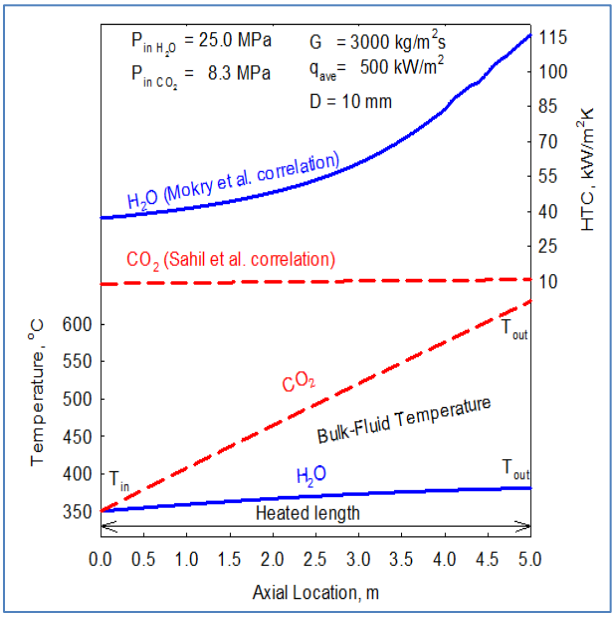

(e)

Figure 6-3: CO_2 and Water comparison for G =3000 kg/m^{2}s; D =10 mm (a) q_{ave}= 25 kW/m^2 (b) q_{ave}= 50 kW/m^2 (c) q_{ave}= 100 kW/m^2 (d) q_{ave}= 250 kW/m^2 (e) q_{ave}= 500 kW/m^2

6.2 Applications of HTC Correlations

The 1-D HTC correlations have widespread applications and can be applied for preliminary calculations involving SCFs flowing in tube geometry. They can also be used to perform parametric and sensitivity analysis by varying various operational parameters numerically. The primary applications for the proposed correlations in SCF technology are discussed below:

1. Preliminary heat-transfer calculations can be performed for SCWR fuel channels and core design as a conservative approach. The correlations can also be applied for preliminary safety analysis and sub channel codes for fuel design support. However, it must be noted that due to the lack of bundle data, validation of these correlations must be performed prior to such applications (see Section 6.3 for limitations on this applications);

2. Calculations of supercritical-water heat-transfer in heat exchangers in SCWR indirect-cycle concepts and for the co-generation of hydrogen at SCW NPPs;

3. Future comparisons with other independent datasets and with data for fuel bundles;

4. Verification of computer codes for SCWR core thermalhydraulics; and

5. Verification of scaling parameters between water and modelling/surrogate fluids such as CO_2, refrigerants, etc.

In addition, the proposed correlation can also be applied towards: (1) advancement of SC-coal-fired thermal power plants that use supercritical fluids as a medium for heat—transfer; (2) use of SC CO_2 in the secondary Brayton cycle for geothermal application; (3) SC CO_2 air–conditioning and refrigeration applications; (4) as a future application in Brayton cycle for Gen IV nuclear reactors (such as calculations of SCW and SC CO_2 heat—transfer in SC steam generators).

6.3 Limitations of New Correlations

Although the 1-D correlations present wide range of applications and are user friendly due to relatively low complexity, they have some serious limitations when applied towards complex geometries and flows as in the case of SCWR designs. Some of the limitations are discussed below:

1. Many new empirical HTC correlations are being suggested world-wide developed from various SC experimental setups. While these correlations show good results for the data-sets they were developed for; they fail to transfer the results when compared against different experimental setups. Results of analysis indicate that the correlations are highly tuned for the reference data-sets they were developed from and thus they have very narrow ranges of applicability. Limited range of applicability for 1-D HTC correlations

poses a significant challenge. There is also a need to standardize SC test apparatus and procedures to obtain a reliable reference SC database that may be then used to data-fit to empirical models.

2. Experimental uncertainly and limited range of usable data near the pseudocritical point make it very difficult to reach any conclusion on behavior very near the pseudocritical temperature with the present analysis. In this thesis only pure empirical models/equations are used with limited understanding of first principle phenomenon's occurring in the transition region. A more detailed study is warranted to study and develop theoretical models using basic first principle equations.

3. Tube data and correlations can be used to make predictions for the conceptual design phases of fuel channels and core designs for Generation IV reactors involving the use of SCFs. However, there remains an associated high uncertainty that could have an impact on the reactor design, power output, and safety margin. Correlations developed for bare tubes are highly tuned for the specific geometry and thus their application to fuel rod bundles is limited. Most of the coolant channels in SCR concepts are more complex than those that have been used to generate the empirical correlations employed in the thermal hydraulic codes. Justification and validation are required to extend the application of correlations based on tube data to the SCWR design and safety analyses. Advanced computational techniques may be applied but measurements with realistic geometries are needed to assess the reliability and accuracy of their predictions (McEligot et. al, 2009). Therefore, additional experiments using complex bundle geometries are necessary for generating relevant experimental data to minimize the uncertainty and validate the prediction methods and analytical toolsets.

4. Consequently, developing SCWR designs requires experimental data for the convective heat transfer from fuel rod bundles to coolant covering relevant ranges of flow rates, pressures and fluid temperatures. The collection, evaluation and assimilation of existing and new data are necessary to establish accurate methods and techniques for the prediction of heat transfer in SCWR cores. Eventually, thermal-hydraulic codes will have to be used for various geometries including rod bundles, grid spacer designs, axial and radial power profiles and coolant velocities. Due to the lack of bundle data,

validation of these 1-D correlations under such conditions is not possible at the moment and hence any preliminary calculations/recommendations have to be considered as tentative. The bare tube 1-D correlations are perhaps too simplistic models that will not be adequate for use in complex geometries involved in SCWR designs.

5. In addition, previous reviews by Pioro and Duffey (2005) concluded that available information on SCW flow in tubes is limited. The range of covered flow conditions in the datasets remains inadequate for the design and safety analyses of SCWR. Insufficient or no data is available at postulated accident conditions which limits the any type of safety analysis.

6.4 Future Work

1. Large amounts of experimental data are available for vertical upward flow of water and other surrogate fluids in tubes covering a wide range of flow conditions (available at IAEA SC database). Compilation of datasets from other test sections can be performed to have a much larger dataset. The newly developed correlations can be tested against different experimental dataset with varying flow conditions and geometrical parameters to test their applicability. The correlations can be refined based on the larger dataset for further accuracy or have added correction factors for specific flow conditions.

2. Further investigation of the DHT and IHT regimes and correlations for predicting onset of DHT regions (q_{dht}) can be further refined. Note that a precise definition of the onset of DHT needs to be developed and universally adapted before further refinements can occur on these correlations. Semi-empirical and numerical solutions may be possible.

3. Pressure drop data compilation can be performed and correlations for predicting frictional pressure drop can be investigated.

4. Investigations of the application of correlations for HX development, bundle data predictions etc.

5. Development and validations of scaling parameters between various supercritical fluids.

6.5 Summary

The main highlights are presented below:

1. Global energy demand is expected to grow in direct proportions to the population growth and nuclear energy is expected to play a big part in future energy mix. Water-cooled NPPs have significantly lower thermal efficiencies (30 – 35%) compared to that of the fossil fired plants (45 – 50%). To ensure economic attractiveness; advanced designs of NPPs (Generation IV) are being considered for development throughout the world with a goal to increase the thermal efficiency to the level of 55 – 62%.

2. The Generation IV International Forum (GIF) Program established in 2002 has narrowed design options of nuclear reactors to six concepts. These concepts are: 1) Gas-cooled Fast Reactor (GFR) or High Temperature Reactor (HTR), 2) Very High Temperature Reactor (VHTR), 3) Sodium-cooled Fast Reactor (SFR), 4) Lead-cooled Fast Reactor (LFR), 5) Molten Salt Reactor (MSR), and 6) SuperCritical Water-cooled Reactor (SCWR). These nuclear-reactor concepts differ one from each other in terms of their design, neutron spectrum, coolant, moderator, operating temperatures and pressures. However, most of these concepts are expected to utilize SCFs (especially SC Water and SC CO_2) in their heat transfer cycles.

3. SCFs are expected to have widespread applications in future for power and heat transfer applications (both conventional and nuclear) as it leads to significant increase in efficiency. In addition, higher temperatures also allow opportunities for hydrogen co-generation, increase in the specific fuel utilization and reduction in the waste heat rejection. SC CO_2 is proposed to be the working fluid in Brayton-cycle power plant applications due to its attractive thermophysical properties, low operational and capital costs, and minimal safety concerns as well as particularly small dimensions of turbomachinery. Supercritical CO_2 cycles can also be optimally used in combined cycles with water or Sodium. Thus, a basic understanding of the thermodynamic behaviour of SCFs is very critical to assist in developments of high temperature and pressure power applications.

4. Applications for SCFs are not limited to power industry. Recent advancements in this area have proposed use of SCFs in much wider applications such as 1) air conditioning systems and other refrigeration cycles 2) enhanced geothermal systems; 3) solar trough plants, and many others.

5. A number of countries are pursuing the development of SCWR technology. While the reactor core and fuel designs differ significantly, there are many similarities between the secondary side cycles and safety features. Most design concepts are still facing challenges, particularly cladding material selection to withstand high temperatures during normal operations and postulated accident scenarios. From thermalhydraulic point of view, one of the important parameters in SCWRs is the fuel-sheath temperature, which is usually limited to 750 – 850°C (design constraint). In this case, the ability to correctly predict the Heat Transfer Coefficients (HTCs) along a fuel-bundle string is essential for the reactor design. Due to lack of experimental data and, corresponding to that, empirical correlations for heat transfer in fuel bundles, heat-transfer correlations based on bare-tube data can be used as a preliminary conservative approach. Improvement in heat-transfer prediction accuracy would provide a realistic estimation of cladding temperature, which may ease the cladding material requirement.

6. SCFs have very unique thermodynamic properties and very drastic variations in properties are observed when a fluid transition to pseudocritical ranges. Three major heat-transfer regimes can be noticed at critical and SC parameter 1) normal heat transfer; 2) improved heat transfer regime and 3) deteriorated heat transfer regime. Heat flux, mass flux, and the geometry are the main parameters that play a major factor in forming of a DHT regime. The conditions under which the deterioration occurs are: 1) the wall temperature must be above and the bulk temperature below the psuedocritical temperature (i.e. $T_b < T_{pc} < T_w$) and 2) the heat flux must be above a certain value, dependent on the flow rate and pressure. Numerical analyses used for DHT predictions generally over predict the test data. Basic empirical and semi-empirical correlations can be developed to predict the onset of DHT regimes using experimental datasets and curve fitting techniques that show good agreement with test data. However, there is no clear unique definition of the onset

of DHT and thus the various correlations found in literature vary significantly from each other.

7. Large amounts of experimental data are available for vertical upward flow of water and surrogate fluids in tubes. These data cover a wide range of flow conditions. However, the amount of data remains limited for relevant conditions to current SCWR design concepts. Nevertheless, these data were applied in the development of methods for calculating supercritical pressure heat-transfer coefficients.

8. Using existing experimental data for SC Water and SC CO_2, updated HTC correlations were proposed.

6.6 Conclusions

1. Literature survey and error analysis of the existing HTC correlation showed that their predicted values can deviate significantly from experimental values, especially within the pseudocritical regions. Dittus-Boelter (1930) correlation, which is the most widely-used correlation at subcritical pressures, significantly overestimates experimental HTC values in bare vertical tubes cooled with supercritical water within the pseudocritical region. The Bishop et al.(1964) and Jackson (2002) correlations also deviate substantially from the experimental data within the pseudocritical region. The Swenson et al.(1965) correlation provides a better fit for the experimental data than the previous three correlations within some flow conditions, but does not follow closely the experimental data within others.

2. New correlations were proposed based on empirical model of the form $\mathbf{Nu_x} = C\mathbf{Re_x^{n_1}Pr_x^{n_2}}\boldsymbol{F}$, where x represents the characteristic temperature (where the properties are calculated) and F represents the correction factors in terms of dimensionless ratios of viscosity, density, thermal conductivity etc. Experimental SKD-1 test loop water data was used to develop new correlations for SCW while data from AECL MR-1 loop was used to develop correlations for SC CO_2. The new correlations showed promising results for HTC and T_w calculations for the reference dataset with uncertainty of about ±25% for HTC values and about ±10-15% for the calculated wall temperature.

3. While these empirical correlations show good results for the data-sets they were developed for; they fail to transfer the results when compared against different experimental setups. Results of analysis indicate that the correlations are highly tuned for the reference data-sets they were developed from and thus they have narrow ranges of applicability. Limited range of applicability for 1-D HTC correlations poses a significant challenge. There is also a need to standardize SC test apparatus and procedures to obtain a reliable reference SC database that may be then used to data-fit to empirical models.

4. Tube data and correlations can be used to make predictions for the conceptual design phases of fuel channels and core designs for Generation IV reactors involving the use of SCFs. However, there remains an associated high uncertainty that could have an impact on the reactor design, power output, and safety margin. Most of the coolant channels in SCR concepts are more complex than those that have been used to generate the empirical correlations employed in the thermal hydraulic codes. Justification and validation are required to extend the application of correlations based on tube data, to the SCWR design and safety analyses. Therefore, additional experiments using complex bundle geometries are necessary for generating relevant experimental data to minimize the uncertainty and validate the prediction methods and analytical toolsets.

5. Nonetheless, the new correlations presented can be used for: (1) a preliminary heat-transfer calculations in SCWR fuel channels as a conservative approach; (2) calculations of SCW heat-transfer in heat exchangers in SCWR indirect-cycle concepts; (3) calculations of heat-transfer in heat exchangers for the co-generation of hydrogen at SCW NPPs; (4) calculations of SCW heat-transfer in heat exchangers for other Generation IV nuclear-reactor concepts with indirect cycles; (5) future comparisons with other independent datasets and bundle data; (6) the verification of computer codes for SCWR-core thermal hydraulics; and (7) the verification of scaling parameters between water and modeling fluids such as carbon dioxide and refrigerants.

In conclusion, the objectives set forth in Section 1.9 were met successfully.

REFERENCES

"Charter of the Generation IV International Forum", 2002. Generation IV International Forum Document (www.gen-4.org/PDFs/GIFcharter.pdf), February.

Bishop, A.A., Sandberg, R.O., and Tong, L.S., 1964. High Temperature Supercritical Pressure Water Loop: Part IV, "Forced Convection Heat Transfer to Water at Near-Critical Temperatures and Super-Critical Pressures," Westinghouse Electric Corporation WCAP 2056, Pittsburgh, Pennsylvania.

Boehm, C., Starflinger, J., Schulenberg, Th., and Oeynhausen, H., 2005. Supercritical steam cycle for lead cooled nuclear systems, Proceedings of the International Conference Global-Nuclear Energy Systems for Future Generation and Global Sustainability, Tsukuba, Japan, October 9–13, Paper No. 035, 6 pages.

Bringer, R.P. and Smith, J.M., 1957. Heat transfer in the critical region, AIChE Journal, pp. 49–55.

Brown, D., 2000. A Hot Dry Rock geothermal energy concept utilizing supercritical CO_2 instead of water, in Proceedings of the Twenty-Fifth Workshop on Geothermal Reservoir Engineering, Stanford University, pp. 233-238.

Chapman, D.J., and Arias, D.A., 2009. An Assessment of the Supercritical Carbon Dioxide Cycle for Use in a Solar Parabolic Trough Power Plant, Proceedings of $SCCO_2$ Power Cycle Symposium, RPI, Troy, NY, April 29-30, 5 pages.

Cheng, X., Schulenberg, T. , 2001. Heat Transfer at Supercritical Pressures Literature Review and Application to an HPLWR, 47 pages.

Cheng, X., Schulenberg, T. , Koshizuka, S., Oka, Y. and Souyri, A., 2002. Thermalhydraulic Analysis of Supercritical Pressures Light Water Reactors, in Proceedings of ICAPP, Hollywood, FL, USA.

*Department of Energy (*DOE), 2009. Materials for Ultra-Supercritical Steam Turbines, ORNL and NETL (www.ms.ornl.gov), and Ultra Supercritical Steam Corrosion, G. Holcomb et al., (www.osti.gov)

Department of Energy (DOE), 2002. A Technology Roadmap for Generation IV Nuclear Energy Systems. Washington, D.C., Department of Energy.

Dittus, F.W. and Boelter, L.M.K., 1930. Heat Transfer in Automobile Radiators of the Tubular Type, University of California, Berkeley, Publications on Engineering, Vol. 2(13), pp. 443-461.

Duffey, R.B., Pioro, I., Zhou, X., Zirn, U., Kuran, S., Khartabil, H., and Naidin, M., 2008. Supercritical Water-Cooled Nuclear Reactors (SCWRs): Current and Future Concepts – Steam Cycle Options, Proc. 16th International Conference on Nuclear Engineering (ICONE16), Orlando, Florida, USA, May 11-15.

Dyadyakin, B.V. and Popov, A.S., 1977. Heat transfer and thermal resistance of tight seven-rod bundle, cooled with water flow at supercritical pressures, (In Russian), Transactions of VTI (Труды ВТИ), No. 11, pp. 244–253.

Fouillac, C., Sanjuan, B., Gentier, S., and Czernichowski-Lauriol, I., 2004. Could Sequestration of CO_2 be Combined with the Development of Enhanced Geothermal Systems?, *Conference on Carbon Capture and Sequestration*, Alexandria, VA.

Gallaway, T., Antal S.P., and Podowski, M.Z., 2009. Thermal-Hydraulics and Dynamics of Supercritical S-CO_2 Reactor, Proceedings of $SCCO_2$ Power Cycle Symposium, RPI, Troy, NY, April 29-30, 9 pages.

Gen IV, 2009. GIF R&D Outlook for Generation IV Nuclear Energy Systems, 21 August. https://www.gen-4.org/gif/upload/docs/application/pdf/2013-09/gif_rd_outlook_for_generation_iv_nuclear_energy_systems.pdf

Gorban', L.M., Pomet'ko, R.S. and Khryaschev, O.A., 1990. Modeling of water heat transfer with Freon of supercritical pressure, (In Russian), ФЭИ-1766, Institute of Physics and Power Engineering (ФЭИ), Obninsk, Russia, 19 pages.

Gupta, S., Farah, A., King, K., Mokry, S. and Pioro, I., 2010. Developing New Heat-Transfer Correlation for Supercritical-Water Flow in Vertical Bare Tubes, Proc. ICONE-18, Xi'an, China, May 17-21, Paper 30024, 9 pages.

Gupta, S., Mokry, S. and Pioro, I., 2011. Developing A Heat-Transfer Correlation for Supercritical-Water Flow in Vertical Bare Tubes and Its Application in SCWRS, Proceedings of the 19th International Conference On Nuclear Engineering (ICONE-19), Osaka, Japan, October 24-25, Paper# 43503, 11 pages.

Hajek, P., 2009. Thermodynamic Aspects of Cycles with Supercritical Fluids, Proceedings of $SCCO_2$ Power Cycle Symposium, RPI, Troy, NY, April 29-30, 7 pages.

He, S., Jiang, P.-X., Xu, Y.-J., et al., 2005. A computational study of convection heat transfer to CO2 at supercritical pressures in a vertical mini tube, International Journal of Thermal Sciences, 44, pp. 521–530.

Hejzlar, P., Dostal, V., and Driscoll, M.J., 2005. Assessment of gas cooled fast reactor with indirect supercritical CO2 cycle, Proceedings of the International Congress on Advances in Nuclear Power Plants (ICAPP'05), Seoul, Korea, May 15–19, Paper No. 5090, 11 pages.

Incropera, F.P, DeWitt D.P, Bergman T.L, and Lavine, A.S, 2007. *Fundamentals of Heat and Mass Transfer*. 6th Edition. John Wiley and Sons, Inc, New York, NY, USA, pp 134-136.

Jackson, J.D. and Hall, W.B., 1979. Forced convection heat transfer to fluids at supercritical pressure, In book: Turbulent Forced Convection in Channels and Bundles, Editors S. Kakaç and D.B. Spalding, Hemisphere Publishing Corp., New York, New York, USA, Vol. 2, pp. 563–612.

Jackson, J.D., 2002. Consideration of the Heat Transfer Properties of Supercritical Pressure Water in Connection with the Cooling of Advanced Nuclear Reactors, Proc. 13th Pacific Basin Nuclear Conference, Shenzhen City, China, October 21-25.

Kato, Ya., Muto, Ya., Ishizuka, T., and Mito, M., 2005. Design of recuperator for the supercritical CO2 gas turbine fast reactor, Proceedings of the International Congress on Advances in Nuclear Power Plants (ICAPP'05), Seoul, Korea, May 15–19, Paper No. 5196, 10 pages.

Kim, J. K., H. K. Jeon, J. Y. Yoo and J. S. Lee, 2005. Experimental study on heat transfer characteristics of turbulent supercritical flow in vertical circular/non-circular tubes, NURETH-11, Avignon, France, Paper 266.

Kirillov, P.L., 2001a. Transition to supercritical parameters — way to improving NPP with water-cooled reactors, *Thermal Engineering* (Теплоэнергетика, стр. 6–10), 48 (12), pp. 973–978.

Kirillov, P.L., 2001b. Supercritical parameters ― future for reactors with water coolant and NPP, (In Russian), *Atomic Energy Abroad*, (6), pp. 6–8.

Kirillov, P.L., Pomet'ko, R.S., Smirnov, A.M., Grabezhnaia, V.A., Pioro, I.L., Duffey, R.B. and Khartabil, H.F., Experimental Study on Heat Transfer to Supercritical Water Flowing in Vertical Tubes, Proceedings of the International Conference GLOBAL-2005 "Nuclear Energy Systems for Future Generation and Global Sustainability, Tsukuba, Japan, October 9–13, 2005, Paper #518, 8 pages.

Koppel, L. B., 1960, Heat Transfer and Thermodynamics in the Critical Region, Ph.D. Thesis in Chemical Engineering. Northwestern University, Illinois.

Krasnoshchekov, E., Protopopov, V., Van, F., and Kuraeva, I., 1967. Experimental Investigation of Heat Transfer for Carbon Dioxide in the Supercritical Region, Proc. 2nd All-Soviet Union

Conf. on Heat and Mass Transfer, Minsk, Belarus', May, 1964, Published as Rand Report R-451-PR, Edited by C. Gazley, Jr., J. Harnett & E. Ecker, Vol. 1, pp.26-35.

Krasnoshchekov, E.A. and Protopopov, V.S., 1959. Heat transfer at supercritical region in flow of carbon dioxide and water in tubes, (In Russian), Thermal Engineering (Теплоэнергетика, стр. 26–30), No. 12, pp. 26–30.

Krasnoshchekov, E.A. and Protopopov, V.S., 1960. About heat transfer in flow of carbon dioxide and water at supercritical region of state parameters, (In Russian), Thermal Engineering (Теплоэнергетика, стр. 94), No. 10, p. 94.

Mathur, G. D., 2000. Carbon Dioxide as an alternative refrigerant for automotive air conditioning systems, in Energy Conversion Engineering Conference and Exhibit, 2000. (IECEC) 35th Intersociety, pp. 371-379

McAdams, W., 1942. *Heat Transmission*, 2nd ed., McGraw-Hill, New York, NY, USA, 459 pages.

McEligot, D.M., Yoo, et al., 2009. Advanced Computational Thermal Studies and their Assessment for Supercritical-pressure Reactors (SCRs), Proceedings of $SCCO_2$ Power Cycle Symposium, RPI, Troy, NY, April 29-30, 4 pages.

Mokry, S., Gospodinov, Y., Pioro, I. and Kirillov, P.L., 2009. Supercritical Water Heat-Transfer Correlation for Vertical Bare Tubes, Proceedings of the International Conference On Nuclear Engineering (ICONE-17), July 12-16, Brussels, Belgium, Paper #76010, 8 pages.

Mokry, S., Pioro, I., Farah, A., and King. K., 2010b.Updated Heat Transfer Correlations for Supercritical Water-Cooled Reactor Applications, Proceedings of the 19th International Conference On Nuclear Engineering (ICONE-19), Osaka, Japan, October 24-25, Paper# 43876, 13 pages.

Mokry, S.J., Kirillov, P.L., Pioro, I.L. and Gospodinov, Y.K., 2010a. Supercritical Water Heat Transfer in a Vertical Bare Tube: Normal, Improved and Deteriorated Regimes, Nuclear Technology, Vol. 172, No. 1, pp. 60-70.

Munson, B., Young, D. and Okiishi, Th., 2005. *Fundamentals of Fluid Mechanics*, 5th ed., New York, NY, J. Wiley & Sons.

National Institute of Standards and Technology, 2007. NIST Reference Fluid Thermodynamic and Transport Properties-REFPROP. NIST Standard Reference Database 23, Ver. 8.0. Boulder, CO, U.S.: Department of Commerce.

Nuclear Energy Today, 2012, Organisation for Economic Co-operation and Development, December 21, 120 pages, NEA#6885, ISBN: 978-92-64-99204-7 Available online at: http://www.oecd-nea.org/pub/nuclearenergytoday/6885-nuclear-energy-today.pdf

Ogata, H., Sato S., 1972. Measurement of forced convection heat transfer to supercritical helium, Proc. Of the 4th Int. Cryogenic Engineering Conference, Eindhoven, Netherlands, May 24-26, pp. 291-294

Oka, Yo., 2003. Research and development of the supercritical-pressure light water cooled reactors, Proceedings of the International Topical Meeting on Nuclear Reactor Thermal Hydraulics (NURETH-10), Seoul, Korea, October 5–9, 11 pages.

Oka, Yo., Koshizuka, S., Ishiwatari, Y. and Yamaji, A., 2010. Super Light Water Reactors and Super Fast Reactors, Springer, 416 pages.

Petuhkov, B.S., Kurganov, V.A., 1983. Heat Transfer and flow resistance un the turbulent pipe flow of a fluid with near-critical state parameters, Teplofizika Vysokikh Temperature, Vol. 21, No. 1, pp. 92-100, Jan.

Petukhov, B.S. and Kirillov, 1958. About heat transfer at turbulent fluid flow in tubes, (In Russian), Thermal Engineering (Теплоэнергетика, стр. 63–68), (4), pp. 63–68.

Pioro, I. and Duffey, R., 2007. Heat Transfer and Hydraulic Resistance at Supercritical Pressures in Power Engineering Applications, ASME Press, New York, NY, USA, 334 pages.

Pioro, I., 2011. The Potential Use of Supercritical Water-Cooling in Nuclear Reactors. Chapter in Nuclear Energy Encyclopedia: Science, Technology, and Applications, Editors: S.B. Krivit, J.H. Lehr and Th.B. Kingery, J. Wiley & Sons, Hoboken, NJ, USA, pp. 309-347 pages.

Pioro, I., 2013. Nuclear Power as a Basis for Future Electricity Production in the World, Chapter #10 in the book: Current Research in Nuclear Reactor Technology in Brazil and Worldwide, Editors: A.Z. Mesquita and H.C. Rezende, INTECH, Rijeka, Croatia, pp. 211-250.

Pioro, I. and Kirillov, P., 2013. Current Status of Electricity Generation in the World, Chapter in the book: Materials and Processes for Energy: Communicating Current Research and Technological Developments, Energy Book Series #1, Editor: A. Méndez-Vilas, Publisher: Formatex Research Center, Spain, pp. 783-795. Free download from: http://www.formatex.info/energymaterialsbook/book/783-795.pdf

Pioro, I., Mokry, S., and Draper, S., 2011. Specifics of thermophysical properties and forced-convective heat transfer at critical and supercritical pressures. *Rev Chem Eng*, 27, pp. 191-214.

Pioro, I.L. and Duffey, R.B., 2003. Literature Survey of the Heat Transfer and Hydraulic Resistance of Water, Carbon Dioxide, Helium and Other Fluids at Supercritical and Near-Critical Pressures, Report AECL-12137/FFC-FCT-409, CRL AECL, April, ISSN 0067-0367, 182 pages.

Pioro, I.L. and Duffey, R.B., 2005. Experimental Heat Transfer to Supercritical Water Flowing inside Channels (Survey), Nuclear Engineering and Design, 235 (22), pp. 2407-2420.

Pioro, I.L. et al., 2008. Supercritical Water-Cooled Nuclear Reactors: Thermodynamic-Cycles Options, Proc. 6th International Conference on Heat Transfer, Fluid Mechanics and Thermodynamics (HEFAT-2008), Pretoria, South Africa, Paper #PI1, June 30-July 02.

Schnurr, N.M., Sastry, V.S., and Shapiro, A.B., 1976. A Numerical Analysis of Heat Transfer to Fluids near the Thermodynamic Critical Point Including the Thermal Entrance Region, Journal of Heat Transfer, Transactions of the ASME, 98 (4), pp. 609-615.

Shiralkar, B.S, and Griffith, P., 1968. The Deterioration in Heat Transfer to Fluids at Super-Critical Pressure and High Heat Fluxes, Department of Mechanical Engineering, Massachusetts Institute of Technology, Report No. 70332-51, March 1, 67 pages.

Shitsman, M.E., 1963, Impairment of the Heat Transmission at Supercritical Pressures, Teplofizika Vysokikh Temperature, Vol. I, No. 3, pp. 267 -275.

SigmaPlot, 2011. Curve Fitting and Regression Analysis.
http://www.sigmaplot.com/products/sigmaplot/curvefitting.php

Smith, D., 1999. Ultra-supercritical CHP: Getting more competitive, *Modern Power Systems*, January, pp. 21–32.

Sohn, M.S., Yoo, Yo.H., and Suh, K.Y., 2005. Recuperator for supercritical carbon dioxide Brayton cycle, Proceedings of the International Congress on Advances in Nuclear Power Plants (ICAPP'05), Seoul, Korea, May 15–19, Paper No. 5584, 5 pages.

Styrikovich, M.A., Margulova, T.K., and Miropolskii, Z.L., 1967. Problems in the development of designs of supercritical boilers, Teploenergetika, Vol.14, No.6, 1967, pp. 4-7

Swenson, H.S., Carver,J.R., and Kakarala, C.R, 1965. Heat Transfer to Supercritical Water in Smooth-Bore Tubes, J. of Heat Transfer, Trans. ASME Series C, 87 (4), pp. 477-484.

Ueda. A., et al., 2005. Experimental studies of CO2-rock interaction at elevated temperatures under hydrothermal conditions, Geochem. J., 39pp. 417-425.

Vanyukova, G.V., Kuznetsov, Yu.N., Loninov, A.Ya., Papandin, M.V., Smirnov, V.P. and Pioro, I.L., 2009. Application of CFD-Code to Calculations of Heat Transfer in a Fuel Bundle of SCW

Pressure-Channel Reactor, Proc. 4th Int. Symp.on Supercritical Water-Cooled Reactors, March 8-11, Heidelberg, Germany, Paper No. 28, 9 pages.

Wan, Y., Xu, T., and Pruess, K., 2011. Impact of Fluid-Rock Interactions on Enhanced Geothermal Systems With CO_2 As Heat Transmission Fluid, in Thirty-Sixth Workshop on Geothermal Reservoir Engineering, Stanford.

Winterton, R.H.S., 1998. Where Did the Dittus and Boelter Equation Come From? Int. J. Heat and Mass Transfer, 41 (4–5), pp. 809–810.

World Coal Institute, 2010, "Improving Efficiencies" (www.worldcoal.org)

Yamagata, K., Nishikawa, K., Hasegawa, S., Fugii, T., Yoshida, S., 1972. Forced convection heat transfer to supercritical water flowing in tubes, Int. J. Heat and Mass Transfer, Vol. 15, pp. 2575-2593

Zahlan, H., Groeneveld, D. and Tavoularis, S., 2010. Look-Up Table for Trans-Critical Heat Transfer, Proc. 2nd Canada-China Joint Workshop on Supercritical Water-Cooled Reactors (CCSC-2010), Toronto, Ontario, Canada, Canadian Nuclear Society (CNS), April 25-29.

APPENDIX A: SAMPLE EQUATIONS FOR CALCULATING T_w AND T_b

A1: Calculation of T_w

Calculation of the internal T_w temperature from the external Temperature sensor was required for the analysis. General solution for the temperature distribution T (r) can be found as a function of radius using the uniform heat general concept within the solid (Incropera et al., 2007).

Consider a long cylindrical tube, insulated at the outer radius r_2 and cooled at the inner radius r_1, with uniform heat generation $\dot{q}$ (W/m^3) within the solid (shown in Figure below - Incropera et al., 2007). This case is similar to our test section, where the internal wall is being cooled by the supercritical coolant.

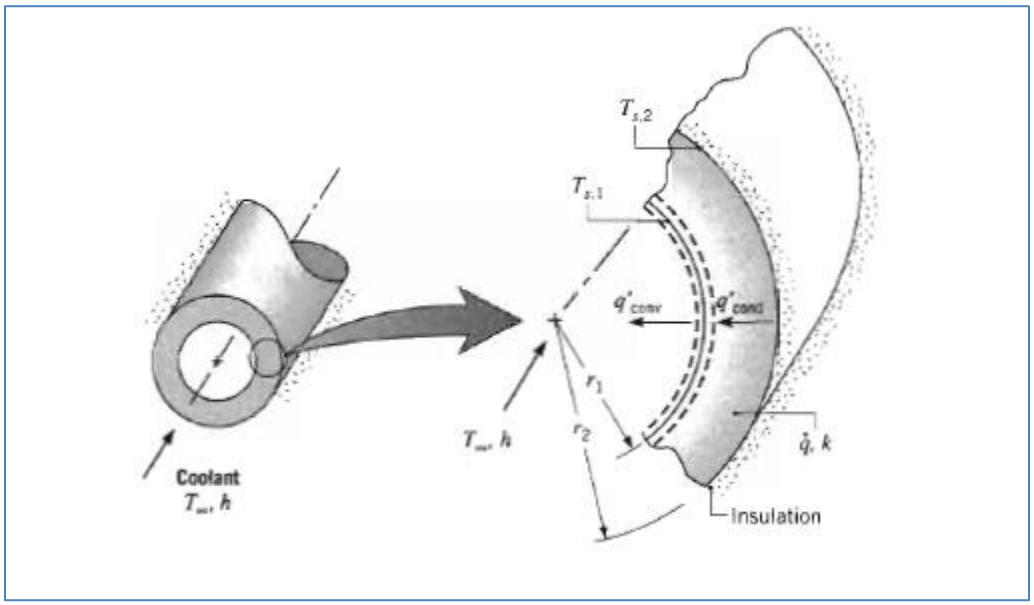

Assumptions:

1. Steady State Conditions.

2. Heat is transferred by one-dimensional radial conduction

3. Constant properties of materials assumed (Our Test section was tested to verify this assumption).

4. Uniform volumetric local heat generation.

5. Outer Surface is adiabatic.

For the prescribed conditions, the generic heat transfer expression can be expressed as

$$\frac{1}{r}\frac{d}{dr}\left(r\frac{dT}{dr}\right)+\frac{\dot{q}}{k}=0$$

This equation can be integrated to obtain a general solution for the temperature distribution as

$$T(r) = -\frac{q}{4k}r^2 + C_1 \ln r + C_2$$

After applying boundary conditions needed to evaluate C1 and C2, the equation can be solved to the general form presented in the Equation B1. Please refer to Incropera et al. for full solution.

Equation B1: Calculating Internal Wall Temperature (Incropera et al. 2007)

$$T_{s,1} = T_{s,2} + \frac{\dot{q}}{4k}(r_2^2 - r_1^2) - \frac{\dot{q}}{2k}r_2^2 \ln\left(\frac{r_2}{r_1}\right)$$

Where $T_{s,1}$ is the internal wall temperature of the cylinder, $T_{s,2}$ is the external temperature, r_2 is the outer radius of the pipe, r_1 is the inner radius of the pie and $\dot{q}$ is the local heat flux.

Equation B1 will be used in the form presetned in Equation B2

Equation B2: Calculating Internal Wall Temperature (Incropera et al. 2007)

$$T_{w_{in}} = T_{w_{ext}} + \frac{q_l}{4k}\left(r_{out}^2 - r_{in}^2\right) - \frac{q_l}{2k}r_{out}^2 \ln\left(\frac{r_{out}}{r_{in}}\right)$$

The various parameters required for the calculation of Equation B2 are described below.

Equation B3: Local Volumetric Heat Flux

$$q_{\ell vol} = \frac{POW_l - HL_l}{A_{hl}}$$

Where:

- Heated area: $A_{h\ell} = \pi\, D\, L_\ell$, where L_ℓ is the local heated length (see **Figure 5-2**).
- Measured power: $POW = V\, I$, where V is the test-section voltage drop, and I is the electrical current.
- Power: $POW_\ell = I^2 \cdot R_{el\ell}$, where $R_{el\ell}$ is the local electrical resistance within the local heated length calculated using a local value of electrical resistivity.
- where HL_ℓ is the local heat loss based on the corresponding external wall temperature measurements

Equation B4: Average Wall temperature of the Pipe

$$T_{w_{avg}} = \frac{T_{w_{in}} + T_{w_{ext}}}{2}$$

Equation B5: Specific Resistivity of Inconel-600 as a function of temperature

$$\rho_{elcal} = (103.1289703317 - 5.4963164982 \cdot 10^4 \cdot T + 6.4711351326 \cdot 10^{-5} \cdot T - 6.111698975 \cdot 10^{-8} \cdot T)10^{-8}\ Ohm \cdot m$$

Where T is the temperature in °C.

Equation B6: Thermal Conductivity as a function of Temperature

$$k_{w_{local}} = 14.2214329176 + 0.0162450563 \cdot T \quad W/mK$$

Equation B7: Local Electrical Resistance

$$R_{el} = \frac{\rho_{elcal} L_\ell}{A_c}$$

Where L_ℓ is the length between the thermocouples and A_c is the cross sectional area of the pipe.

Calculation

Solving for the internal wall temperatures at a particular thermopcouple requires iterations using the average wall temperature of the pipe. However the average temperature requires the internal wall temperature, which is what is being solved for, so an internal wall temperature has to be assumed.

In the case for the carbon dioxide test the assumed internal wall temperature is taken as the external wall temperature at the point of measurement subtracted by 5.

1. First assume a value for the internal wall temperature as:

$$T_{assumed-w_{int}} = T_{w_{ext}} - 5$$

2. Then calculate the average wall temperature using C4

$$T_{w_{avg}} = \frac{T_{assumed-w_{int}} + T_{w_{ext}}}{2}$$

3. Solve for the local resivity (B5) and thermal conductivity (B6) subbing $T_{w_{avg}}$ for T.

4. Using the local resitivity calculate the electrical resistance .
5. Then solve for local and the heat loss:

Equation B8: Local Power

$$POW_{local} = I^2 R_{el-local}$$

Equation B9: Heat Loss

$$HL_\ell = 0.47(T_{ext} - T_{amb})\left(\frac{L_\ell}{L}\right)$$

6. Finally solve for volumetric heat flux (C3) and sub into C2 for internal wall temperature

Equation B10: Calculating the internal wall temperature based on previously discussed parameters

$$T_{w_{in}NEW} = T_{w_{ext}} + \frac{q_{\ell vol}}{4k}\left(r_{out}^2 - r_{in}^2\right) - \frac{q_{\ell vol}}{2k} r_{out}^2 \ln\left(\frac{r_{out}}{r_{in}}\right)$$

7. Compare T_{avg} to the average between the new internal wall temperature calculated from step 6 to the external wall temperature.

   a. If $\frac{T_{w_{in}NEW}+T_{ext})}{2} - T_{avg} > 0.01$
   Then
   Set $T_{assumed-w_{in}} = T_{w_{in}NEW}$
   Then repeat from step 2.

   b. Otherwise set $T_{w_{in}NEW}$ as the internal wall temperature for this datapoint.

A2: Calculation of T_b (Method of Adding Enthalpies)

The following are the steps used for calculating bulk-fluid temperature at different points in the tube.

1. Take the temperature and pressure and input this data into Refprop, or similar software, to find the enthalpy of the fluid at those particular conditions. For the first datapoint this will be the inlet temperature and pressure of the test section.

2. Calculate local power with the following equation:

Equation B11: Local Power

$$Q = q_{local}\, \pi D_{hy} L_l$$

3. Use the local power to calculate the enthalpy of the next data point:

Equation B12: Enthalpy

$$H_{n+1} = \frac{Q_n}{\dot{m}} + H_n$$

Where Q_n is the local power (Watts), H_n (Joules/kg) is the enthalpy and local power at the current point and $\dot{m}$ is the mass flow rate (kg/s).

4. Then take H_{n+1} and the pressure of the fluid and use these values to find the corresponding temperature of the fluid from Refprop. This temperature will be the bulk-fluid temperature for the next data point.
5. For other datapoints repeat steps 2-4 until all bulk-fluid temperatures have been calculated.

APPENDIX B: MATLAB CODE FOR CALUCLATION OF T_{pc}

```
%%§§§§§§§§§§§§§§§§§§§§§§§§§§§§§§§§§§§§§§§§§§§§§§§§§§§§§§§§§§§§§§§§§§§§§§§§§§§§§§§§
% A program to calculate the pseudocritical Temperature for a given set of
% Pressure Array
%
% Written by Sahil Gupta, UOIT
%$$$$$$$$$$$$$$$$$$$$$$$$$$$$$$$$$$$$$$$$$$$$$$$$$$$$$$$$$$$$$$$$$$$$$$$$$$$$$$$$$$

%% General Formatting
clear all;
clc
format long g;

%% INPUT PARAMETERS
fluid='CO2'; %defining the working fluid
T_cr=refpropm('T','C',0,'',0,fluid);% Gives the Critical Temperature of the Fluid

%% PRESSURE ARRAY INPUT
P_b = xlsread('PressureArray.xlsx','sheet1','A:A');   %[MPa]
P_b= P_b*1000; % [kPa]

%% Code for Calculation of Tpc Array
Tpc=zeros;
inc=0.05; % Step Increment of Temperature
for m=1:length(P_b)
   condition=0;
cp(1)=refpropm('C','T',T_cr,'P',P_b(m),fluid);
cp(2)=refpropm('C','T',T_cr+inc,'P',P_b(m),fluid);
T = T_cr + inc;
   while condition==0
      T = T + inc;

      cp(3)=refpropm('C','T',T,'P',P_b(m),fluid);

      if ((cp(2)>cp(1))&(cp(2)>cp(3)))
         condition=1;
         Tpc(m)=T-inc-273.15;
      else
         cp(1)=cp(2);
         cp(2)=cp(3);
      end;

   end
end
```

SAMPLE MATLAB CODE FOR CALCULATION OF T_w FROM T_{ext} (USING INCROPERA AND DEWITT EQUATION-2002)

```
clc
```

```
clear
%% Given Constant Parameters
fluid='CO2'; %[working fluid]
L=2.208; % Total Heated Length (m)
ID= 8.058/1000; % [m] [inside diameter]
OD=10/1000; % [m] [Outside diameter]
L_l=0.1;% Thermocople locations (m)
A_c= pi()*(1/4)*(OD^2-ID^2);% m^2 Area of Cross-Section
A_f=pi()*(1/4)*ID^2;% m^2 Flow Area
A_h=pi()*ID*L; %[m^2] Total Heated Area
A_h_local=pi()*ID*L_l;% m^2 Area of Heated Length
% k=14.2214329176+0.0162450563*T; % Thermal Conductivity of Inconel 600
% [W/mK] and T is in C

%% Specific Test Input Conditions
P_in=8.364*1000; % kPa % INPUT FROM PT8
G=1944; %kg/m^2.s [Mass flux]
Q=26.8438*10^3; % [W] Total Power % INPUT FROM JS101
I= 559.288; % INPUT FROM JS 101 (Amps) % INPUT FROM JS101AMP
T_amb = 22.34385; % (C) Ambient Temperature %INPUT FROM TE133
T_in=21.24769231; % C (Inlet Temperature) % INPUT FROM TE103

T_w_ext_c=[
149.6869231
171.8284615
182.6776923
195.4530769
210.9046154
234.3430769
246.16
243.3415385
243.0815385
236.6623077
226.8430769
227.2092308
222.8292308
224.9407692
227.2476923
228.9907692
228.0092308
220.4053846
220.5853846
222.6607692
226.93
230.5146154
235.4207692
233.6438462
];% External Measured Wall Temperatues C
%% Specific Test Calculated conditions
q_ave=Q/A_h; % W/m^2 [heat flux]
m= G*A_f; % kg/s [mass flow rate]

%% Inlet Wall Temperature Calculations
for i=1:24
   T_w_int_assumed =T_w_ext_c(i)-5;
   check=0;
```

```
    while(check==0)
        % Calculations of Properties
        T_w_avg=(T_w_int_assumed+T_w_ext_c(i))/2;
        rho_el=(103.1289703317-5.4963164982*10^-4*T_w_avg+6.4711351326*10^-5*T_w_avg^2-
6.111698975*10^-8*T_w_avg^3)*10^-8; % Ohm.m
        k_w_local=14.2214329176 +0.0162450563*T_w_avg; % Local Thermal Conductivity W/m.K
        R_el_local=rho_el*L_l/A_c; % [Ohms] Local Electrical Resistance
        Pow_local=I^2*R_el_local;% W Local Power
        HL_l= 0.47*(T_w_ext_c(i)-T_amb)*L_l/L;% W Local Heat Loss to Ambient Temperature
        q_local = (Pow_local-HL_l)/A_h_local; % W/m^2
        q_vol_local= (Pow_local-HL_l)/(A_c*L_l); % Volumetric Heat Flux W/m^3
        T_w_int_c= T_w_ext_c(i)+(q_vol_local/(4*k_w_local))*((OD/2)^2-(ID/2)^2)-
(q_vol_local/(2*k_w_local))*(OD/2)^2*log(OD/ID);
        if(abs((T_w_int_c+T_w_ext_c(i))/2- T_w_avg)>0.01)
           T_w_int_assumed=T_w_int_c;
        else
            T_w_int_c_final(i)=T_w_int_c;
            q_local_final(i)=q_local;
            q_vol_local_final(i)=q_vol_local;
            check=1;
        end
    end
end
T_w_int_c_final'

%
%%%%%%%%%%%%%%%%%%%%%%%%%%%%%%%%%%%%%%%%%%%%%%%%%%%%%%%%%%%%%%%%%%%%%
%%%%%%%%%%%

%% Performing Bulk Temperature Calculations(Method of Added Enthalpies)
%Calculations
j=1;
H(j)=refpropm ('H','T',T_in +273.15,'P',P_in,fluid);
%Q=q_ave*A_h_local;
for j=1:22
    if j==1
        Q(j)=q_local_final(j)*pi()*ID*0.056;
        H(j+1)=Q(j)/m + H(j);
        T_b(j)=refpropm('T','P',P_in,'H',H(j+1),fluid);
    else
        Q(j)=(q_local_final(j-1)*L_l/2+q_local_final(j)*L_l/2)*pi()*ID;
        H(j+1)=Q(j)/m + H(j);
        T_b(j)=refpropm('T','P',P_in,'H',H(j+1),fluid);
    end
end
T_b_c=T_b-273.15;
T_b_c'
```

APPENDIX C: SAMPLE MATLAB CODE FOR CALCULATION OF T_w and *HTC* VALUES THROUGH VARIOUS CORRELATIONS

```
%§§§§§§§§§§§§§§§§§§§§§§§§§§§§§§§§§§§§§§§§§§§§§§§§§§§§§§§§§§§§§§§§§§§§§§§§§§§§§
% A program to calculate the wall temperature and heat transfer coefficient
% using iterations from known equations
% Written by Sahil Gupta, UOIT
%
%
%       Each refpropm property is represented by one character:
%           P   Pressure [kPa]
%           T   Temperature [K]
%           D   Density [kg/m3]
%           H   Enthalpy [J/kg]
%           V   Dynamic viscosity [Pa*s]
%           L   Thermal conductivity [W/(m K)]
%
%This code works with all the correlations. They are commented out. Use the
%applicable correlation.
%§§§§§§§§§§§§§§§§§§§§§§§§§§§§§§§§§§§§§§§§§§§§§§§§§§§§§§§§§§§§§§§§§§§§§§§§§§§§§

%%clearing the variables and the screen, and formatting the output
clear all;
clc
format long g;
%% INPUT PARAMETERS
fluid='CO2'; %defining the working fluid
D = 8.058/1000;     %[m]  Inside Diameter (Hydraulic)

%%  BULK FLUID INPUT
temp_b=xlsread('InputParameters.xlsx','sheet1','A:A');% [C]
temp_b = temp_b + 273.15;% [K]

%% PRESSURE ARRAY INPUT
P_b = xlsread('InputParameters.xlsx','sheet1','B:B');  %[MPa]
P_b= P_b*1000; % [kPa]

%% Defining value Holder Arrays
rho_b = zeros;
rho_w = zeros;
rho_f =zeros;

viscosity_b = zeros;
viscosity_w = zeros;
viscosity_f = zeros;

therm_cond_b = zeros;
therm_cond_w = zeros;
therm_cond_f = zeros;

enthalpy_b = zeros;
enthalpy_w = zeros;
enthalpy_f = zeros;

Cp_b=zeros;
```

```
Cp_w=zeros;
Cp_f=zeros;
Cp_avg = zeros;

Pr_avg_b = zeros;
Pr_avg_w = zeros;
Pr_avg_f = zeros;

Re_b= zeros;
Re_w=zeros;
Re_f=zeros;

Nu = zeros;
h = zeros;
h_f=zeros;

temp_w = zeros;
temp_f=zeros; % Defining the Film Temperature.

temp_w_f= zeros;
temp_w_f_C= zeros;

TOL_f=zeros;

Tpc=zeros;

%% calculation of the bulk fluid properties for every temperature

for k = 1:length(temp_b)
   rho_b(k)= refpropm('D','T',temp_b(k),'P',P_b(k),fluid); % [kg/m^3]
   %disp(['Density_b = ', num2str(rho_b),'kg/m^3'])
   viscosity_b(k) = refpropm('V','T',temp_b(k),'P',P_b(k),fluid); % [Pa-s]
   %disp(['viscosity_b = ', num2str(viscosity_b),'Pa-s'])
   Cp_b(k)=refpropm('C','T',temp_b(k),'P',P_b(k),fluid);

   therm_cond_b(k) = refpropm('L','T',temp_b(k),'P',P_b(k),fluid);
   %disp(['thermal conductivity _b = ', num2str(therm_cond_b),'W/(m-K)'])
   enthalpy_b(k) = refpropm('H','T',temp_b(k),'P',P_b(k),fluid);
   %disp(['Enthalpy_b = ', num2str(enthalpy_b),'J/kg'])
end

%% Calculation of Tpc Array
for m=1:length(temp_b)
   startT=30+273.15; % [ K]
   inc=0.05;
   condition=0;
cp(1)=refpropm('C','T',startT,'P',P_b(m),fluid);
cp(2)=refpropm('C','T',startT+inc,'P',P_b(m),fluid);
T = startT + inc;
   while condition==0
      T = T + inc;

      cp(3)=refpropm('C','T',T,'P',P_b(m),fluid);

      if ((cp(2)>cp(1))&&(cp(2)>cp(3)))
         condition=1;
```

```
        Tpc(m)=T-inc-273.15;
    else
        cp(1)=cp(2);
        cp(2)=cp(3);
    end;

  end
end

%% Constant givens

%% Mass FLUX INPUT
G = xlsread('InputParameters.xlsx','sheet1','C:C');%[kg/m^2-s]

%% HEAT FLUX INPUT
q = xlsread('InputParameters.xlsx','sheet1','D:D');%[kW/m^2] Heat flux
q=q*1000; %[W/m^2] heat flux

%% Heated Length INPUT
H_l=xlsread('InputParameters.xlsx','sheet1','E:E'); % Heated Lenght (mm)
H_l=H_l/1000;% Heated Lenght (m)

%% properties of fluid at wall temperature

P_w =P_b;%assuming constant pressure in the tube %[kPa]
P_f=P_b;  % assuming constant pressure in the tube %[kPa]

for j = 1:length(temp_b)

%assuming first temperature to start iterations
temp_w(1) = temp_b(j)+5; %[K] Assuming Wall Temperature For Iterations

%iterations to solve for temperature of the wall and heat transfer
%coefficient values
check = true;
i = 1;
TOL = 0.3; % Within 0.3 degrees
M = 100;  % # of times Iterations will be performed before changing the Tolerance.

%disp(['Point number = ', num2str(j)]);
%the loop includes the equations used to calculate each value

  while (check == true)
    temp_f(i)=(temp_b(j)+temp_w(i))/2;  % [K]
    %disp(['Iteration number = ', num2str(i)]);
  %% CALCULATION OF THERMO PHYSICAL PROPERTIES USING NIST
    enthalpy_w(i)= refpropm('H','T',temp_w(i),'P',P_w(j),fluid); % [J/kg]
    enthalpy_f(i)= refpropm('H','T',temp_f(i),'P',P_f(j),fluid); % [J/kg]
    %disp(['Enthalpy at wall = ', num2str(enthalpy_w(i)),'   [J/kg]'])

    rho_w(i)= refpropm('D','T',temp_w(i),'P',P_w(j),fluid); %  [kg/m^3]
    rho_f(i)= refpropm('D','T',temp_f(i),'P',P_f(j),fluid); %  [kg/m^3]
    %disp(['Density at wall = ', num2str(rho_w(i)),'     [kg/m^3]'])

    Cp_w(i)=refpropm('C','T',temp_w(i),'P',P_w(j),fluid);
    Cp_f(i)=refpropm('C','T',temp_f(i),'P',P_f(j),fluid);
```

```
        Cp_avg(i) = (enthalpy_w(i) - enthalpy_b(j))/(temp_w(i) - temp_b(j)); % [J/kg*K]
        %disp(['Average Cp = ', num2str(Cp_avg(i)),'    [J/kg*K]'])

        viscosity_w(i) = refpropm('V','T',temp_w(i),'P',P_w(j),fluid);
        viscosity_f(i) = refpropm('V','T',temp_f(i),'P',P_f(j),fluid);

        therm_cond_w(i) = refpropm('L','T',temp_w(i),'P',P_w(j),fluid);
        therm_cond_f(i) = refpropm('L','T',temp_f(i),'P',P_f(j),fluid);

        Pr_avg_b(i) = viscosity_b(j)*Cp_avg(i)/therm_cond_b(j);
        Pr_avg_w(i) = viscosity_w(i)*Cp_avg(i)/therm_cond_w(i);
        Pr_avg_f(i) = viscosity_f(i)*Cp_avg(i)/therm_cond_f(i);

        Re_b(i) = G(j)*D/viscosity_b(j);
        Re_w(i) = G(j)*D/viscosity_w(i);
        Re_f(i) = G(j)*D/viscosity_f(i);

    %% Below are the different HTC correlations. USE 1 At a Given Time
     %% EXISTING CORRELATIONS
        %% MOKRY SC CO2 CORRELATION ICONE 19
        %h(i) = (therm_cond_b(j)/D)*(0.0121*Re_b(i)^0.86*Pr_avg_b(i)^0.23*(rho_w(i)/rho_b(j))^0.59); % Mokry
et. al.ICONE 19 SCCO

        %% MOKRY WATER CORRELATION ICONE 19
        %h(i) = (therm_cond_b(j)/D)*(0.0061*Re_b(i)^0.904*Pr_avg_b(i)^0.684*(rho_w(i)/rho_b(j))^0.564); %
Mokry et. al.ICONE 19 SC WATER

        %% SWENSON ORIGINAL CORRELATION 1965
        %h(i) = (therm_cond_w(i)/D)* (0.00459*Re_w(i)^0.923*Pr_avg_w(i)^0.613*(rho_w(i)/rho_b(j))^0.231);
%Swenson original

        %% Krasnoshchekov et al. (1967) Equation 11.4 & 11.11
        %Xi=(1.82*log(Re_b(i))-1.64)^-2; % Equ 11.6
        %Nu_o=((Xi/8)*Re_b(i)*Pr_avg_b(i))/(12.7*sqrt(Xi/8)*(Pr_avg_b(i)^(2/3)-1)+1.07); % Eq. 11.5

        %% Krasnoshchekov and Protopopov Eq 11.4 ( 1959,1960)

%h(i)=(therm_cond_b(j)/D)*Nu_o*((viscosity_b(j)/viscosity_w(i))^0.11)*((therm_cond_b(j)/therm_cond_w(i))^-
0.33)*((Cp_avg(i)/Cp_b(j))^0.35);

        %% Krasnoshchekov et al. (1967) Equation 11.11
%       if (temp_w(i)/Tpc(j)<=1 ||temp_b(j)/Tpc(j)>=1.2)
%           n=0.4;
%           h(i)=(therm_cond_b(j)/D)*Nu_o*((rho_w(i)/rho_b(j))^0.3)*((Cp_avg(i)/Cp_b(j))^n);
%
%       elseif (1<=temp_w(i)/Tpc(j)&& temp_w(i)/Tpc(j)<=2.5)
%           n=0.22+0.18*(temp_w(i)/Tpc(j));
%           h(i)=(therm_cond_b(j)/D)*Nu_o*((rho_w(i)/rho_b(j))^0.3)*((Cp_avg(i)/Cp_b(j))^n);
%
%       elseif (1<=temp_b(j)/Tpc(j) && temp_b(j)/Tpc(j)<=1.2)
%           n1=0.22+0.18*(temp_w(i)/Tpc(j));
%           n=n1+(5*n1-2)*(1-temp_b(j)/Tpc(j))
%           h(i)=(therm_cond_b(j)/D)*Nu_o*((rho_w(i)/rho_b(j))^0.3)*((Cp_avg(i)/Cp_b(j))^n);
%       else
%           disp ('Error: IN CALCULATING HTC USING KRASNOSHCHEKOV')
%           break;
```

```
%       end
%

      %% Jackson et al. (2002) Equation 11.32
%       if (temp_b(j)<temp_w(i)&& temp_w(i)<Tpc(j))
%          n=0.4;
%
h(i)=(therm_cond_b(j)/D)*0.0183*(Re_b(i)^0.82)*(Pr_avg_b(i)^0.5)*((rho_w(i)/rho_b(j))^0.3)*((Cp_avg(i)/Cp_b(j
))^n);
%       elseif (1.2*Tpc(j)<temp_b(j) && temp_b(j)<temp_w(i))
%          n=0.4;
%
h(i)=(therm_cond_b(j)/D)*0.0183*(Re_b(i)^0.82)*(Pr_avg_b(i)^0.5)*((rho_w(i)/rho_b(j))^0.3)*((Cp_avg(i)/Cp_b(j
))^n);
%       elseif (temp_b(j)<Tpc(j) && Tpc(j)<temp_w(i))
%          n=0.4+0.2*((temp_w(i)/Tpc(j))-1);
%
h(i)=(therm_cond_b(j)/D)*0.0183*(Re_b(i)^0.82)*(Pr_avg_b(i)^0.5)*((rho_w(i)/rho_b(j))^0.3)*((Cp_avg(i)/Cp_b(j
))^n);
%       elseif ( (Tpc(j)<temp_b(j)&& temp_b(j)<1.2)|| (temp_b(j)<temp_w(i)))
%          n=0.4+0.2*((temp_w(i)/Tpc(j))-1)*(1-5*((temp_b(j)/Tpc(j))-1))
%
h(i)=(therm_cond_b(j)/D)*0.0183*(Re_b(i)^0.82)*(Pr_avg_b(i)^0.5)*((rho_w(i)/rho_b(j))^0.3)*((Cp_avg(i)/Cp_b(j
))^n);
%       else
%           disp ('Error: IN CALCULATING HTC USING Jackson corr.')
%           break;
%       end


      %% SAHIL WATER CORRELATIONS - ICONE 19 - JEGTP
      %h(i)
=(therm_cond_w(i)/D)*(0.0033*Re_w(i)^0.9413*Pr_avg_w(i)^0.7643*(viscosity_w(i)/viscosity_b(j))^0.3978*(rho
_w(i)/rho_b(j))^0.1563); %Mod Swenson 2 [JEGTP]
      %h(i)
=(therm_cond_w(i)/D)*(0.0033*Re_w(i)^0.9413*Pr_avg_w(i)^0.7643*(viscosity_w(i)/viscosity_b(j))^0.3978*(rho
_w(i)/rho_b(j))^0.1563*(1+exp(-H_l(j)/(24*D)))^0.3); %Mod Swenson2_entrance [JEGTP]

      %% NEW CORRELATIONS (SAHIL) - THESIS 2011 - ICONE 20
      %h(i) =(therm_cond_w(i)/D)*(0.0038*(Re_w(i)^0.9571)*(Pr_avg_w(i)^(-
0.1391))*((rho_w(i)/rho_b(j))^0.8363)*((therm_cond_w(i)/therm_cond_b(j))^(-
0.7537))*((viscosity_w(i)/viscosity_b(j))^(-0.2222))); % WALL Approach FINAL#1
      %h(i)
=(therm_cond_w(i)/D)*(0.0036*(Re_w(i)^0.9519)*((rho_w(i)/rho_b(j))^0.6671)*((therm_cond_w(i)/therm_cond_b
(j))^(-0.732))); % WALL Approach#2
      %h(i) =(therm_cond_b(j)/D)*(0.0094*(Re_b(i)^0.8922)*(Pr_avg_b(i)^(-
0.1413))*((rho_w(i)/rho_b(j))^0.9266)*((therm_cond_w(i)/therm_cond_b(j))^(0.2162))*((viscosity_w(i)/viscosity_
b(j))^(-1.1279))); % BULK Approach
      %h(i)
=(therm_cond_f(i)/D)*(0.0043*(Re_f(i)^0.9354)*((rho_w(i)/rho_b(j))^0.5716)*((therm_cond_w(i)/therm_cond_b(j
))^(-0.5243))); % FILM Approach

     %%
      temp_w(i+1) = (q(j)/h(i) + temp_b(j));

      %% This Section Displays a warning if the calc Tw is out of Bounds
```

```
        if temp_w(i+1)>2000
          disp ('Error: OUT OF BOUNDS TEMP>2000K AT LOCATION ')
          j
          H_l(j)
          temp_w_f(j) =0;
          break
        end
         if temp_w(i+1)<216.59
          disp ('Error: OUT OF BOUNDS TEMP<216.59K AT LOCATION')
          j
          H_l(j)
          temp_w_f(j) =0;
          break
        end
      %% iterations stop when the successive values of wall temperature are within TOL absolute difference
        if abs((temp_w(i+1) - temp_w(i)))<TOL
          h_f(j) = h(i);
          temp_w_f(j) = temp_w(i+1);
          temp_w_f_C(j) = temp_w_f(j)-273.15;
          break
        end
      %% If Iterations Do not Converge after M Trials Tolerance can be increased
        if i>M
          TOL = TOL + 0.2;
          if abs((temp_w(i+1) - temp_w(i)))<TOL
            h_f(j) = h(i);
            temp_w_f(j) = temp_w(i+1);
            temp_w_f_C(j) = temp_w_f(j)-273.15;
            break
          else
            TOL = TOL+0.2;
            M = M + 10;
          end
        end
      %%
      i= i+1;

  end
  TOL_f(j) = TOL;
end

%$$$$$$$$$$$$$$$$$$$$$$$$$$$$$$$$$$$$$$$$$$$$$$$$$$$$$$$$$$$$$$
%$$ DISPLAY OF FINAL VALUES
temp_b_C = temp_b - 273.15;
disp('Wall Temperature (C)')
temp_w_f_C_real=real(temp_w_f_C);
h_f_real=real(h_f)/1000;
```

APPENDIX D: S.GUPTA PUBLICATIONS

PAPERS IN REFEREED JOURNALS

1. **Gupta, S.**, Saltanov, Eu., Mokry, S.J., Pioro, I., Trevani, L. and McGillivray, D., 2013. Developing Empirical Heat-Transfer Correlations for Supercritical CO_2 Flowing in Vertical Bare Tubes, Nuclear Engineering and Design, Vol. 261, pp. 116-131.
2. Mokry, S., Pioro, I.L., Farah, A., King, K., **Gupta, S.**, Peiman, W. and Kirillov, P., 2011. Development of Supercritical Water Heat-Transfer Correlation for Vertical Bare Tubes, Nuclear Engineering and Design, Vol. 241, pp. 1126-1136.

PAPERS PUBLISHED IN REFEREED PROCEEDINGS OF INTERNATIONAL AND NATIONAL CONFERENCES AND SYMPOSIUMS

1. Pioro, I., Mokry, S., **Gupta, S.,** Saltanov, Eu., Dragunov, A., Draper, Sh., and Mann, D., 2013. Heat Transfer at Supercritical Pressures in Power-Engineering Applications, Proceedings of the 13th UK Heat Transfer Conference (UKHTC2013), Imperial College London, UK, September 2–3, 8 pages.

2. **Gupta, S.,** Saltanov, Eu. and Pioro, I., 2013. Heat-Transfer Correlation for Supercritical Carbon Dioxide Flowing in Vertical Bare Tubes, Proceedings of the 21st International Conference on Nuclear Engineering (ICONE-21), July 29-August 2, Chengdu, China, Paper #16453, 12 pages.

3. **Gupta, S.,** Saltanov, Eu. and Pioro, I., 2013. Few Challenges Associated with Developing 1-D HTC Correlations For , Proceedings of the 34th Annual Canadian Nuclear Society Conference and 37th CNS/CNA Student Conference, Toronto, ON, Canada, June 9-12, Paper #68, 5 pages.

4. Pioro, I., Mokry, S., **Gupta, S.,** and Saltanov, E., 2012. Heat-transfer for Supercritical Water and CO_2 with Upward Flow in Vertical Bare Tubes, Transactions of the European Nuclear Conference (ENC-2012), Manchester, UK, December 9 – 12, Paper ENC2012-A0202, 11 pages.

5. Surendran, P., **Gupta, S.,** Preda, T. and Pioro, I., 2012. Comparison of Existing Supercritical Carbon Dioxide Heat Transfer Correlations for Horizontal and Vertical Bare Tubes, Proceedings of the 20th International Conference On Nuclear Engineering (ICONE-20) – ASME 2012 POWER Conference, July 30 - August 3, Anaheim, California, USA, Paper #54630, 8 pages.

6. **Gupta, S.,** McGillivray, D., Surendran, P., Trevani, L. and Pioro, I., 2012. Developing Heat-Transfer Correlations for Supercritical CO_2 Flowing in Vertical Bare Tubes, Proceedings of the 20th International Conference On Nuclear Engineering (ICONE-20) – ASME 2012 POWER Conference, July 30 - August 3, Anaheim, California, USA, Paper #54626, 13 pages.

7. Zvorykina, A., **Gupta, S.,** Peiman, W., Pioro, I. and Fialko, N., 2012. Current Status and Future Applications of Supercritical Pressures in Power Engineering, Proceedings of the 20th International Conference On Nuclear Engineering (ICONE-20) – ASME 2012 POWER Conference, July 30 - August 3, Anaheim, California, USA, Paper #54558, 16 pages.

8. Pioro, I., **Gupta, S.** and Mokry, S., 2012. Heat-Transfer Correlations for Supercritical Water and Carbon Dioxide Flowing Upward in Vertical Bare Tubes, Proceedings of the ASME 2012 Summer Heat Transfer Conference - HT2012, July 8-12, Rio Grande, Puerto Rico, Paper #HT2012-58514, 12 pages.

9. **Gupta, S.,** Mokry, S. and Pioro, I., 2011. Developing a Heat-Transfer Correlation for Supercritical-Water Flowing in Vertical Tubes and Its Application in SCWR, Proceedings of the 19th International Conference On Nuclear Engineering (ICONE-19), Makuhari, Japan, May 16-19, Paper 43503, 11 pages.

10. Thind, H., **Gupta, S.,** Pioro, I. and Harvel, G., 2011. Heat-Transfer Analysis of SCW to SCW Double-Pipe Heat Exchanger for Indirect-Cycle SCW NPPs, Proceedings of the 5th International Symposium on SCWR (ISSCWR-5), Vancouver, BC, Canada, March 13-16, Paper P84, 14 pages.

11. Mokry, S., Farah, A., King, K., **Gupta, S.,** Pioro, I. and Kirillov, P., 2010. Development of a Heat-Transfer Correlation for Supercritical Water Flowing in a Vertical Bare Tube, Proceedings of the 14th International Heat Transfer Conference (IHTC-14), Washington, D.C., USA, August 7-13, Paper #22908, 13 pages.

12. Mokry, S., Farah, A., King, K., **Gupta, S.** and Pioro, I., 2010. Updated Heat-Transfer Correlations for Supercritical Water in Vertical Bare Tubes, Proceedings of the 7th International Conference on Heat Transfer, Fluid Mechanics and Thermodynamics (HEFAT-2010), July 19-21, Antalya, Turkey, Paper #860.

13. King, K., Farah, A., **Gupta, S.,** Mokry, S. and Pioro, I., 2010. Comparison of Three-Rod Bundle Data with Existing Heat-Transfer Correlations for Bare Vertical Tubes, Proceedings of the 18th International Conference On Nuclear Engineering (ICONE-18), Xi'an, China, May 17-21, Paper 29991, 7 pages.

14. Farah, A., King, K., **Gupta, S.,** Mokry, S., Peiman, W. and Pioro, I., 2010. Comparison of

Selected Forced-Convection Supercritical-Water Heat-Transfer Correlations for Vertical Bare Tubes, Proceedings of the 18th International Conference On Nuclear Engineering (ICONE-18), Xi'an, China, May 17-21, Paper 29990, 10 pages.

15. **Gupta, S.,** Farah, A., King, K., Mokry, S. and Pioro, I., 2010. Developing New Heat-Transfer Correlation for Supercritical-Water Flow in Vertical Bare Tubes, Proceedings of the 18th International Conference On Nuclear Engineering (ICONE-18), Xi'an, China, May 17-21, Paper 30024, 9 pages.

16. Mokry, **Gupta, S.,** S., Farah, A., King, K. and Pioro, I.L., 2010. Analysis of Updated Supercritical Water Heat Transfer Correlations for Vertical Bare Tubes, Proceedings of the 18th International Conference On Nuclear Engineering (ICONE-18), Xi'an, China, May 17-21, Paper 30192, 12 pages.

17. **Gupta, S.,** Farah, A., King, K., Mokry, S. and Pioro, I., 2010. Development of Heat-Transfer Correlation for Water Flowing in Vertical Bare Tubes at Supercritical Conditions, Proceedings of the 31st Annual Conference of Canadian Nuclear Society and 34th CNS/CNA Student Conference, Montreal, QC, Canada, May 24−27, 13 pages.

18. Farah, A., King, K., **Gupta, S.,** Mokry, S., Peiman, W. and Pioro, I., 2010. A Study of Selected Forced-Convection SuperCritical-Water Heat-Transfer Correlations for Vertical Bare Tubes Based on a Wide-Range Dataset, Proceedings of the 31st Annual Conference of Canadian Nuclear Society and 34th CNS/CNA Student Conference, Montreal, QC, Canada, May 24−27, 13 pages.

19. Farah, A., King, K., **Gupta, S.,** Mokry, S. and Pioro, I., 2010. Comparison of Selected Heat-Transfer Correlations for Supercritical Water Flowing Upward in Vertical Bare Tubes, Proceedings of the 2nd Canada-China Joint Workshop on Supercritical Water-Cooled Reactors (CCSC-2010), Toronto, Ontario, Canada, April 25-28, Paper No. 25, 12 pages.

20. Mokry, S., Farah, A., **Gupta, S.,** King, K. and Pioro, I., 2010. Comparative Study and Advancement on a Supercritical-Water Heat-Transfer Correlation for Vertical Bare Tubes, Proceedings of the 2nd Canada-China Joint Workshop on Supercritical Water-Cooled Reactors (CCSC-2010), Toronto, Ontario, Canada, April 25-28, Paper No. 21, 17 pages.

21. Mokry, S., Farah, A., King, K., **Gupta, S.,** Pioro, I. and Kirillov, P., 2009. Development of Supercritical Water Heat-Transfer Correlation for Vertical Bare Tubes, Proceedings of the International Conference "Nuclear Energy for New Europe" (NENE), Bled, Slovenia, Sep. 14-17, Paper 210, 14 pages.

APPENDIX E: AWARDS AND HONOURS BY S. GUPTA

1. Winner of "Student Best Paper Competition" for the paper "Development of a New Heat-Transfer Correlation For Supercritical-Water Flow in Vertical Bare Tubes" - 18th International Conference On Nuclear Engineering (ICONE-18), May 17 21, Xi'an, China, 2010, Paper #30024

2. Best Paper/Presentation Award at the 34th CNS/CAN Student Conference, Montreal, Quebec, May 25th, 2010

3. Winner of "Student Best Paper Competition" for the paper "Developing a Heat-Transfer Correlation For Supercritical-Water Flowing in Vertical Tubes and Its Application in SCWRS" - 19th International Conference On Nuclear Engineering (ICONE-19), Oct 24 25, Osaka, Japan, 2011, Paper #43503.

4. Akiyama Medal (Awarded by Japan Society of Mechanical Engineers) for the best paper in student track "Developing Heat-Transfer Correlations for Supercritical CO2 Flowing in Vertical Bare Tubes" - 20th International Conference on Nuclear Engineering (ICONE-20) – ASME 2012 POWER Conference, July 30 August 3, Anaheim, California, USA, Paper #54626.

5. Recipient of 2013 R.E Jervis Award given by Canadian Nuclear Society (CNS) and Canadian Nuclear Association (CNA) in recognition of excellence in research and development in Nuclear Engineering - Canadian Nuclear Society's 34th Annual Conference, 2013 June 9-12 at the Toronto Marriott Downtown Eaton Centre, 525 Bay St., Toronto.

6. Chinese Nuclear Society (CNS) S.Qian best paper award for the paper "Heat-Transfer Correlation For Supercritical-Carbon Dioxide Flowing in Vertical Tubes" - 21st International Conference On Nuclear Engineering (ICONE-21), July 29 - Aug 2, Chengdu, China, 2013, Paper #16453.